NEW OPTOELECTRONIC DEVICES USING GaAs-GaAlAs EPITAXY

Thesis by

Chien- Ping Lee

In Partial Fulfillment of the Requirements

for the degree of

Doctor of Philosophy

California Institute of Technology

Pasadena, California

1978

(Submitted May 26, 1978)

To My Parents

ACKNOWLEDGMENTS

It is a pleasure to express my sincere appreciation to my advisor, Professor Amnon Yariv, for his guidance, encouragement, and support throughout the course of this research. It has been a pleasant and unforgettable experience working in the quantum electronic group under his supervision.

I would like to thank Dr. Shlomo Margalit, whom I collaborated with during the last one and half years. His scientific guidance and stimulating discussions are deeply appreciated. I would also like to thank Dr. Ilan Samid for introducing me to the laboratory work and the epitaxial crystal growth. I am also grateful to Mr. Desmond Armstrong for the skillful assistance with the experimental apparatus.

Special thanks go to Professor Peter Goldreich for his care and encouragement during my first year in Caltech as well as in this country.

I would also like to express my appreciation to my friends, Israel Ury and Pei-Chuang Chen, for reading the manuscript and Mrs. Ruth Stratton and Mrs. Verona Carpenter for typing part of the thesis.

Finally, I would like to thank my parents and my wife, Alice, for their love, encouragement, and support. Alice also helped in the computer programming and the vacuum evaporation of the metal contacts used in this work.

Financial support received from the National Science Foundation, the Office of Naval Research, the International Bussiness Machines Corporation, the Corning Glass Works Foundation and the California Institute of Technology is greatly appreciated.

ABSTRACT

Three subjects related to epitaxial GaAs-GaAlAs optoelectronic devices are discussed in this thesis. They are:

1. Embedded Epitaxy

This is a technique of selective multilayer growth of GaAs-$Ga_{1-x}Al_xAs$ single crystal structures through stripe openings in masking layers on GaAs substrates. This technique results in prismatic layers of GaAs and $Ga_{1-x}Al_xAs$ "embedded" in each other and leads to controllable uniform structures terminated by crystal faces. The dependence of the growth habit on the orientation of the stripe openings has been studied. Room temperature embedded double heterostructure lasers have been fabricated using this technique. Threshold current densities as low as 1.5 KA/cm^2 have been achieved.

2. Barrier Controlled PNPN Laser Diode

It is found that the I-V characteristics of a PNPN device can be controlled by using potential barriers in the base regions. Based on this principle, GaAs-GaAlAs heterostructure PNPN laser diodes have been fabricated. GaAlAs potential barriers in the bases control not only the electrical but also the optical properties of the device. PNPN lasers with low threshold currents and high breakover voltage have been achieved. Numerical calculations of this barrier controlled structure are presented in the ranges where the total current is below the holding point and near the lasing threshold.

3. Injection Lasers on Semi-Insulating Substrates

GaAs-GaAlAs heterostructure lasers fabricated on semi-insulating substrates have been studied. Two different laser structures achieved

are: (1) Crowding effect lasers, (2) Lateral injection lasers. Experimental results and the working principles underlying the operation of these lasers are presented. The gain induced guiding mechanism is used to explain the lasers' far field radiation patterns. It is found that Zn diffusion in $Ga_{1-x}Al_xAs$ depends on the Al content x, and that GaAs can be used as the diffusion mask for Zn diffusion in $Ga_{1-x}Al_xAs$. Lasers having very low threshold currents and operating in a stable single mode have been achieved. Because these lasers are fabricated on semi-insulating substrates, it is possible to integrate them with other electronic devices on the same substrate. An integrated device, which consists of a crowding effect laser and a Gunn oscillator on a common semi-insulating GaAs substrate, has been achieved.

TABLE OF CONTENTS

	Page
CHAPTER I - INTRODUCTION	1
I.1 Optical Communication and GaAs-Based Integrated Optics	1
I.2 GaAs-GaAlAs Heterostructure Lasers	5
I.3 Outline of the Thesis	12
References for Chapter I	14
CHAPTER II - GaAs-GaAlAs EMBEDDED HETEROSTRUCTURE EPITAXY AND EBBEDDED LASERS	16
II.1 Introduction	16
II.2 Embedded Epitaxy	18
II.2.1 Fabrication procedure	19
II.2.2 Growth structure	22
II.3 Embedded Heterostructure Lasers	30
References for Chapter II	45
CHAPTER III - BARRIER CONTROLLED GaAs-GaAlAs PNPN LASER DIODE	47
III.1 Introduction	47
III.2 PNPN Device Operation	51
III.3 Design of the Barrier Controlled GaAs-GaAlAs PNPN Laser	56

Page

III.4 Current-Voltage Characteristics Below the Holding Point 61

III.4.1 Boundary conditions 63

III.4.2 Solution of the diffusion equation 66

III.4.3 Transport factors 70

III.4.4 I-V characteristics 73

III.4.5 Numerical results 76

III.5 Characteristics Near the Lasing Threshold 84

III.6 Experimental Results 91

References for Chapter III 101

CHAPTER IV - GaAs-GaAlAs HETEROSTRUCTURE LASERS ON SEMI-INSULATING SUBSTRATES 103

IV.1 Introduction 103

IV.2 GaAs-GaAlAs Heterostructure Lasers on Semi-Insulating Substrates using Carrier Crowding 106

IV.2.1 Crowding effect 108

IV.2.2 Device structure and fabrication 117

IV.2.3 Experimental results 121

IV.3 GaAs-GaAlAs Heterostructure Lasers on Semi-Insulating Substrates using Lateral Injection 131

IV.3.1 Zn diffusion in $Ga_{1-x}Al_xAs$ 135

IV.3.2 Device structure and fabrication 139

IV.3.4 Experimental results 144

IV.4 Gain Induced Guiding 150

Page

IV.5 Monolithic Integration of Injection Lasers with Electronic Devices 160

IV.5.1 Integration of a crowding effect laser with a Gunn oscillator on a semi-insulating substrates 161

IV.5.2 Integration of injection lasers with MESFET'S 166

References for Chapter IV 169

CHAPTER V - EXPERIMENTAL TECHNIQUES 173

V.1 Introduction 173

V.2 GaAs-GaAlAs Liquid Phase Epitaxy 174

V.2.1 Growth system 175

V.2.2 Growth procedure 178

V.3 Laser Diode Fabrication 181

V.4 Optical Measurements 185

V.4.1 Threshold current, differential quantum efficiency and spectrum 185

V.4.2 Near field measurements 186

V.4.3 Far field measurements 188

References for Chapter V 191

CHAPTER I

INTRODUCTION

I.1 Optical Communication and GaAs-Based Integrated Optics

Optical communication in the spectral range of visible light or the near infrared has been of great interest since the advent of lasers as coherent light sources. The enormous amount of information carring capability of laser light makes it attractive for various communication applications. Owing to the shorter wavelengths of the optical waves compared with those of radio waves, light signals can be transmitted through small size waveguides such as glass fibers, thin film dielectric waveguides, etc. instead of bulky copper cables used for radio waves.

Use of glass fibers in the optical communication system has been of particular interest recently. The combination of small size, light weight and large bandwidth makes fibers most suitable for today's already crowded communication systems. Low loss fibers with transmission losses of about 1 dB/km in the 0.8 μm - 1.6 μm spectral range have recently been achieved(1). Long distance fiber communication is promising, as stronger, less lossy and less dispersive fibers are made.

In order to realize efficient optical communication, one needs along with the fibers, source terminals, detection terminals, and repeater stations. The source terminal should consist of a light source which is capable of generating light having small attenuation and dispersion in the fiber medium and a modulator which converts information into optical signals. The repeater stations perform the functions of detecting the attenuated light signals and regenerating them into intense signals

for the next leg of the journey; the detection terminals detect and process the signals. It is essential that all these terminals and stations are reliable and have dimensions comparable to the sizes of fibers so that efficient coupling between them and the fibers can be obtained. The objectives, however, are difficult to achieve with conventional optical technology, because each optical circuit in a terminal or a station consists of several components which are usually heavy, bulky, and require careful alignment and protection. In addition, the interface between different components is complicated and usually limits the performance. In an effort to reduce the sizes of the components and fabricate them on a common base, a new technology called "integrated optics" has been developed[2].

Much as integrated electronic circuits are presently fabricated having small dimensions, integrated optics has an eventual goal of fabricating complex optical circuits with densely packed components in small solid configurations. All the components of an optical circuit will be fabricated in thin films on the surface of a common substrate, and all the functions of light generation, modulation, waveguiding and detection will be confined in those thin film structures. The whole circuit will be compact, rigid and free from the problems of vibration and alignment. The simplicity, reliability, low cost, and large information carrying capability of these monolithic integrated optical circuits will add a new dimension to future communication and information processing systems.

The basic and the most important problem of monolithic integration is to find the proper material which has the versatility of performing the various functions mentioned above. There are many materials

which have been used to perform satisfactorily one or two of these functions. But there is only one which is able to fulfill all these requirements. This material is GaAs. The versatility of GaAs in terms of its electrical and optical properties has long been recognized, and various useful electronic and optical GaAs devices have been fabricated. Using GaAs as the base material for integrated optics was first suggested by Yariv[3].

Let us examine some of the properties of GaAs and the various devices which can be fabricated on a chip of GaAs:

(1) GaAs is a direct bandgap semiconductor which can be used to fabricate lasers and light emitting diodes(LED). The wavelength of the emitted light is in the range of 0.8 - 0.9 μm which coincides with one of the low loss windows of the fiber transmission spectrum. Today, CW, room temperature GaAs lasers are probably the most reliable light sources for fiber communication systems.

(2) GaAs can be easily alloyed with aluminum to form the ternary compound $Ga_{1-x}Al_xAs$. The nearly identical lattice constants of these two materials make it possible to grow epitaxially $Ga_{1-x}Al_xAs$ layers on GaAs with relatively few defects. Both of the electrical and optical characteristics of this ternary compound depend on the Al content x. This makes it possible to form heterojunction devices and waveguides using GaAs-$Ga_{1-x}Al_xAs$ multilayer structures.

(3) Both the electrooptic figure of merit and the photo-elastic figure of merit of GaAs are among the largest[4], making it applicable to a variety of switching and modulating devices.

(4) Efficient and fast light detectors can be easily fabricated using PN junctions in GaAs.

(5) The fabrication procedures of GaAs integrated optical circuits are compatible with standard semiconductor planar technology. Various techniques such as diffusion, ion implantation, metalization, lithography pattern formation, etc. which have been used for GaAs microwave devices are available for optical devices.

(6) The existence of semi-insulating GaAs makes the integration of electronic devices and optical devices possible.

In the past most of the effort in GaAs integrated optics was centered on individual devices such as low threshold lasers, waveguides, detectors, modulators and switches, etc. The integration of these devices on a common GaAs substrate is still in its primitive stage. One of the obstacles to integration derives from the injection lasers' mirrors, which are formed by cleaving the crystal along a pair of crystal planes, and therefore, preclude the monolithic integration of other optical components. This obstacle was overcome using a "mirrorless concept" which employs a periodically corrugated laser structure to provide the necessary feedback for lasing. Two kinds of lasers, which have been fabricated using this method, are distributed feedback (DFB) lasers and distributed Bragg reflector (DBR) lasers[5]. Other schemes such as etched mirrors[6], and as-grown mirrors[7], have also been developed with an aim to solve this problem. Another obstacle which had not been overcome untill recently was the use of highly conductive N type GaAs substrates, which makes it difficult to obtain electrical isolation between devices. A new technique of fabricating lasers and related

devices on semi-insulating GaAs substrates was developed by us recently.[8] The use of non-conductive (semi-insulating) substrates provides the necessary electrical isolation needed for integration and brings the possiblity of integrating optical devices with electronic devices. It is possible that GaAs based optics will in the near future take full advantage of GaAs microwave technology to achieve a considerable amount of integration.

I.2 GaAs-GaAlAs Heterostructure Lasers

Lasing action by stimulated recombination of carriers injected across a PN junction of semiconductors was predicated by Basov in 1961[9]. The first working injection lasers were reported the following year[10]. These early lasers were fabricated on GaAs wafers with diffused PN junctions. Stimulated recombination takes place in the region near the junction and coupled out from the laser cavity via two cleaved mirrors. (see Fig. 1-1a) These lasers had simple structures and are now referred to as homostructure lasers. Lasers of this type have very high room-temperature threshold current densities ($\sim$50 KA/cm^2) because the active (recombination) regions, as determinated by the carrier diffusion lengths, are wide, and the waveguides for the light in the PN junctions are poor.

In 1963 Kroemer[11] and Alferov et al.[12] suggested that the injection lasers could be improved by the use of heterostructures in which the recombination or active region is bounded by the wider bandgap regions. Such structures can provide both carrier and optical confinement to a thin active region, because the wider bandgap provides

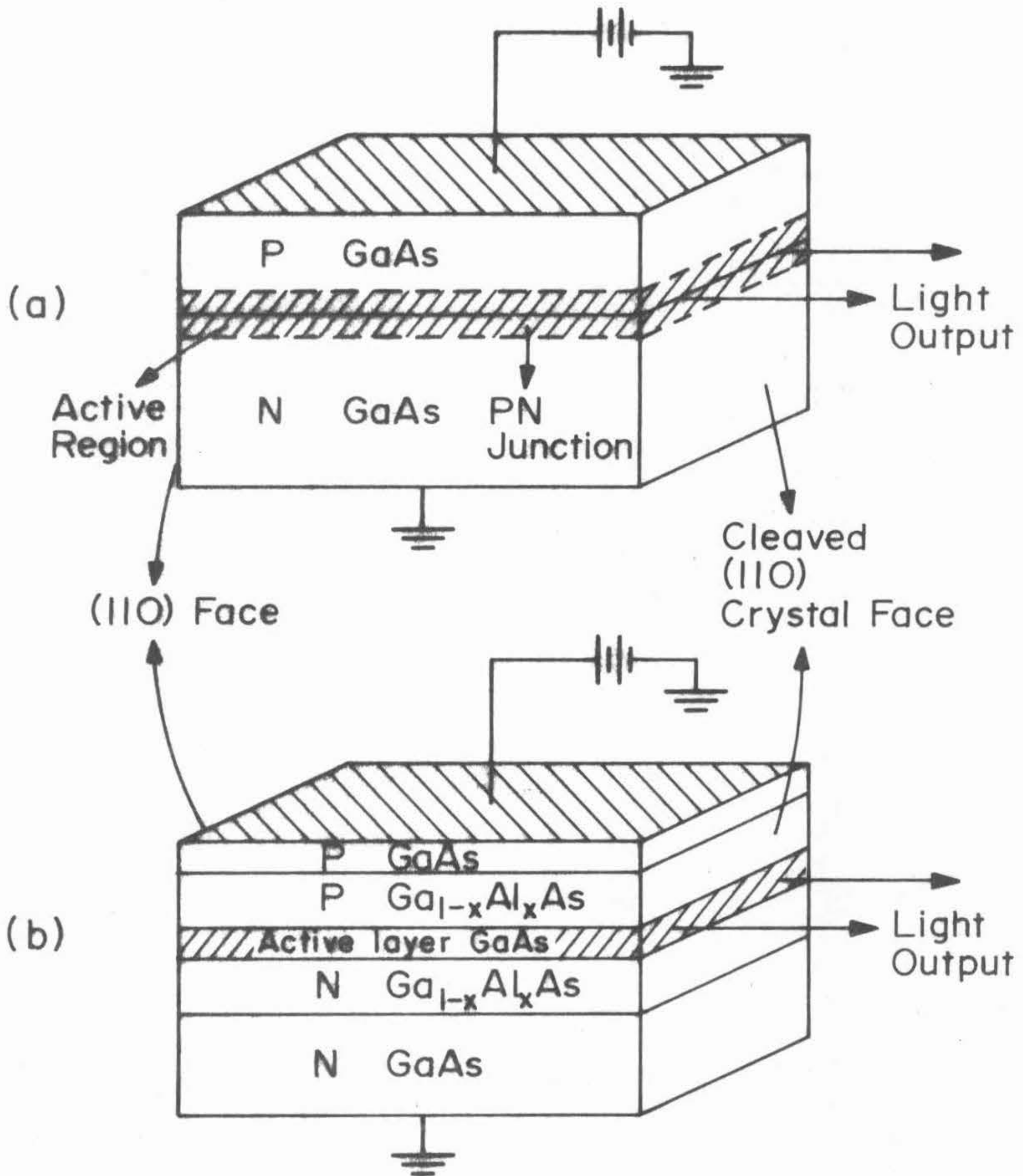

Fig. 1-1 Schematic drawings of (a) a GaAs homostructure laser, and (b) a GaAs-GaAlAs double heterostructure laser.

a potential barrier to carriers, and has a lower index of refraction so as to provide waveguiding. However this idea was not realized until $Ga_{1-x}Al_xAs$ layers were successfully grown on GaAs substrates by liquid phase epitaxy[13].

$Ga_{1-x}Al_xAs$ is an alloy of GaAs and Al. This alloy is formed by replacing a fraction x of the Ga atoms in the GaAs crystal by Al atoms. The fraction x can be varied continuously from 0 to 1. The addition of Al atoms in the crystal has only a very small effect on the lattice parameters, so epitaxial layers of $Ga_{1-x}Al_xAs$ can be easily grown on GaAs substrates with a very small amount of interface defects. This property is very important for lasers, because defects at the interfaces may form non-radiative recombination traps for carriers, and hence influence the lasing performance. The material properties of $Ga_{1-x}Al_xAs$ have been studied extensively. Its index of refraction decreases with Al content x, while the bandgap increases. It is a direct bandgap material when x is less than 0.37, and becomes indirect when x is higher. The energy of the bandgap increases from 1.43 eV at x=0 to $\sim$1.92 eV at x=0.37. The curve of the bandgap energy versus composition is shown in Fig. 1-2.

In the late 1960's, due to efforts by Alferov et al.[14], Panish et al.[15], and Kressel et al.[16], GaAs-GaAlAs heterostructure injection lasers were fabricated. The first kind of these lasers involved only one GaAs-GaAlAs heterojunction in the laser. Light and injected carriers were confined by the heterojunction only at one boundary of the recombination region. These lasers were named single heterostructure (SH) lasers. They had threshold currents considerably lower than those of

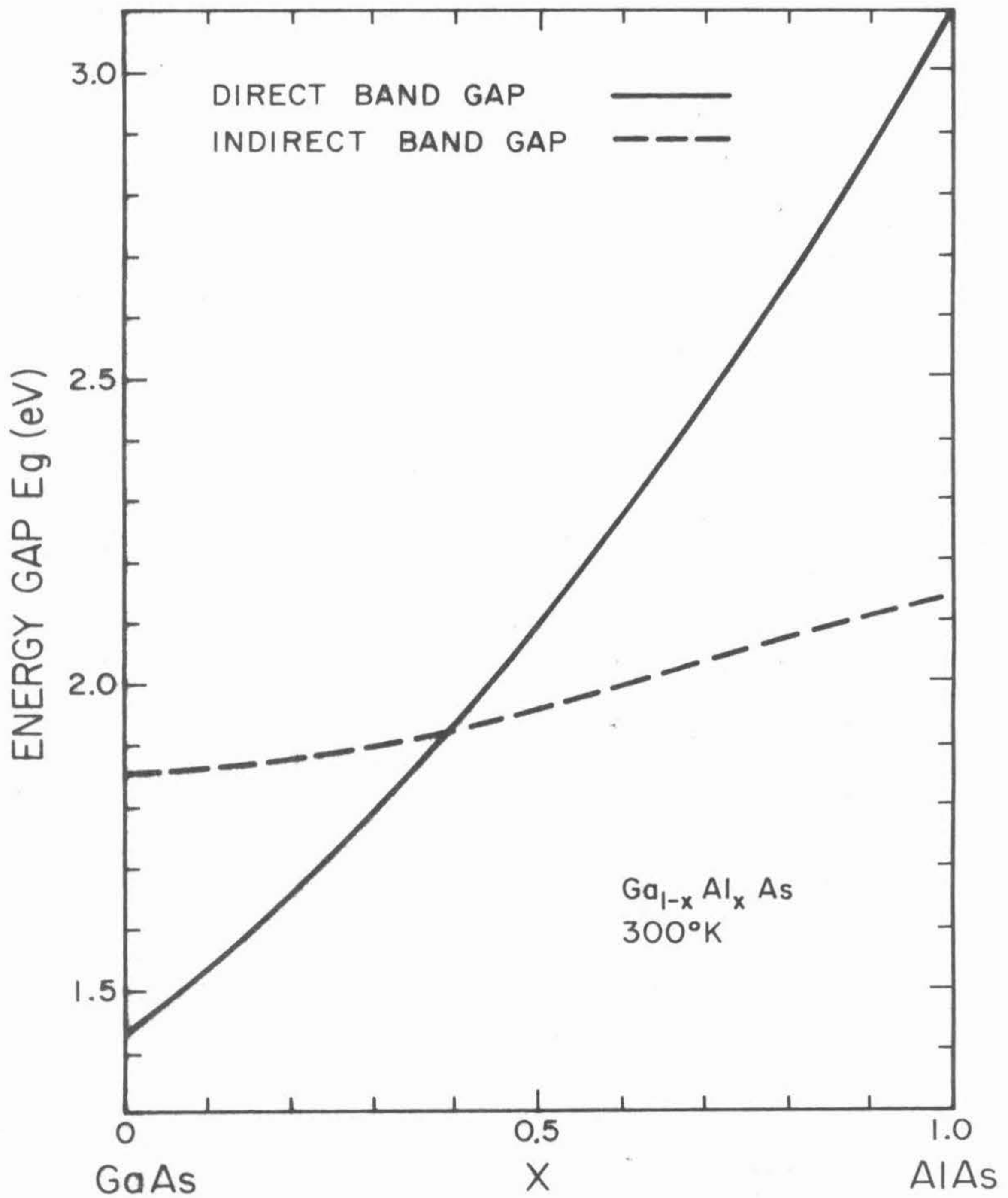

Fig. 1-2 Bandgap energy of $Ga_{1-x}Al_xAs$ versus composition.

homostructure lasers but still too high for room temperature continuous operation. Later, an improved structure, which contains two GaAs-$Ga_{1-x}Al_xAs$ heterojunctions, one on each side of the active region (GaAs), was developed. In this structure, called double heterostructure (DH), light and carriers are confined in the active region by heterojunctions on both sides. (see Fig. 1-1b) Room-temperature threshold current densities of about 1 KA/cm^2 have been achieved. Today the GaAs-$Ga_{1-x}Al_xAs$ double heterostructure laser is probably the most important light source being developed for use in optical communication systems. It was the first junction laser capable of continuous operation at room temperature with long life.

A typical structure of a double heterostructure laser is shown in Fig. 1-3. It consists of four epitaxial layers on an N type GaAs substrate. The two $Ga_{1-x}Al_xAs$ layers serve as the confining layers for the GaAs active region, which is either P or N type with a small doping concentration. Typical thicknesses of the active layer lie in the range of 0.2 - 0.3 μm. The P GaAs top layer is used to obtain better ohmic contacting since contacts on GaAlAs are poor. The mechanism of operation of this laser can be understood via the band diagram shown in Fig. 1-4. When the diode is forward biased, the electrons injected from the N $Ga_{1-x}Al_xAs$ layer are confined by the P $Ga_{1-x}Al_xAs$ potential barrier, and the holes injected from the P $Ga_{1-x}Al_xAs$ region are confined by the N $Ga_{1-x}Al_xAs$ barrier. As a result, the minority carriers are effectively trapped in the narrow bandgap active region where stimulated recombination takes place. Since the active regions are usually made much narrower than the carrier diffusion lengths, the threshold current densities,

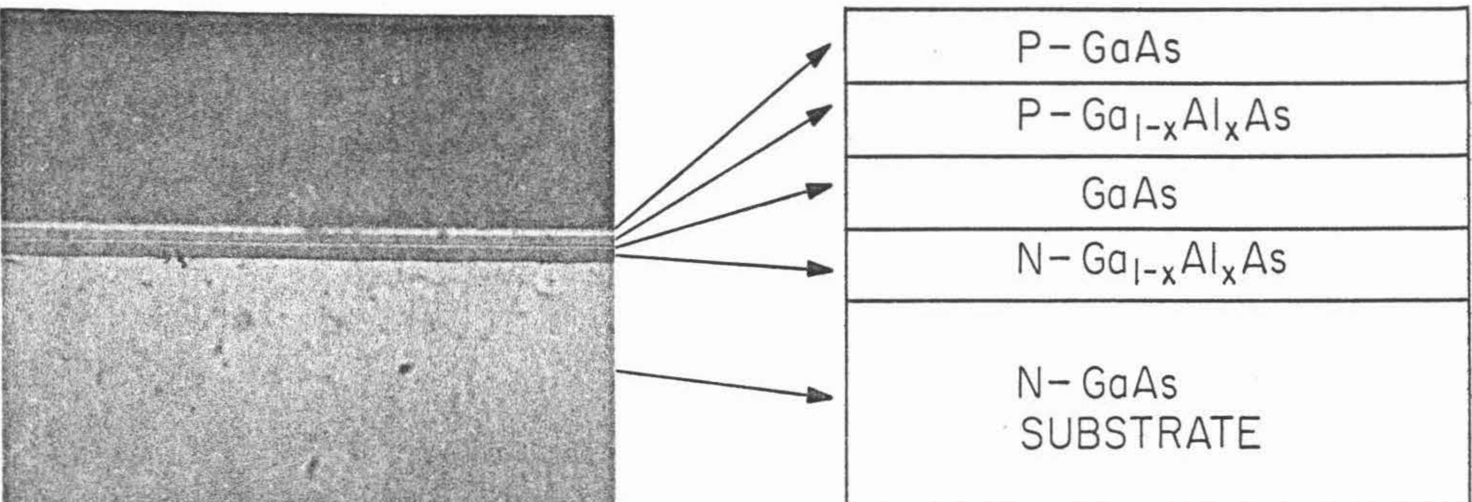

Layer	Material	Thickness (μm)	Al Content	Dopant	Carrier Concentration cm^{-3}
1	$Ga_{1-x}Al_xAs$	2.2	0.4	Sn	5×10^{17}
2	GaAs	0.3	–	–	10^{16}
3	$Ga_{1-x}Al_xAs$	1.7	0.4	Ge	5×10^{17}
4	GaAs	1.2	–	Ge	10^{18}

Fig. 1-3 The structure of a GaAs-GaAlAs double heterostructure laser and the parameters of the layers.

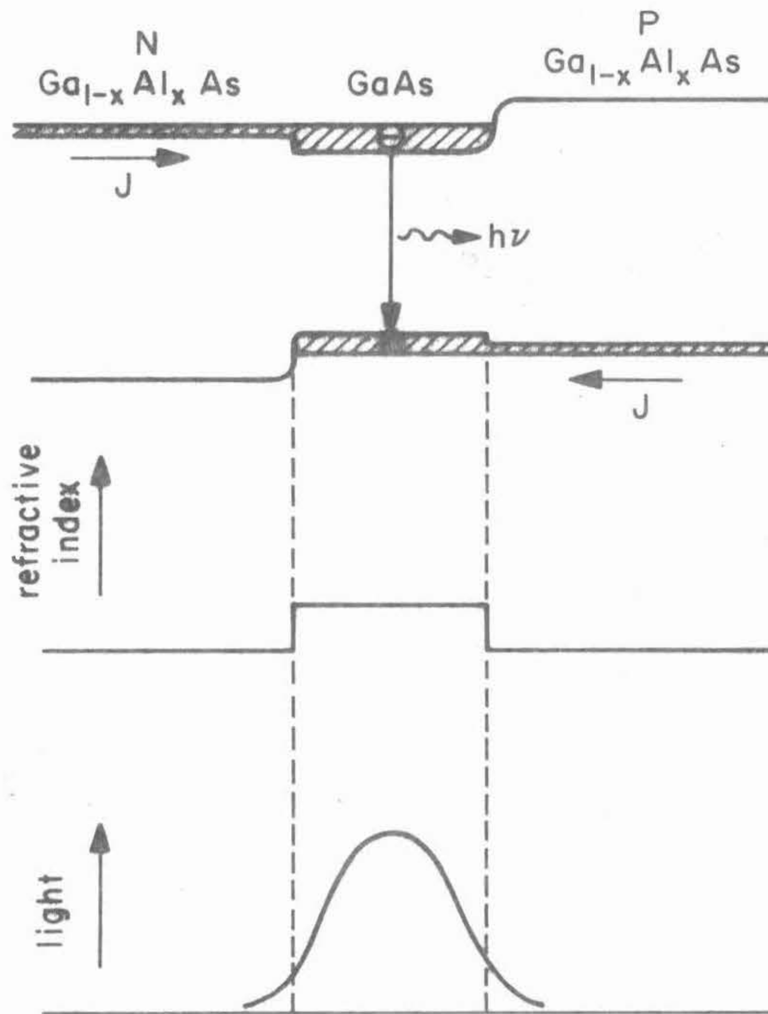

Fig. 1-4 Schematic representation of the band edges with forward bias, refractive index changes and optical field distribution of a double-heterostructure laser diode.

which are proportioal to the volume of the active regions, are much lower than those which can be achieved with homostructure or single heterostructure lasers. This reduction in threshold also benefits from better coupling of the optical field to the active region compared to the other two structures described above. This is due to the fact that the $Ga_{1-x}Al_xAs$ confining layers have a lower index of refraction than the GaAs active layer.

I.3 Outline of the Thesis

Three subjects will be discussed in the following chapters. All three deal with GaAs-GaAlAs laser devices although they have implications to other semiconductor devices.

Chapter II describes a new epitaxial growth technique called "Embedded Epitaxy". This technique involves selective multilayer epitaxial growth of GaAs-$Ga_{1-x}Al_xAs$ through stripe openings in masking layers on GaAs substrates. The growth habit (structure) has features which are favorable to the fabrication of stripe geometry lasers, waveguides and integrated optics components which require planar definition. We shall describe this growth habit and its dependence on the orientation of the stripe openings. Stripe geometry embedded lasers fabricated using this technique will be described and their characteristics discussed.

In chapter III we shall describe a GaAs-GaAlAs heterostructure PNPN laser diode which is capable of having high breakover voltage and low lasing threshold current at the same time. The concept of using $Ga_{1-y}Al_yAs$ potential barrier to control the carrier transport in the device is introduced. Analysis of this barrier-controlled device will be given

and the numerical results presented. Experimental results of devices with no barrier, one barrier and two barriers will be presented, and the effects of the barriers on the devices' electrical and optical characteristics discussed.

Chapter IV is concerned with a totally new field of research in integrated optics - the fabrication of GaAs-GaAlAs injection lasers on semi-insulating substrates and the integration of these lasers with other electronic devices. We shall describe two kinds of lasers, which have been demonstrated, and the working principles underlying them. The fabrication procedures will be given and the experimental results discussed. Zinc diffusion in $Ga_{1-x}Al_xAs$, a technique which we found very useful in the fabrication of these lasers, will be described; its dependence on the Al content x will be discussed. Gain induced guiding, which explains some of the interesting behavior of our lasers, will be introduced and analyzed. The integration of these lasers with other electronic devices occupies the last section of this chapter. The first demonstrated integrated device, a crowding effect laser and a Gunn oscillator integrated on a single semi-insulating GaAs substrate, will be described; other integration schemes are suggested and will be discussed.

Chapter V describes in some detail the experimental techniques which have been used in this research, including: liquid phase epitaxial growth, laser fabrication, and device characterization.

REFERENCES FOR CHAPTER I

(1) N. Niizeki, "Single mode fiber at zero-dispersion wavelength", Topical Meeting on Integrated and Guided Wave Optics, Salt Lake City, 1978, Paper MB-1

(2) P. K. Tien, "Integrated optics and new wave phenomena in optical waveguides", Rev. Mod. Phys. 49, 361 (1977)

(3) A. Yariv, "Active integrated optics", in Fundamental and Applied Laser Physics, Proc. of the 1977 Esfanhan Symposium, John Wiley & Sons, New York (1973)

(4) V. Evtuhov and A. Yariv, "GaAs and GaAlAs devices for integrated optics", IEEE J. Trans. Microwave Theory Tech. 23, 44 (1975)

(5) A. Yariv and M. Nakamura, "Periodic structures for integrated optics", IEEE J. Quantum Electron. QE-9,233 (1977)

(6) C. E. Hurwitz, J. A. Rossi, J. J. Hsieh, and C. M. Wolfe, "Integrated GaAs-GaAlAs double-heterostructure lasers", Appl. Phys. Lett. 27, 241 (1975)

(7) D. W. Bellavance and J. C. Campbell, "Room temperature mesa lasers grown by selective liquid phase epitaxy", Appl. Phys. Lett. 29, 162 (1976)

(8) C. P. Lee, S. Margalit, and A. Yariv, "GaAs-GaAlAs heterostructure lasers on semi-insulating substrates",to be published in IEEE Trans. Electron Device (1978)

(9) N. G. Basov, O. N. Krokhin, and Y. M. Popov, "Production of negative-temperature states in PN junctions of degenerate semiconductors", Pis'ma Zh. Eksp. Theor. Fiz. 40, 1879 (1961)

(10) R. N. Hall, G. E. Fenner, J. D. Kingsley, T. J. Soltys, and R. O. Carlson, "Coherent light emission from GaAs junctions", Phys. Rev. Lett. 9, 366 (1962)

M. I. Nathan, W. P. Dumke, G. Burns, F. N. Dill, and G. J. Lasher, "Stimulated emission of radiation from GaAs PN junctions", Appl. Phys. Lett. 1, 62 (1962)

(11) H. Kroemer, "A proposed class of heterojunction lasers", Proc. IEEE, 51, 1782 (1963)

(12) Zh. I. Alferov and R. F. Kazarinov, Author certificate 1032155 /26-25, USSR (1963)

(13) H. Rupperecht, J. M. Woodall, and D. G. Pettit, "Efficient visible electroluminescence at $300^{\circ}K$ from $Ga_{1-x}Al_xAs$ PN junctions grown by liquid phase epitaxy", Appl. Phys. Lett. 11, 81 (1967)

(14) Zh. I. Alferov, V. M. Andreev, V. I. Korol'kov, E. L. Portnoi, and D. N. Tret'yakov, "Injection properties of $n\text{-}Al_xGa_{1-x}As$ - p-GaAs hererojunctions", Sov. Phys. Semicond. 2, 843 (1969)

(15) I. Hayashi, M. B. Panish, and P. W. Foy, " A low threshold room-temperature injection laser", IEEE J. Quantum Electron. QE-5, 211 (1969)

(16) H. Kressel and H. Nelson, "Close confinement GaAs PN junction lasers with reduced optical loss at room temperature", RCA Rev. 30,106 (1969)

CHAPTER II

GaAs-GaAlAs EMBEDDED HETEROSTRUCTURE EPITAXY AND EMBEDDED LASERS

II.1 Introduction

GaAs-GaAlAs laser epilayers are usually grown uniformly over the GaAs substrate. The area of the substrate is about 1 cm^2. This area, however, is too large for a single ordinary optical or electronic device. In an integrated optical circuit each component has dimensions of the order of 10 μm on each side and demands high quality edge smoothness and high resolution pattern formation. Two dimensional definition, therefore, is very important in the fabrication of monolithic integrated optical circuits. Conventional thin-film definition techniques such as mesa etching(1), selective diffusion(2), ion beam machining(3), proton bombardment(4), etc. have been used for this purpose. Optical and electronic devices, which are made by these methods, include stripe geometry lasers, waveguides, detectors, distributed feedback lasers, etc(5). However all these methods are independent of the epitaxial growth. They are usually applied after the layers are prepared. It is impossible to eliminate the possibilities of damage to the crystal during the fabrication steps. The best way to overcome this problem is to develop techniques in the growth of high quality epitaxial layers as well as the transverse definition and,at the same time, these layers are shaped into appropriate configurations to perform their specific functions. In this chapter we describe a new technique of liquid phase epitaxy which fulfills these requirements. The GaAs-GaAsAs multilayers are grown selectively on window openings

defined by masking layers which cover the GaAs substrate. The positions of the active devices are thus defined by the windows in the masks.

The masks have the desirable property that no growth takes place on them and they are stable at the growth temperatures. The structure of the crystal grown in the window areas depends on the orientation of the windows and terminates with as-grown crystal faces. Smooth and mirror-like surfaces are usually observed on the three-dimensional crystal structure. Detailed description of the growth procedure and the crystal structure is given in section II.2.

Four-layer GaAs-GaAlAs double heterostructures grown selectively through thin stripe openings in the masks are suitable for stripe geometry lasers. The resulting structure has prismatic layers of GaAs and GaAlAs embedded in each other and the GaAs active layer can be grown in such a way that it is totally surrounded by the GaAlAs low index confining layers. We thus use the term "embedded epitaxy" for this growth technique. Lasers with very low threshold current densities have been fabricated using this technique. The details are given in section II.3.

Embedded epitaxy is useful not only for laser fabrication but also as an attractive method for fabricating other optical and electronic devices which require planar definition. For future applications it may be useful in fabricating monolithic integrated optical circuits which consists of various electro-optical components on a single chip of GaAs. Using this technique one is able to make the monolithic circuits by a single step epitaxial growth instead of processing the sample after the growth.

II.2 Embedded Epitaxy

As described in the introduction to this chapter, embedded epitaxy is an attractive method for two-dimensional thin-film definition. This is especially true for GaAs-GaAlAs heterostructure devices which require several epitaxial layers. A unique feature of this technique is that it results in three-dimensional structure with as-grown crystal faces instead of a two-dimensional planar structure.

The first selective epitaxial growth of GaAs was reported by F. W. Tausch et al. in 1965[(6)]. They used vapor phase epitaxial growth technique to deposit a layer of GaAs onto the substrate only in certain areas which are exposed by windows in SiO_2 film. Later on, D. W. Shaw extended the technique to include selective deposition in holes etched into GaAs substrates[(7)]. Their efforts were directed to the investigation of the layer crystallography and surface morphology. Selective liquid phase epitaxy was reported by T. Kawakami et al. in 1973[(8)]. One layer of $Ga_{1-x}Al_xAs$ ($0 \leq x \leq 0.9$) was grown on stripe-shaped windows on Al_2O_3 masked GaAs substrates, and the dependence of the growth morphology on the Al content was studied. All these experiments, however, involve only one layer growth, which is not enough for most of the electro-optical devices that require multilayers. The first successful selective liquid phase epitaxy of GaAs-GaAlAs heterostructures-embedded epitaxy- was accomplished by us[(9)]. The structure of the grown layers is controllable, and growth on very narrow stripe openings (~15 μm) has been achieved.

II.2.1 Fabrication procedure

The substrates used in our experiments are [100]-oriented polished GaAs wafers with (N type) Si doping $n = 3x10^{18}cm^{-3}$. The wafers were cleaved into rectangles with areas 15mm x 8mm at two perpendicular cleavage planes (011) and (01$\bar{1}$). Following cleaning,the substrates were etched slightly with $H_2SO_4:H_2O_2:H_2O$ (4:1:1), masking layers were deposited or grown on the wafers. We have used Al_2O_3 and $Ga_{0.4}Al_{0.6}As$ as the masks for growth. SiO_2 masks used previously for single layer GaAs growth are probably not suitable for the growth of GaAlAs because the aluminum in the melt may react with the silicon oxide. We found sputtered Al_2O_3 masks stable and adhering throughout the multilayer growing processes. The sputtered layer is about 3000Å thick and can be easily etched away using hot phosphoric acid (80^oC). Very smoothly edged openings can be formed in the oxide. Another mask used extensively by us is $Ga_{1-x}Al_xAs$ with Al content x = 0.6. Because of aluminum, $Ga_{0.4}Al_{0.6}As$ is chemically very active and is oxidized when exposed to air. The oxidized surface rejects wetting between the Ga solution and the substrate, and therefore, no epitaxial growth can take place on top of it. This layer is prepared by epitaxial growth and can be etched away using standard etchants for GaAs like $H_2SO_4:H_2O_2:H_2O$ (4:1:1), Br-methanol or selective etchants, which do not attack GaAs, like HF, KI, etc.

Windows in the masking layers were formed using standard photo-lithographic techniques. The masks in the window areas have to be completely removed because growth can not take place even when a very thin masking layer remains. The wafers were cleaned and briefly etched

in $H_2SO_4:H_2O_2:H_2O$ (4:1:1) immediately before they were transfered to the growth system. (Our system is the standard horizontal sliding boat system. Details of the growth procedures are described in chapter V.) The temperature was set at 818°C before the start of the growth. Typical cooling rates used were 0.04^{o}/min - 0.1^{o}/min. These values are much lower than those we usually use for growth on unmasked wafers. This is due to our finding that the rate of growth through small openings is much faster than that on unmasked wafers, and the bigger the windows the thinner are the grown layers. This feature can be explained as follows: The total amount of growth on a substrate is determined by the amount of excess supersaturated GaAs or GaAlAs in the solution, and this value is controlled by the cooling rate and is independent of the size of the windows[8]. Consequently the rate of growth increases as the area available for growth is smaller. In order to have good control of the layer thickness and the growth structure one has to use very small cooling rates so that the growth rate can be lowered. An example of the cooling cycle for a four-layer double heterostructure embedded epitaxial growth is shown in Fig. 2-1. The mask was Al_2O_3 and the windows were 25μm wide stripes oriented in the [110] direction with a separation of 250μm between neighboring stripes. The cross section of the structure grown is shown in the upper half of Fig. 2-1. The cooling rate was chosen to be 0.04^{o}/min. The rate of growth was about ten times higher than that of the ordinary planar growth. During the entire cooling cycle the temperature cooled was almost an order of magnitude less than that used for growth on unmasked wafers.

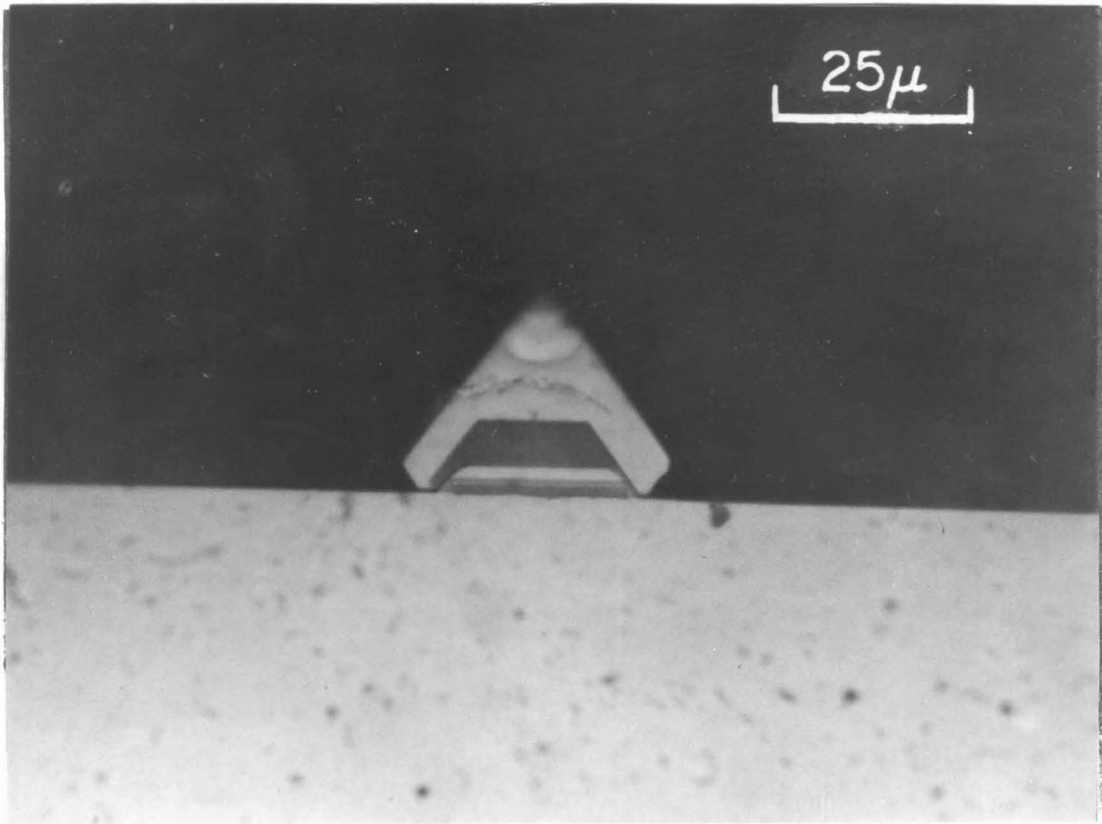

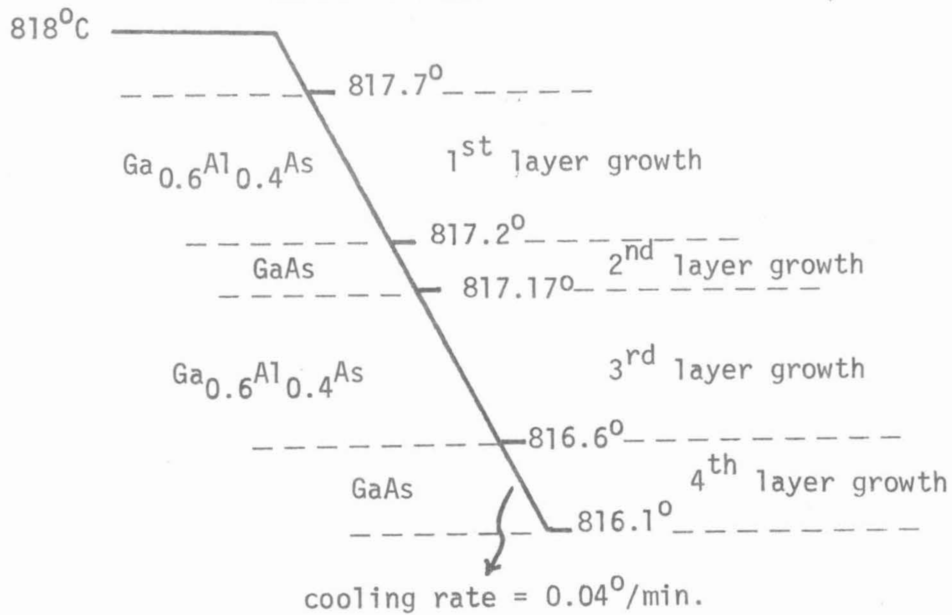

Fig. 2-1 A photomicrograph of the cross section of a four-layer embedded growth and it's cooling cycle during the growth.

II.2.2 Growth structure

Ordinary epitaxial growth is performed on unmasked wafers and results in uniform planar epilayers which are parallel to the surface of the substrate. In selective epitaxy, the growth is limited to certain small areas which are exposed by windows in a protective mask. The resulting growth in the windows has a three-dimensional structure instead of two-dimensional planar layers. The structure depends on the shape and the orientation of the windows and thus tell us the growth habit.

In our experiments we studied the growth through stripe-shaped windows, because our interests were mainly in the fabrication of stripe geometry lasers and waveguides. A series of stripe openings of widths ranging from 5μm to 25μm were defined in the masking layer on GaAs substrates with surfaces oriented in [100] direction. On some of the wafers the stripes were opened parallel to the [011] crystal cleavage plane, and on others stripes were oriented in [001] direction which is oriented at 45° to the [011] direction. The growth was carried out as described in the previous section. The nature of the growth on these two types of stripes are very different[10].

Fig. 2-2a is a scanning electron microscope (SEM) picture of the growth which took place on a [011] oriented stripe window opened in the Al_2O_3 mask. The growth was limited to the stripe opening of 25μm wide, and no growth was observed on the oxide away from the window. As the picture shows it is a three-dimensional trapezoid structure terminated at three crystal faces. The top face is parallel to the substrate (100) surface. The two side walls form an angle about 55°

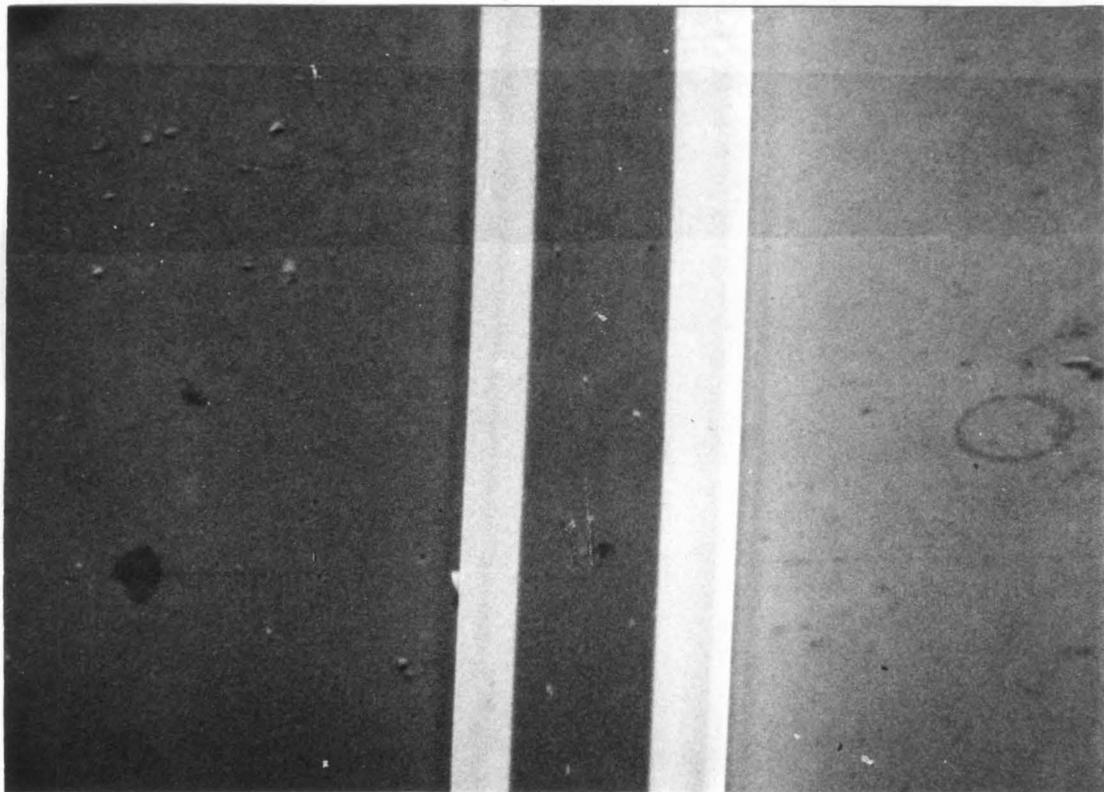

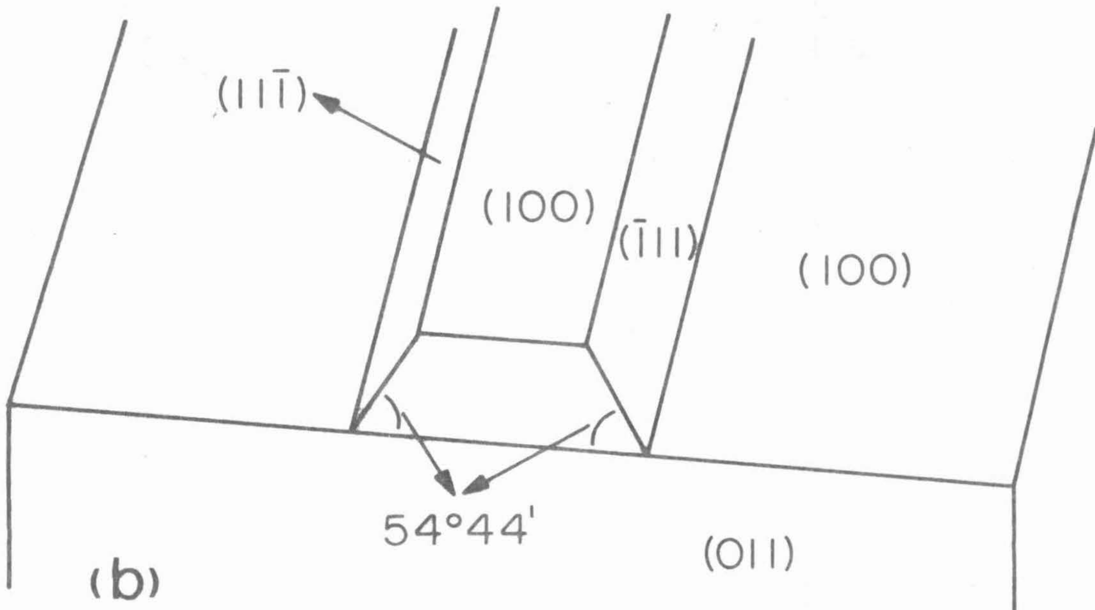

Fig. 2-2 (a) An SEM micrograph of an embedded growth on a [011] oriented stripe window opened in an Al_2O_3 mask. (b) The growth structure and the orientation of the crystal faces.

with the (100) face. This identifies them as (111) surfaces which ideally form an angle of $54^{o}44'$ with the (100) face. Fig. 2-2b is a schematic drawing of the structure showing the orientation of each face. The cross section of the growth is shown in Fig. 2-3. It is a four-layer double heterostructure. The layers were revealed using $HF:HNO_3:H_2O$ (1:3:4) staining solution. The first and the third layers are $Ga_{0.6}Al_{0.4}As$ (dark layers in the figure). The second and the fourth layers are GaAs (white layers in the figure). The resulting structure consists of prisms which are embedded epitaxially in outer crystalline layers of similar material. An interesting feature of the structure is that the second layer (GaAs) is totally surrounded by $Ga_{0.6}Al_{0.4}As$. No growth of GaAs was observed on the side faces of the first $Ga_{0.6}Al_{0.4}As$ layer. We found that this is true as long as this layer is very thin or the growth time of this layer is very short. This fact indicates that the selective growth of GaAs probably starts on the GaAlAs (100) faces, and later proceeds to the (111) faces.

In a regular double heterostructure laser the thin GaAs layer sandwiched between the GaAlAs layers is the lasing active region. The neighboring GaAlAs layers provide the electrical and the optical confinement for the carriers and the laser light. In our embedded structure the GaAs active layer is not only sandwiched between the GaAlAs layers in the direction perpendicular to the substrate surface but is also surrounded by them in the transverse direction. This structure thus has electrical and optical confinements on all sides of the active region, and is suitable for the fabrication of stripe geometry lasers with very defined optical modes.

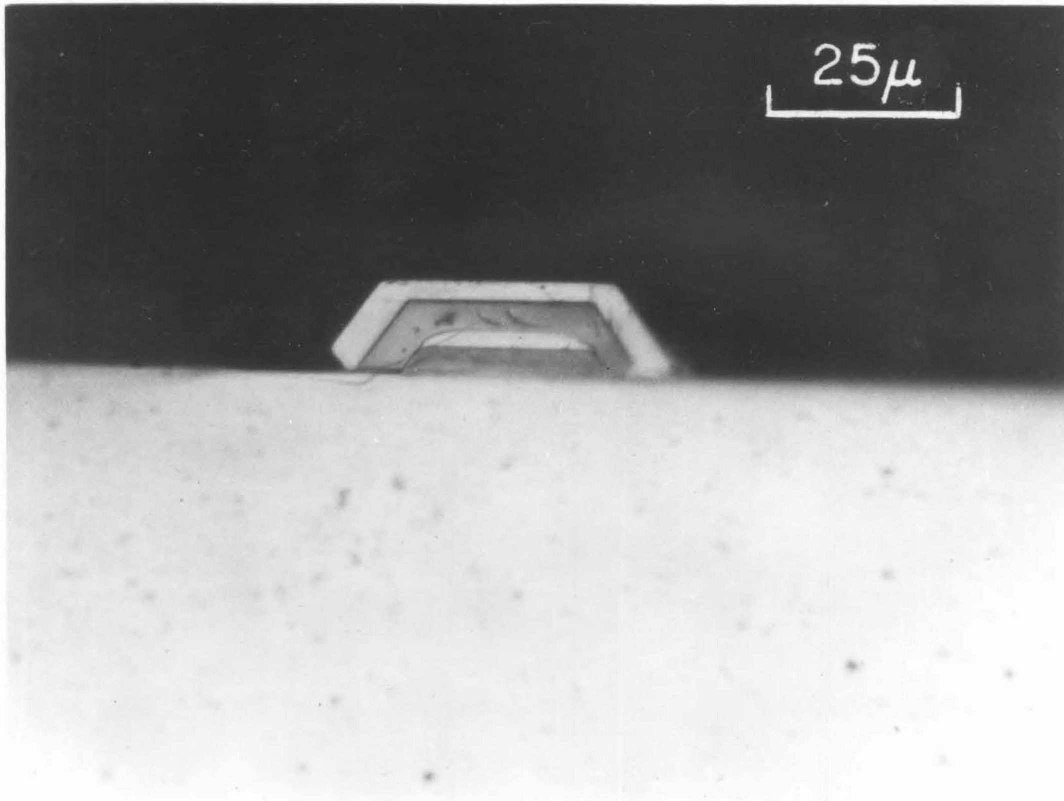

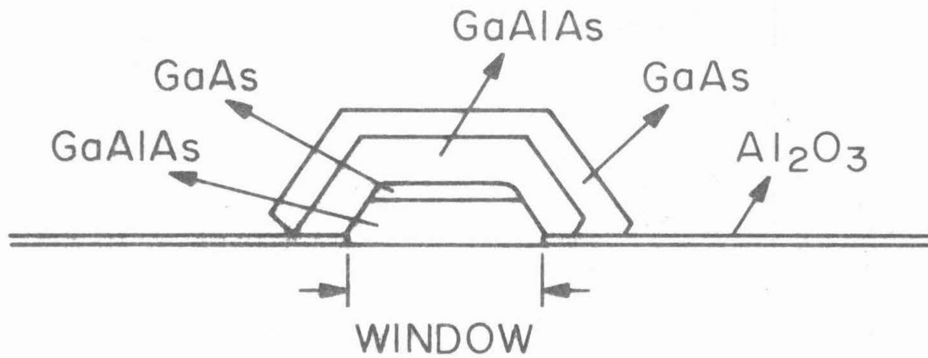

Fig. 2-3 The cross section of a double-heterostructure embedded growth on a [011] oriented stripe opening.

The growth taking place on the stripe openings oriented in the [001] direction, which is 45° to the crystal cleavage plane, has a different structure. Figure 2-4 is a scanning electron microscope picture of the growth. It is no longer trapezoidal, but rectangular. The top surface is (100). The side faces are perpendicular to the surface of the substrate which identifies them as (010) and ($0\bar{1}0$) crystal faces. Figure 2-4b shows schematically the orientation of the growth surfaces. The cleavage planes of the crystal in this case are not perpendicular to the stripes. It is, therefore, difficult to cut the sample at 90° with respect to the stripes. In order to see the cross section of the growth one has to cleave the sample at one of the cleavage planes oriented at 45° with respect to the direction of the stripes. Figure 2-5a,b consists of two photographs of the cross sections of two growths. The faces shown in the figure are (011) cleavage planes. The real cross sections should have lateral dimensions smaller than those shown in the figure by a factor of cos 45°(= $1/\sqrt{2}$).

Both of the growths shown in Fig. 2-5 are four-layer double-heterostructures. The first and the third layer are $Ga_{0.6}Al_{0.4}As$, and the second and the fourth layers are GaAs. The inner layers are surrounded by the outer layers. The widths of the stripe windows are 8 μm and 18 μm for Fig. 2-5a and Fig. 2-5b, respectively. As shown in the pictures, the growth extends from the window areas to the oxide and is much wider than the openings. This overgrowth is much bigger than that of the growth on stripes oriented in the [011] direction.

The resulting structures of the embedded epitaxy are usually very uniform. Since the faces of the growths are crystal planes, they are

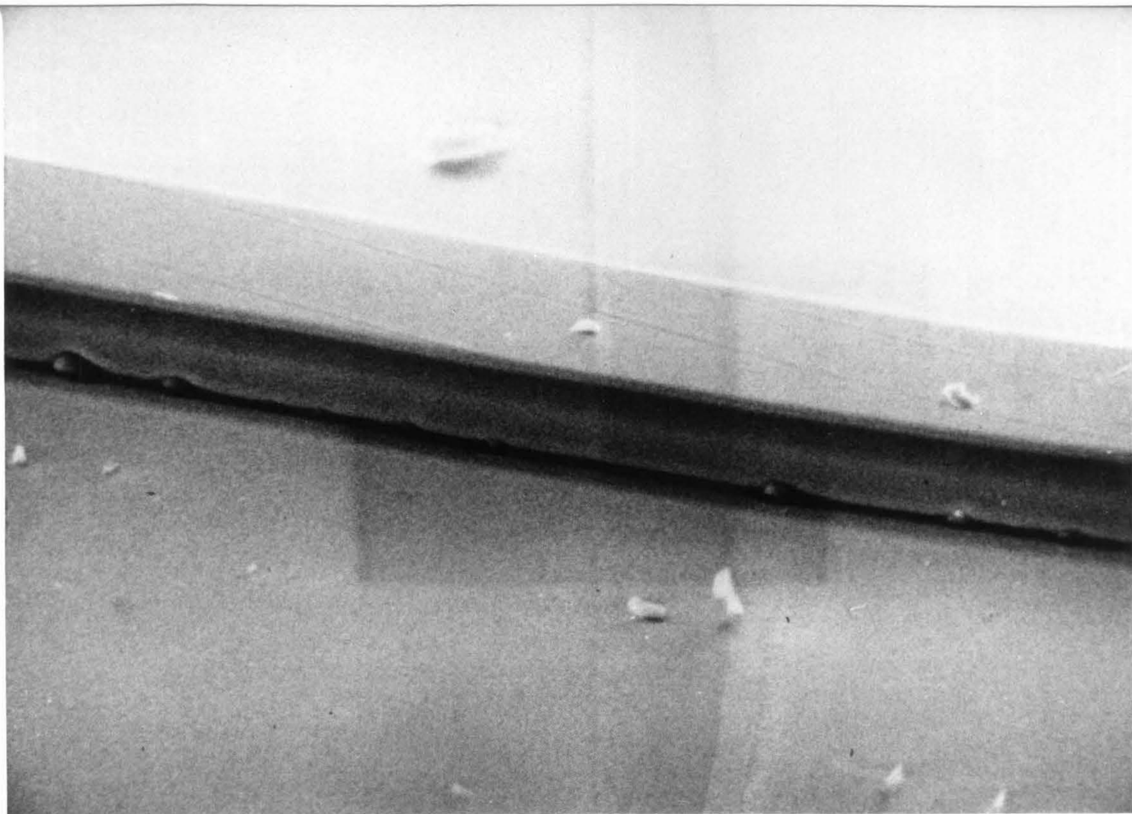

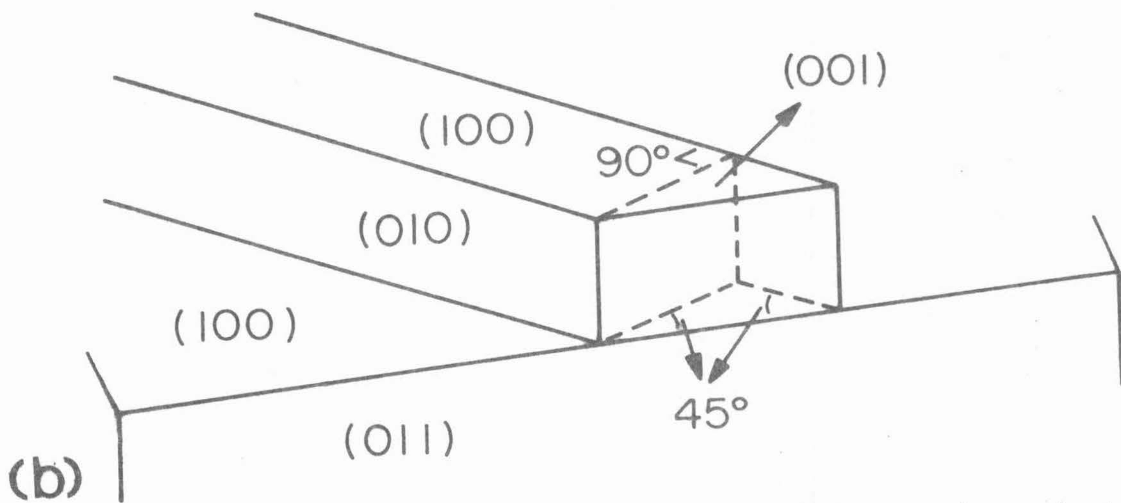

Fig. 2-4 (a) An embedded growth grown through a stripe opening oriented in the [001] direction. (b) The growth structure and the orientations of the crystal faces.

Fig. 2-5 The cross sections of two embedded double hetero-structures grown through [001] oriented stripe openings with widths of (a) 8 μm, and (b) 18 μm.

(a)

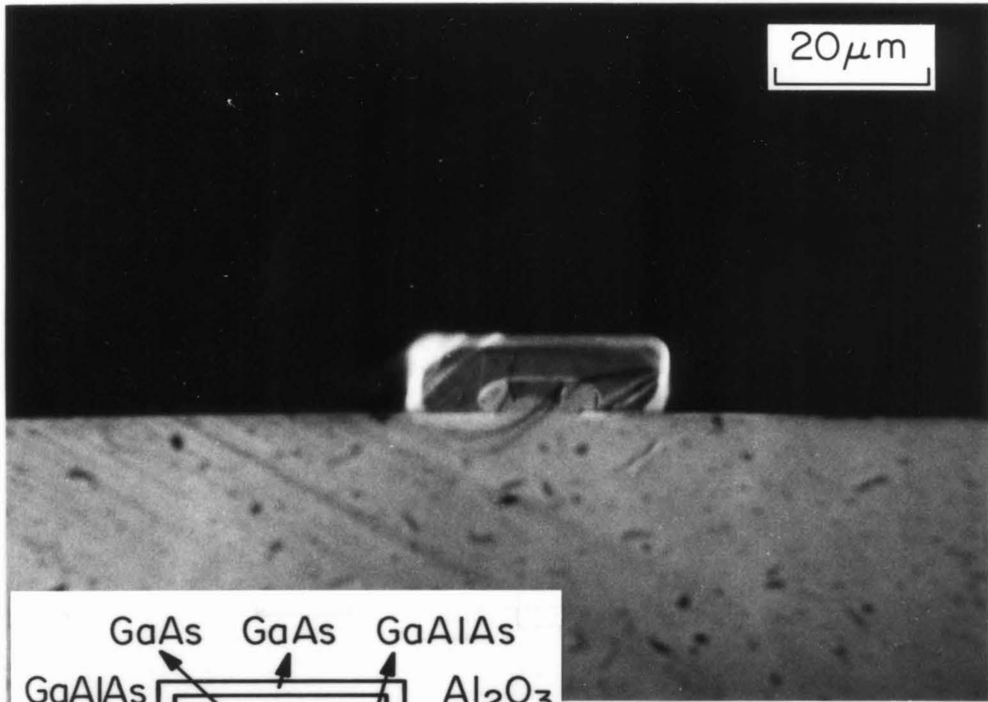

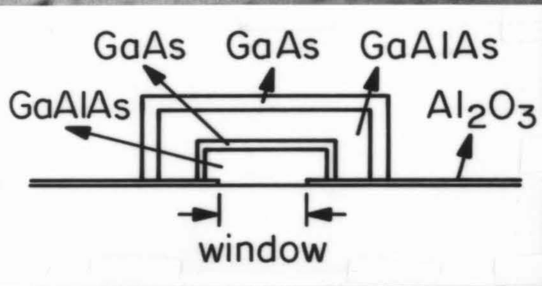

(b)

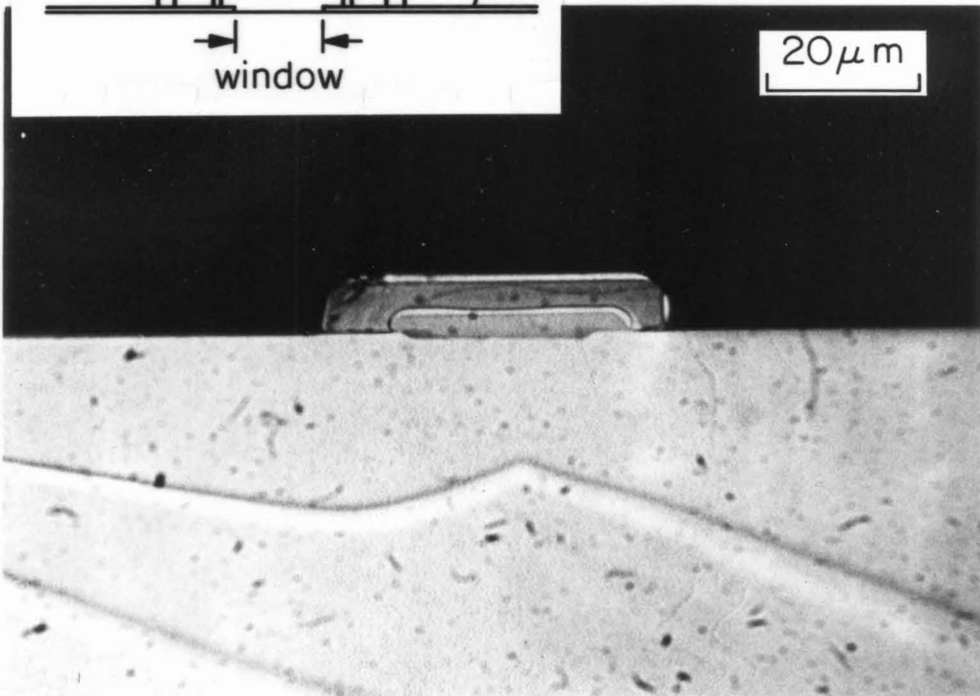

smooth and mirror-like. Figure 2-6a,b consists of two pictures of the top view of a sample before and after the growth. The stripe-shaped windows opened in Al_2O_3 masking layer are 15 μm wide and oriented in the [001] direction. After the growth, the stripe openings are filled with crystal, and no growth is found on the oxide away from the windows. As the picture shows the growth is extremely uniform along the stripes.

II.3 Embedded Heterostructure Lasers

As discussed in the previous chapter, GaAs-GaAlAs heterostructures lead to laser performance which is superior to that obtained with homostructures. This is due to the thin active region which incorporates both optical and carrier confinement. However, in conventional lasers this is true only for the direction perpendicular to the junction plane. In the lateral direction the laser cavity is usually defined by two sawed faces and has a width of about 100 μm. Lasers fabricated in this way have broad active regions, and the threshold currents are usually higher than 1A. The lasing action in these broad area lasers is usually non-uniform along the active region in the transverse direction. The light is generated in several small regions or "filaments", bright spots as viewed at the laser mirror, instead of uniformly in the active region.[11] The filaments are randomly and unpredictably distributed and tend to be unstable as the driving current increases. This non-uniform behavior is due at least partly to the nonuniformities in geometry, current flow, doping, and material quality, etc. In order to reduce the number of filaments, or possibly to get single filament, and uniform light distribution in the active region, one has to reduce the lateral dimension of

Fig. 2-6 The top-view photographs of a sample (a) before and (b) after the selective growth. The mask is Al_2O_3. The stripe openings are 15 μm wide and oriented in the [001] direction.

(a)

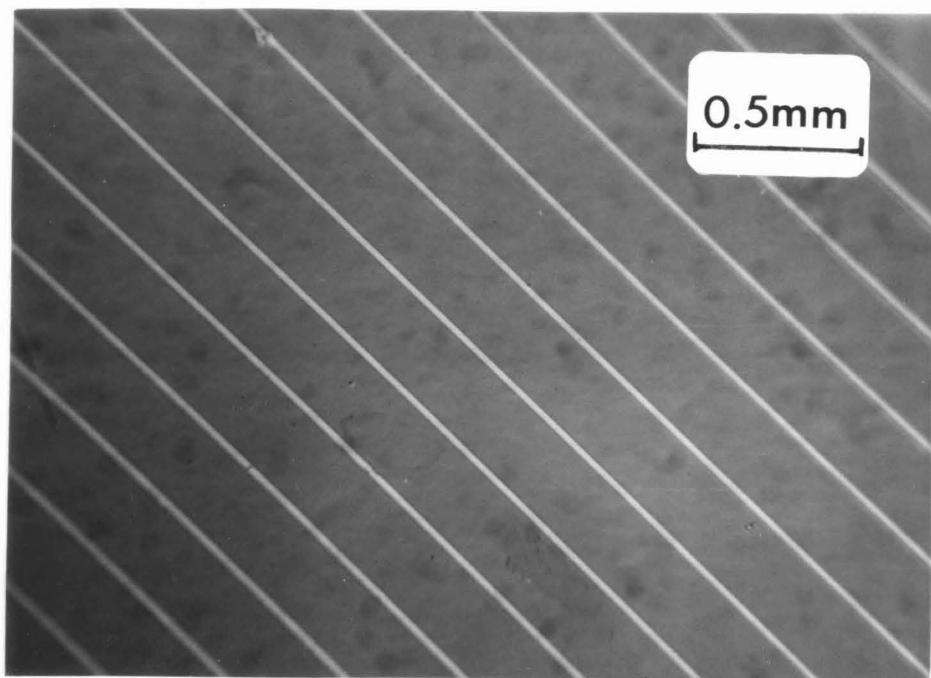

(b)

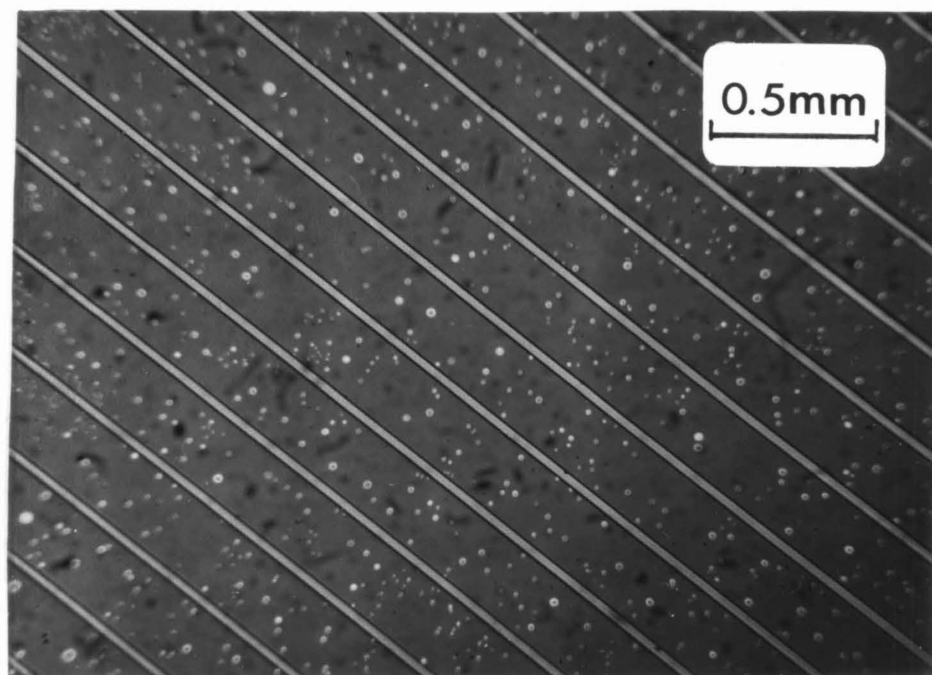

the laser cavity and restrict the current flow to a narrow stripe. Lasers with this current confinement are called stripe geometry lasers. They require less current because the current at threshold is proportional to the active area. Various techniques have been used to fabricate the stripe-geometry lasers. In these lasers the current injection is limited to a rectangular region (the stripe) with a width in the range of 5-30 μm. They have threshold currents much lower than those of broad area lasers and have controllable transverse modes. However, the threshold current densities, defined as the ratio of the threshold current and the area of current injection,of most of these stripe-geometry lasers are higher than those of broad area lasers, because of the lack of good electrical and optical confinement in the transverse direction.

As described in the previous section, embedded epitaxy is suitable for the fabrication of stripe geometry lasers. The embedded structure, as the one shown in Fig. 2-3, has the second layer (GaAs) totally surrounded by the GaAlAs layers. Since GaAlAs has a wider bandgap and a lower refractive index than GaAs, both carriers and optical field can be confined in this GaAs active region. This confinement, which is on all sides of the GaAs layer, enables the embedded-structure lasers to lase at threshold current densities lower than most of the conventional stripe-geometry lasers.

The first embedded lasers were achieved by growing selectively four-layer double heterostructures on 25 μm wide stripes opened in Al_2O_3 mask.(12) They had room temperature threshold current densities of about 5 kA/cm^2. This value is higher than that obtained from broad area lasers. The reason for this relatively high current was excessive

leakage current passing through the two corners of the trapezoidal-shaped growth, where the P GaAlAs layer touches the N GaAs substrate. We have solved this problem by using a different technique to prepare the masks. The mask consists of two layers, P GaAs and N GaAlAs. The top GaAlAs layer serves as a mask for growth, and the combination of these two serves as a barrier for the current. The lasers fabricated in this way did not have the current leakage problem, and had a room temperature threshold current density of 1.5 kA/cm^2,[13] which is considerably lower than those of the conventional stripe geometry lasers.

The fabrication procedure of the embedded laser grown through a GaAs-GaAlAs mask is shown in Fig. 2-7. Two layers: a 3 μm P GaAs (M1, Ge doped) and a 1.4 μm N $Ga_{0.4}Al_{0.6}As$ (M2, Sn doped) were grown on top of a (100) N type GaAs substrate as shown. A series of 25 μm wide stripe windows were next opened in the layers using standard photolithographic techniques. The stripes were parallel to the [011] direction and the etching solution $H_2SO_4:H_2O_2:H_2O$ (5:1:1) was used to eliminate completely the epitaxially grown layers from the window areas so that the bottom of the etched channels consisted of the N GaAs substrate. A top view of the sample at this stage is shown in Fig. 2-8a.

After etching, the sample was placed back in the growth system and a four-layer double heterostructure was grown through the windows. The top view picture of the sample after this growth is shown in Fig. 2-8b. The growth took place inside the etched channels with no growth on the surface of the masking layer away from the windows. The layer composition is as follows: (S1) N-(Sn doped) $Ga_{0.6}Al_{0.4}As$ 7 μm thick, (S2) P-(Ge doped) GaAs active layer ∿ 0.2 μm thick, (S3) P-(Ge doped)

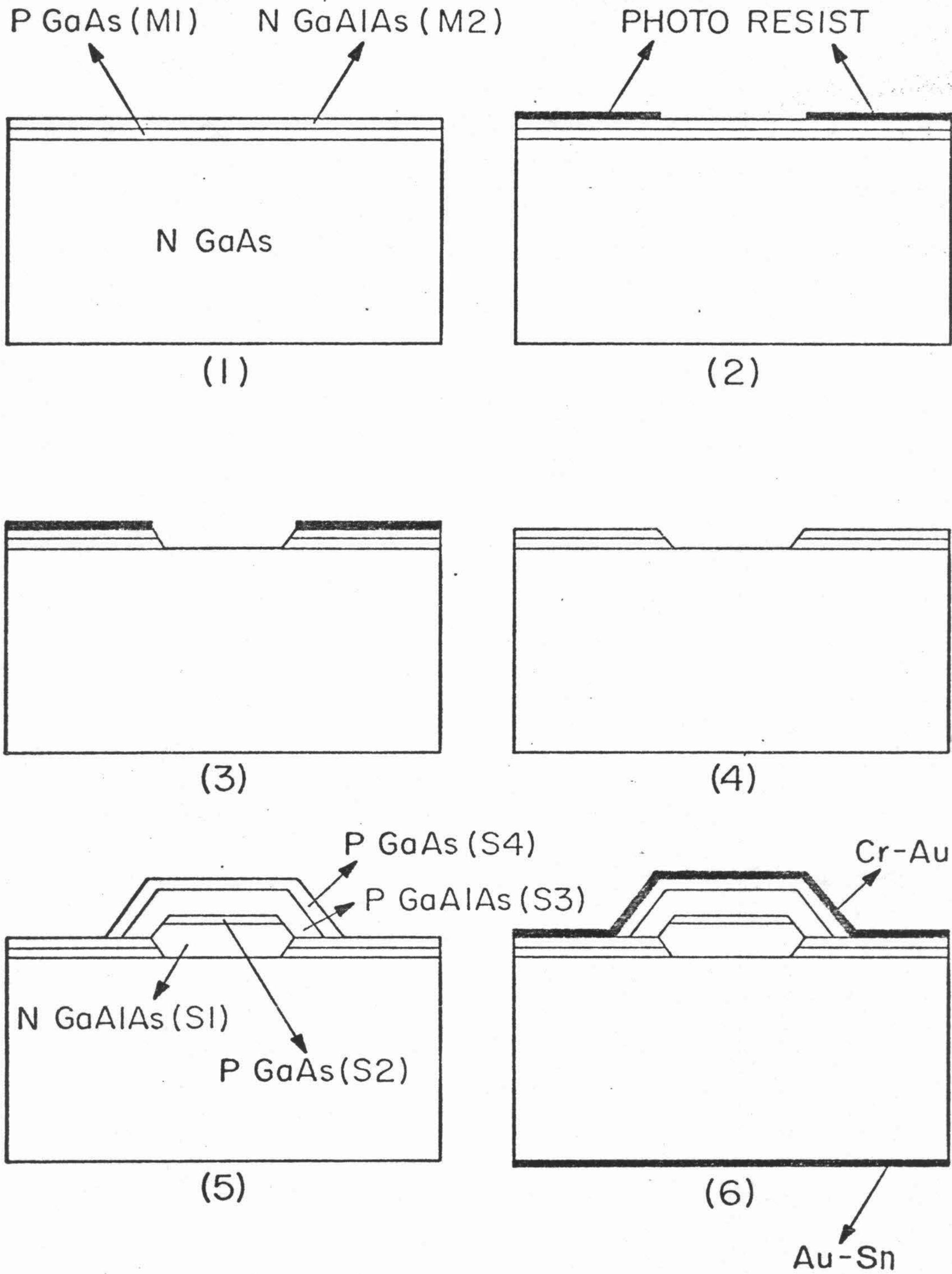

Fig. 2-7 Fabrication steps of an embedded laser: (1) masking layer growth, (2) photoresist stripe defining, (3) etching, (4) photoresist removal , (5) embedded growth, (6) metalization.

Fig. 2-8 The top-view photographs of a sample (a) before and (b) after the embedded growth. The mask for growth is GaAlAs-GaAs. (a) corresponds to step (4) in Fig. 2-7, and (b) corresponds to step (5).

Stripe Openings

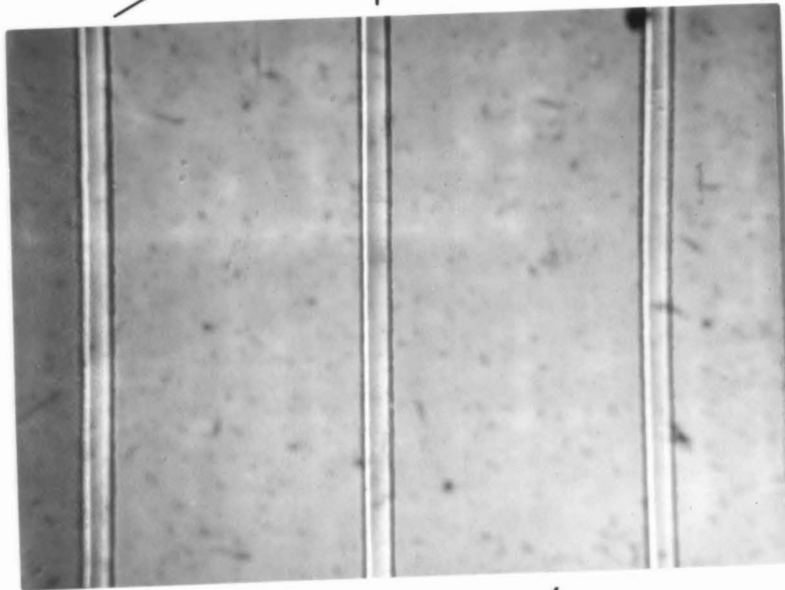
(a)

GaAlAs Mask
100 μm

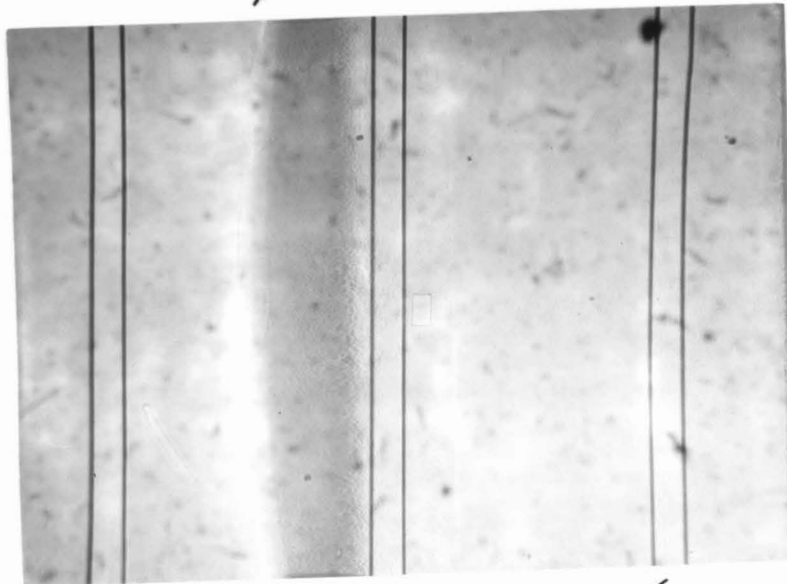
(b)
Embedded Growth

$Ga_{0.6}Al_{0.4}As$ layer 8 μm thick, (S4) P^{+}-(Ge doped) GaAs contact layer 0.5 μm thick. A photograph of the cross section of the resulting structure is shown in Fig. 2-9. During the growth a cooling rate of 0.1°/min was used in growing the mask, while the embedded double heterostructure was grown using a rate of 0.05°/min. The slower cooling rate in growing through the mask is necessitated by the faster growth rate in this case.

Ohmic contacts were applied using evaporation of Cr-Au on the P side and Au-Sn electrodeless plating and alloying to the N side. The wafer was cleaved normal to the stripes' direction into bars 550 μm wide to form the Fabry-Perot laser resonators, and separated into individual lasers by cleaving between the stripes. The individual lasers were mounted in indium-plated copper heat sinks.

The reason for the layer sequence used in this laser can be understood by referring to Fig. 2-10. Under forward biasing conditions of the laser in the stripe (positive voltage applied to the top contact) the junction (N $Ga_{0.4}Al_{0.6}As$ - P GaAs) outside the stripe is reverse biased and conducts negligible current. Another bypass current path (i.e., current not injected into the active region) involves the forward biased P GaAlAs-N GaAlAs junctions between layers S1 and S3 on either side of the active region. The ratio of the currents flowing through the active junction (N GaAlAs-P GaAs) and the GaAlAs junctions can be estimated as follows. From the junction equations the currents flowing across these two kinds of junction are

$$I_i = S_i J_{0i} \, e^{qV_i/mkT} \tag{2-1}$$

where J_{0i} is the saturation current density, S_i is the area of the current injection, m is a constant, and V_i is the voltage applied to the

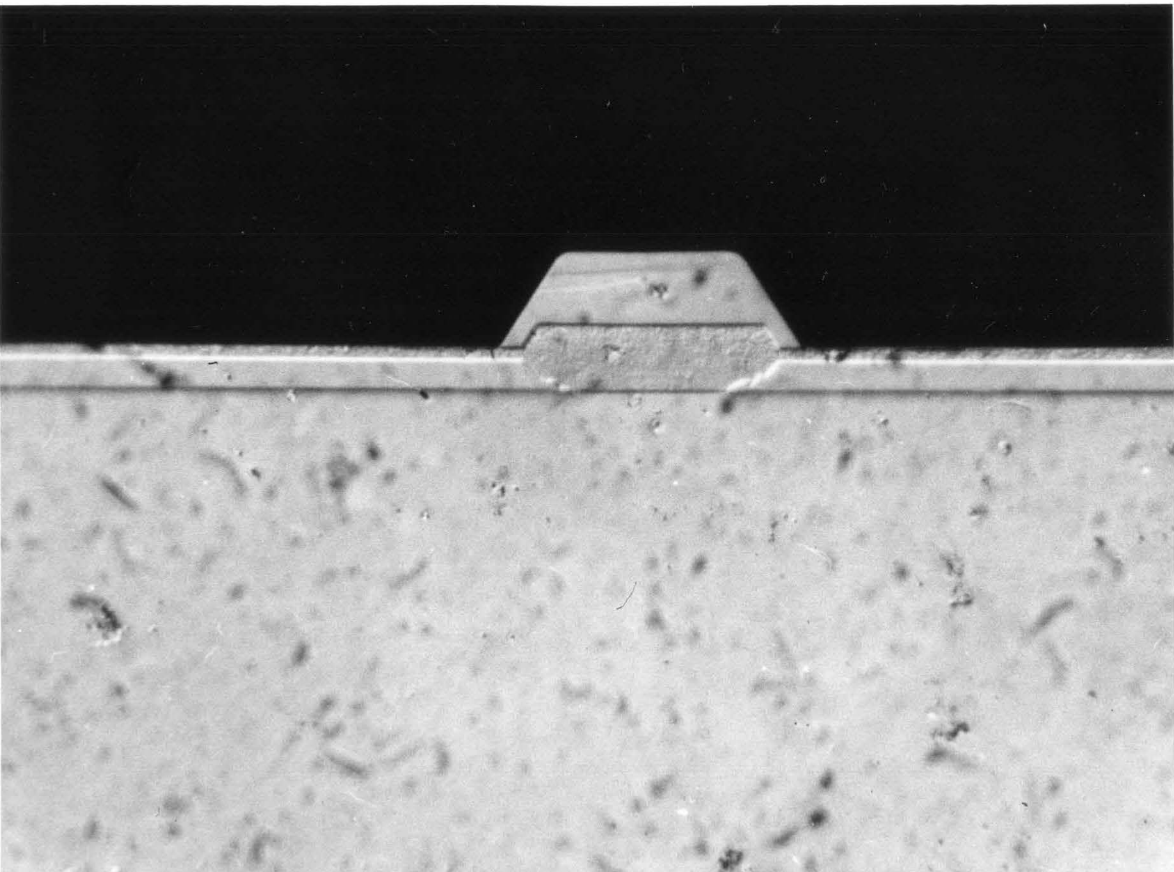

Fig. 2-9 Photograph of the cross section of an embedded double-heterostructure laser grown through a window opened in a GaAlAs-GaAs mask.

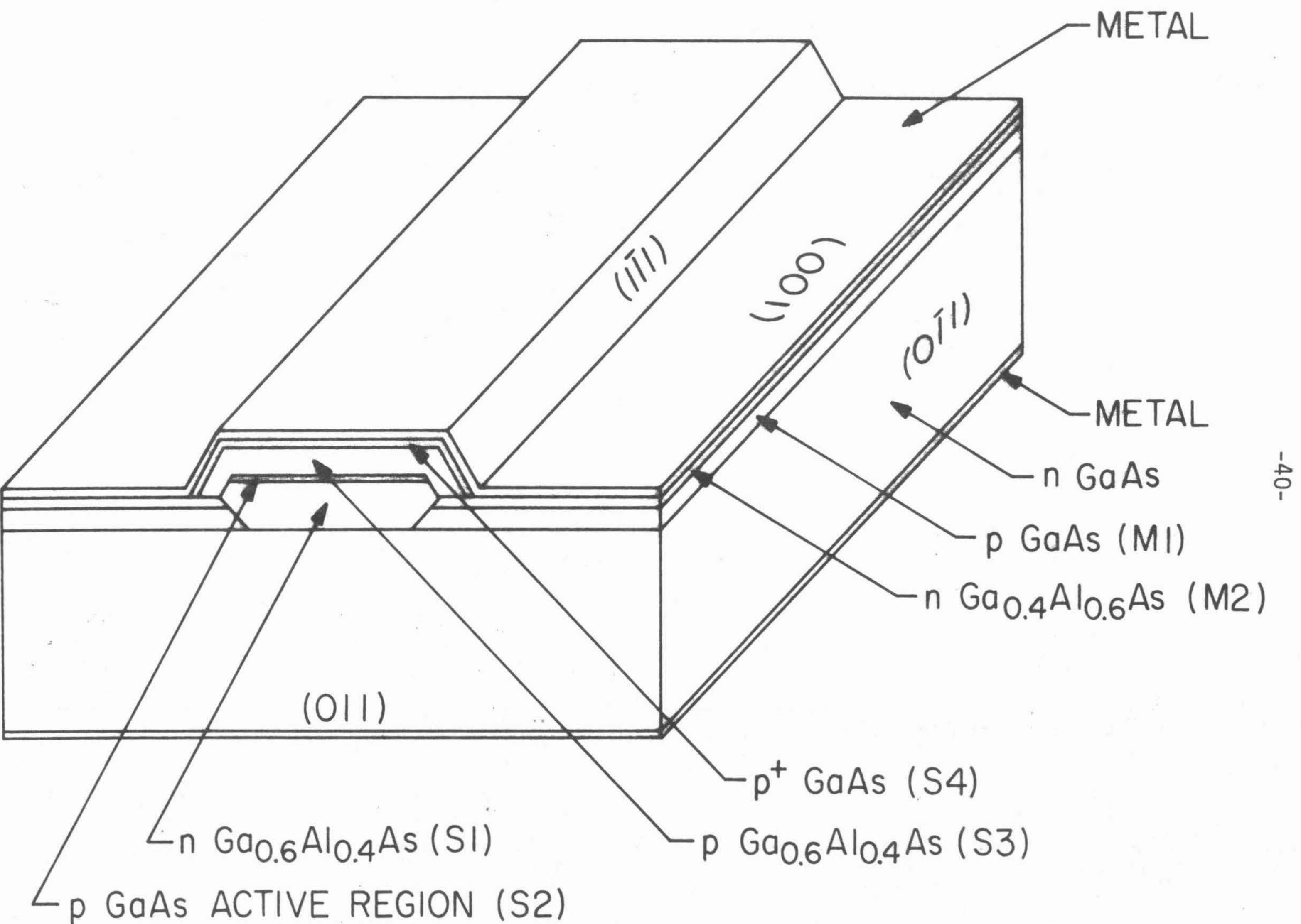

Fig. 2-10 Schematic drawing of an enbedded laser made with a GaAlAs-GaAs mask.

junction. The subscript i=1,2 indicates the active and the GaAlAs junction, respectively. Because these two kinds of junctions are next to each other and the total dimension is small, V_1 and V_2 are approximately the same ($V_1 \simeq V_2$). Therefore the ratio of the currents becomes

$$\frac{I_1}{I_2} = \frac{S_1}{S_2}\frac{J_{01}}{J_{02}} \qquad (2\text{-}2)$$

The ratio of J_{01}, the saturation current density of the heterojunction N GaAlAs - P GaAs, and J_{02}, the saturation current density of the wider bandgap homojunction N GaAlAs - P GaAlAs, is approximately given by[14]

$$\frac{J_{01}}{J_{02}} = e^{\Delta Eg/kT} \qquad (2\text{-}3)$$

where ΔEg is the energy difference between the bandgaps of GaAs and GaAlAs. Substituting eq. (2-3) into eq. (2-2) we get

$$\frac{I_1}{I_2} = \frac{S_1}{S_2} e^{\Delta Eg/kT} \qquad (2\text{-}4)$$

For Al content x = 0.4 in the $Ga_{1-x}Al_xAs$ confining layers, ΔEg is about 20 kT at room temperature. The ratio (S_1/S_2) of the current injection areas is about 20, as seen from Fig. 2-10. Therefore,

$$\frac{I_1}{I_2} \simeq 20\ e^{20} \qquad (2\text{-}5)$$

The current that passes through the GaAlAs junction is negligible compared with the current passing through the active junction. The possible leakage path through the small area interface between layers S1 and M2 was not effective in bypassing current, possibly because of poor electrical contact between them and between the metal and the top GaAlAs layer

(M2), which is covered by native oxide.

A plot of a laser's light intensity versus current is shown in Fig. 2-11. Measurements were made with 100 nsec pulses at a repetition rate of 500 Hz. The curve is linear with current up to more than two times of threshold. The threshold current was 220 mA, and the diode had an active region dimension of 550 μm x 26 μm x 0.25 μm. The corresponding threshold current density is $\sim$1.5 kA/cm^2, which is also typical for most of the lasers tested. This value is lower than those of conventional stripe geometry lasers with the same dimensions, and is comparable to the threshold achieved with conventional broad area lasers. This low threshold current density is a result of electrical and optical confinement in both the vertical and the lateral directions of the active region in the embedded structure.

Figure 2-12 is a microphotograph of the light distribution on a laser's end mirror. The picture was taken through an optical microscope equipped with an image converter. The shape of the cross section of the laser is visible due to the background illumination. The light intensity distribution along the active region is uniform and well confined from all sides.

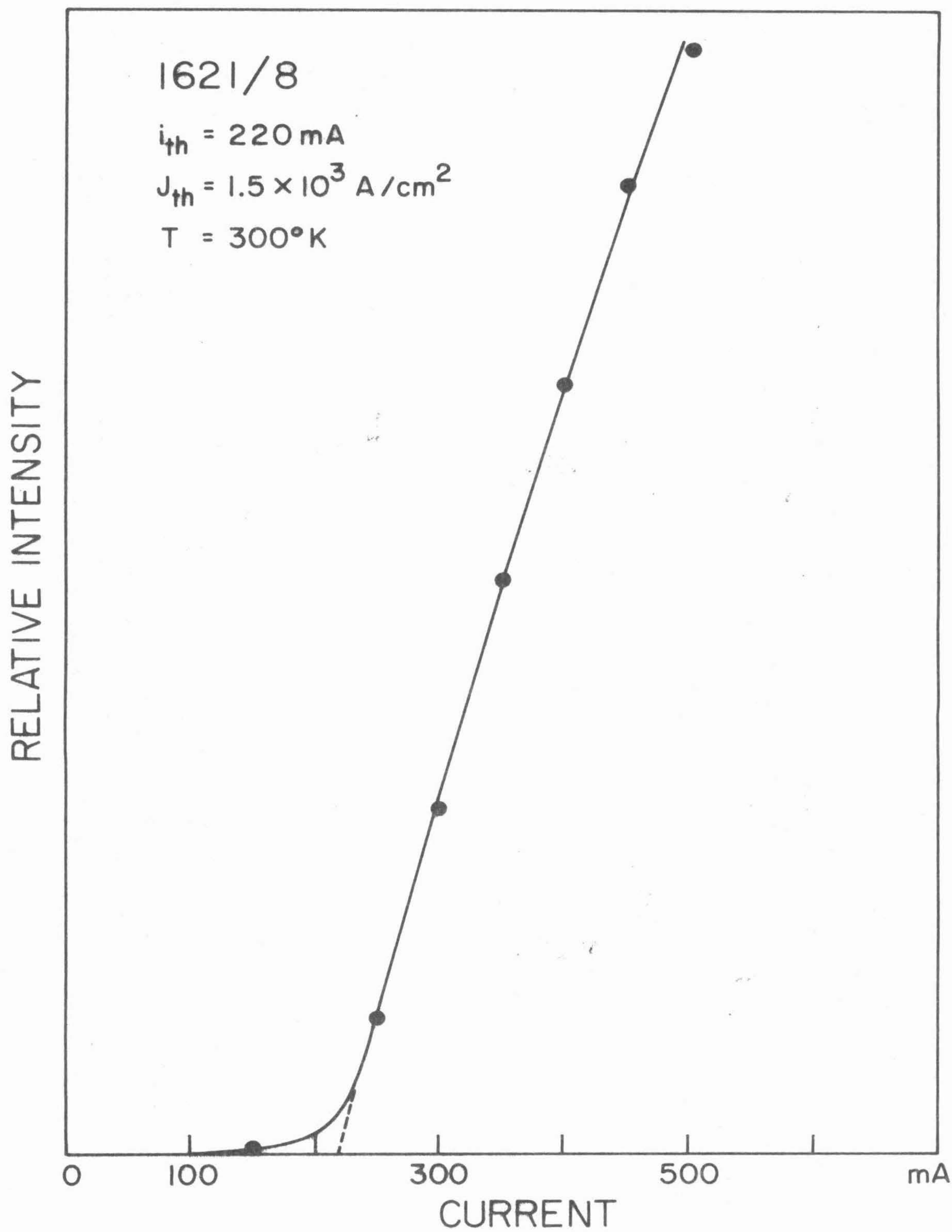

Fig. 2-11 Light intensity vs. driving current of a typical embedded laser.

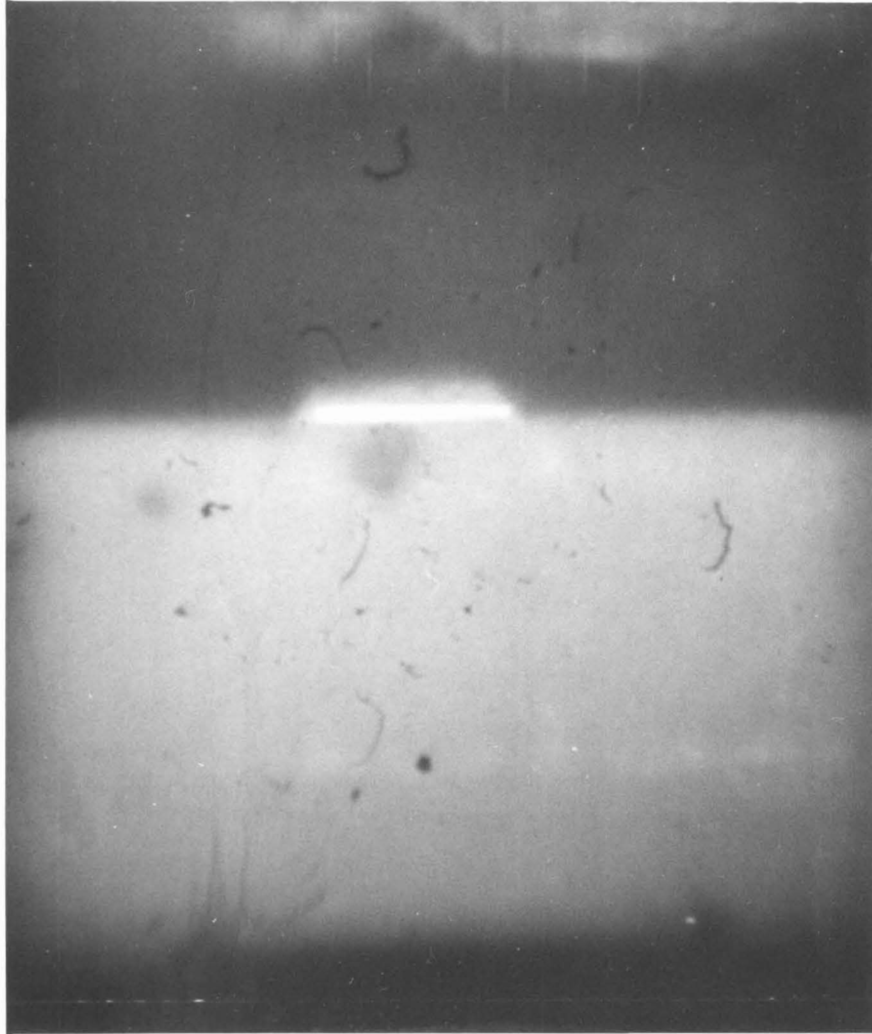

Fig. 2-12 A photograph showing the light distribution at a cavity mirror of an embedded laser.

REFERENCES FOR CHAPTER II

(1) J. C. Tracy, W. Wiegman, R. A. Logan, and F. K. Reinhart, "Three-dimensional light guides in single-crystal GaAs-$Al_xGa_{1-x}As$", Appl. Phys. Lett. 22, 511 (1973)

T. Tsukada, R. Ito, H. Nakashima,and O. Nakada, "Mesa-stripe-geometry double heterostructure injection lasers", IEEE J. Quantum Electron. QE-9, 356 (1973)

(2) H. Yonezu, I. Sakuma, K. Kobayashi, Y. Kamejima, M. Ueno, and Y. Nannichi, "GaAs-$Al_xGa_{1-x}As$ double heterostructure planar stripe laser", Japan J. Appl. phys. 12, 1585 (1973)

E. Garmire, D. F. Lovelace, and H. B. Thompson, "Diffused two-dimensional optical waveguides in GaAs", Appl. Phys. Lett. 21, 87 (1973)

(3) H. L. Garvin, E. Garmire, S. Somekh, H. Stoll, and A. Yariv, "Ion beam micromachining of integrated optics components", Appl. Opt. 12, 455 (1973)

(4) J. C. Dyment, L. A. D'Asaro, and J. C. North, " Optical and eleltrical properties of proton bombarded P-type GaAs", Bull. Am. Phys. Soc. 16, 329 (1971)

(5) V. Evtuhov and A. Yariv, "GaAs-GaAlAs devices for integrated optics", IEEE Trans. Microwave theory tech. 23, 44 (1975)

(6) F. W. Taush,Jr. and A. G. Lapierre,III. "A novel crystal growth phenomenon: single crystal GaAs overgrowth onto silicon dioxide", J. Electrochem. Soc. 112, 706 (1965)

(7) D. W. Shaw, "Selective epitaxial deposition of GaAs in holes", J. Electrochem. Soc. 113, 904 (1966)

(8) T. Kawakami and K. Sugiyama, "Selective liquid phase epitaxy of AlGaAs", Japan J. Appl. Phys. 12, 1808 (1973)

(9) I. Samid, C. P. Lee, A. Gover, and A. Yariv, "Embedded hetero-structure epitaxy : a technique for two dimensional thin-film definitions", Appl. Phys. Lett. 27, 405 (1975)

(10) C. P. Lee, I. Samid, A. Gover, and A. Yariv, "Embedded multilayer heterostructure epitaxy of $Ga_{1-x}Al_xAs$-GaAs", Third American Conf. on Crystal Growth, Stanford (1975)

(11) G. H. B. Thompson, "A theory for filamentation in semiconductor lasers including the dependence of dilectric constant on injection carrier density", Opto-Electron. 4, 257 (1972)

(12) C. P. Lee, I. Samid, A. Gover, A. Yariv, "Embedded GaAs-GaAlAs heterostructure lasers", Topical Meeting on Integrated Optics, WC6-1, Salt Lake City (1976)

(13) C. P. Lee, I. Samid, A. Gover, A. Yariv, "Low-threshold room-temperature embedded heterostructure lasers", Appl. Phys. Lett. 29, 365 (1976)

(14) S. M. Sze, Physics of Semiconductor Devices (John Wiley & Sons, Inc. New York, 1969)

CHAPTER III

BARRIER CONTROLLED GaAs-GaAlAs PNPN LASER DIODE

III.1 Introduction

The concept of the PNPN device was first described by W. Shockley in 1950.[1] The first working device and the principles underlying its operation were reported by J. Moll and coworkers of the Bell Laboratories in 1956.[2]

A simple four-layer PNPN structure and its basic current-voltage (I-V) characteristic curve are shown in Fig. 3-1. Under forward bias it displays three different operating regions. In region 1 the device is in the blocking or "off" state with very high impedence. After the breakover point the curve turns to region 2, which is a negative resistance unstable region. The voltage at the turning point ($dV/dI = 0$). is called the breakover voltage. In region 3 the curve shows positive resistance again but with a small resistance. This region is called the forward conducting or "on" state. The point where the curve changes from negative resistance to positive resistance is called the holding point and the current at this point is the holding current. When the device is reverse biased it has the characteristic of a conventional PN diode. In region 4 the device is in the reverse blocking state, while region 5 is the reverse breakdown region.

A PNPN device when operated in the forward direction is thus a bistable device which can change from a high-impedence low-current state to a low-impedence high-current state or vice versa. As a two terminal device, the PNPN diode (or the Shockley diode as it is sometimes called) can be switched from the "off" state to the "on"

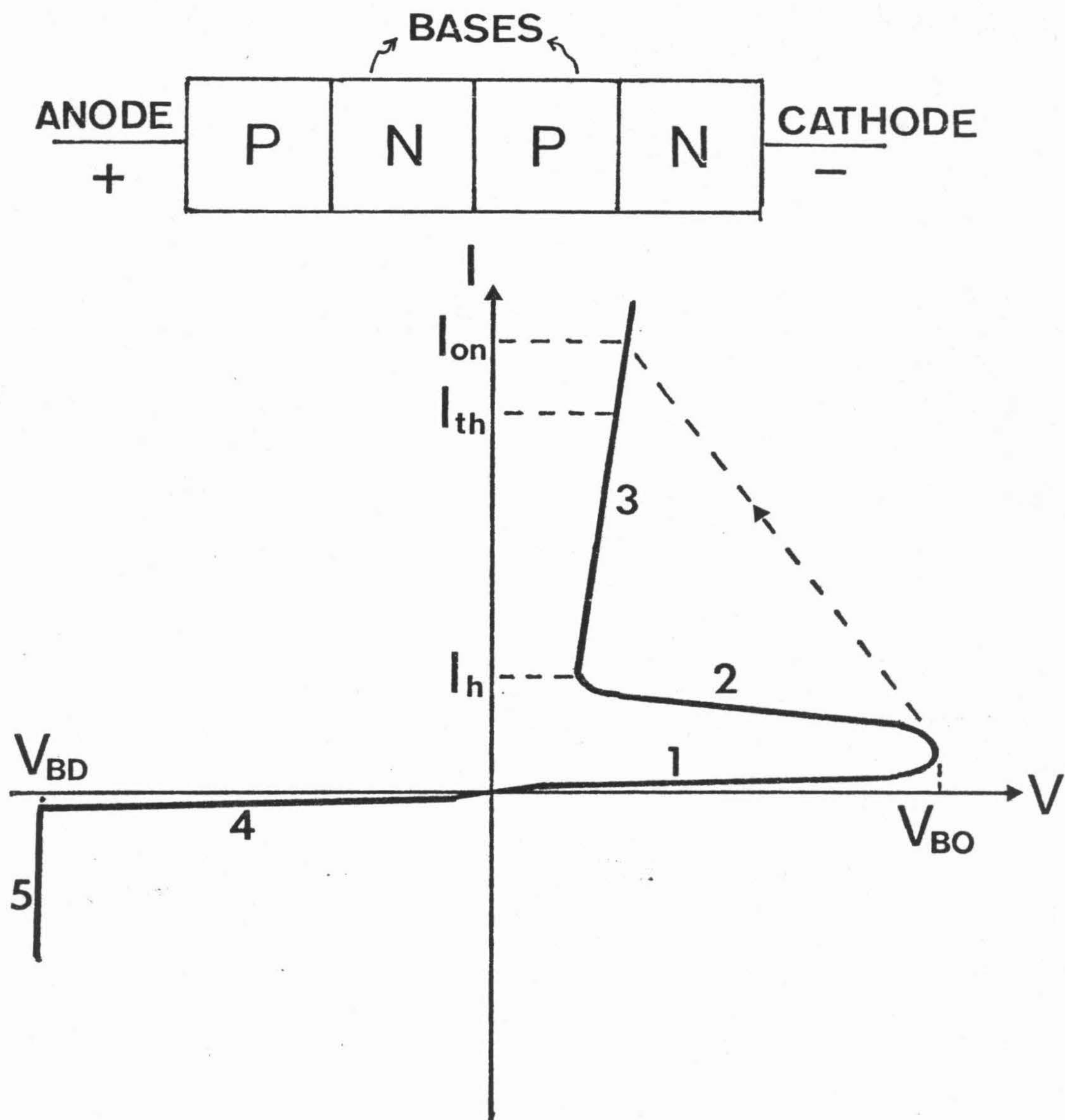

Fig. 3-1 A PNPN device and its I-V characteristic. In the forward region, 1 is the forward blocking state, 2 is the negative resistance region, 3 is the forward conduction state. V_{BO} is the breakover voltage, I_h is the holding current. In the reverse region, 4 is the reverse blocking state and 5 is the breakdown region. V_{BD} is the breakdown voltage.

state when the terminal voltage exceeds the breakover voltage. When the device is operated with three terminals it is referred to as a semiconductor-controlled-rectifier (SCR). The switching of a SCR is usually controlled by the triggering current injected from the gate electrode, which is located on one of the two middle layers, or bases, of a PNPN structure (see Fig. 3-1). A PNPN device can also be switched from "off" to "on" by shining light on the base regions. The photons absorbed in the bases generate electron-hole pairs, and these carriers form the triggering current for the device.

Since their introduction in the fifties PNPN devices used silicon as the material. Recently the importance of GaAs has been realized and their exists a considerable amount of interest in GaAs junction devices. Owing to its relatively large energy gap (1.42 eV) and small minority carrier lifetime ($\sim 10^{-8}$sec) GaAs devices offer the potential of high temperature and high frequency (or fast switching) applications.(3) PNPN devices made from GaAs have been reported by several authors.(4-6) The multilayer structures were prepared by sequential impurity diffusions or epitaxial growth.

Our motivation for fabricating GaAs-GaAlAs PNPN laser diodes was a desire to combine the lasing properties of GaAs-GaAlAs heterostructure with the switching capability of the PNPN device so that the combined device could work as a laser switch. The operation of this device can be understood by referring again to Fig. 3-1. Supposing that the lasing threshold current of the PNPN laser is I_{th} and the current to which the device switches after being turned on is I_{on}, the device will emit laser light if $I_{on} \geq I_{th}$. As a switch it can be

turned on by simply applying a voltage greater than the breakover voltage or by external triggering either with an electrical pulse or an optical pulse. When triggered by an optical pulse the device can function as an optical repeater. As the weak light signal is incident on the device, which is under forward bias just below the breakover voltage, the device will be turned on and emit intense and coherent laser light. In optical communication systems,repeaters are very important for long distance fiber transmissions. A light signal, after a long distance of propagation through an optical fiber, may become weakened and distorted because of absorption in the fiber medium and scattering at the boundaries. A repeater station can pick up this weak signal and regenerate an intense laser signal for another journey down the fiber.

The condition for a PNPN laser diode to emit laser light after being turned on is $I_{on} \geq I_{th}$. In order to obtain a sufficient turn-on current one requires a device with a large breakover voltage (V_{BO}). As will be discussed in the following sections, a large breakover voltage has been realized traditionally by increasing the widths of the base regions (the middle two layers of the PNPN structure). Increasing base widths, however is in contradiction to the requirement of low threshold lasers. This is due to the fact that the base regions are also the active regions of the lasers so that increasing widths lead to lower density of inverted population and hence to higher threshold current densities for the lasers. In this chapter we describe a new method which overcomes this problem. This method involves adding GaAlAs,

a larger bandgap material, to the base regions. The GaAlAs layers serve as potential barriers for the carriers passing through the bases and thus control the current transport in the device. These barrier layers not only change the electrical properties but also affect the optical properties of the device because GaAlAs has a lower index of refraction than GaAs. With this technique it is possible to fabricate PNPN lasers with a thin active region while still retaining a large breakover voltage. Lasers with threshold current densities comparable to those of conventional double heterostructure lasers have been achieved.

III.2 PNPN Device Operation

The basic operation of a PNPN device can be easily understood using a two-transistor analogue.[8] A PNPN structure can be considered as an NPN transistor and a PNP transistor connected in such a way that the collector of each transistor is attached to the base of the other as shown in Fig. 3-2 a,b,c. The relationship between emitter, collector and base currents (I_E, I_C and I_B, respectively) and the dc common-base current gain α for a PNP transistor is shown in Fig. 3-2d. I_{CO} is the collector to base reverse saturation current. Similar relationships can be obtained for the NPN transistor, except that the currents are reversed. From Fig. 3-2b it is clear that the collector of the NPN transistor supplies the base current for the PNP transistor. The base drive for the NPN transistor is provided by the collector of the PNP transistor along with the gate current I_g. Thus a regenerative situation results when the total loop gain exceeds one.

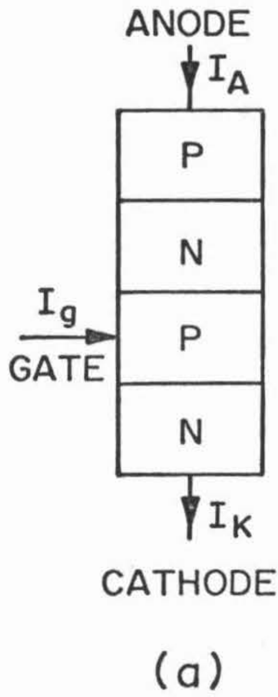

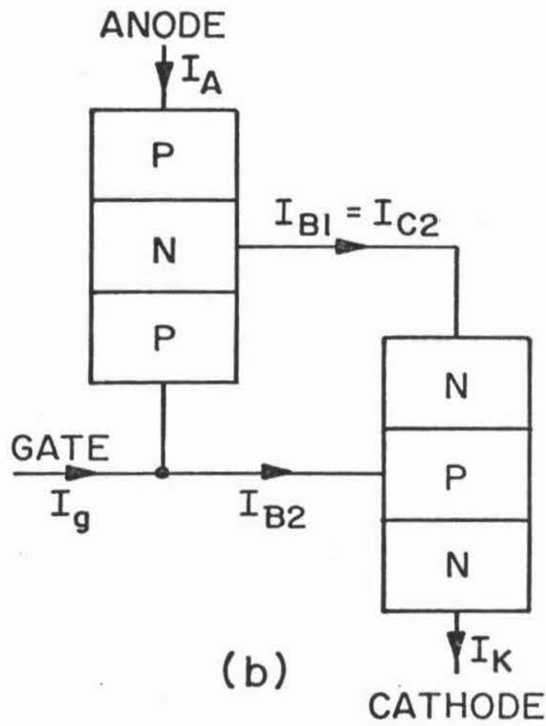

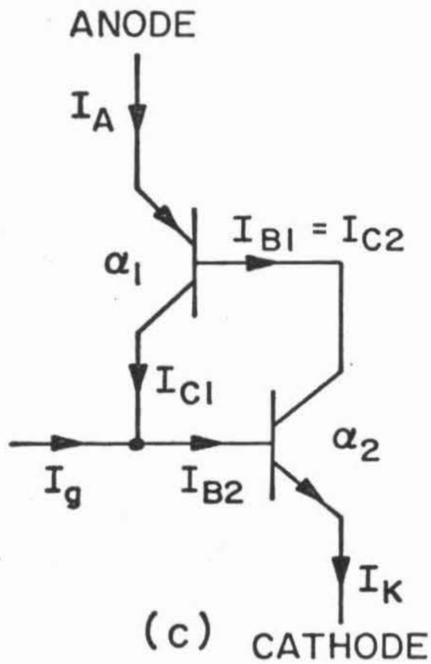

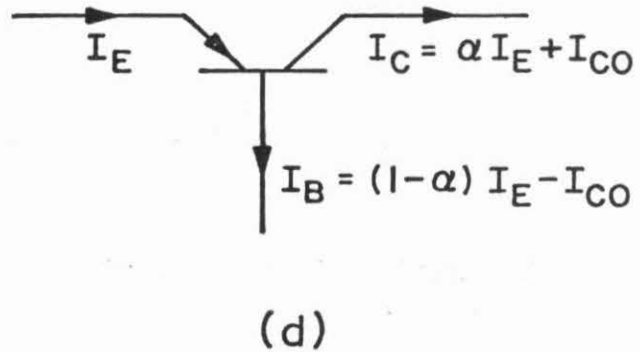

Fig. 3-2 (a) A PNPN device. (b) Two transistor analogue of the device. (c) Same as (b), using transistor notation. (d) Current relationships in a PNP transistor.

Starting with the basic two equations for the two transistors

$$I_{C1} = \alpha_1 I_A + I_{C01} \qquad (3\text{-}1)$$

$$I_{C2} = \alpha_2 I_K + I_{C02} \qquad (3\text{-}2)$$

where I_A, I_K are the anode and the cathode currents of the device as shown in Fig. 3-2c. Using the relations $I_{B1} = I_{C2}$ and $I_{B1} = I_A - I_{C1}$, we get

$$I_{B1} = (1 - \alpha_1)I_A - I_{C01} = \alpha_2 I_K + I_{C02} \qquad (3\text{-}3)$$

or

$$(1 - \alpha_1)I_A + \alpha_2 I_K = I_{C01} + I_{C02} \qquad (3\text{-}4)$$

Substituting $I_A + I_g = I_K$ into eq. (3-4) yields

$$I_A = \frac{\alpha_2 I_g + I_{C01} + I_{C02}}{1 - \alpha_1 - \alpha_2} \qquad (3\text{-}5)$$

If the gate current is provided through the base of the PNP transistor, exactly the same solution results. When $\alpha_1 + \alpha_2$ approaches 1 the denominator of eq. (3-5) approaches 0 and switching will occur.

For a more accurate analysis, one can view the PNPN device as a four terminal device as shown in Fig. 3-3. I_{g1} and I_{g2} are the base currents entering the N and the P base regions respectively. In the forward "off" state, the middle collector junction is reverse biased with voltage V_2 across the depletion region between x_1 and x_2. Because of avalanche multiplication, hole current $I_p(x_1)$ entering the depletion region at x_1 becomes $M_p I_p(x_1)$ at $x = x_2$. A similar state of affairs

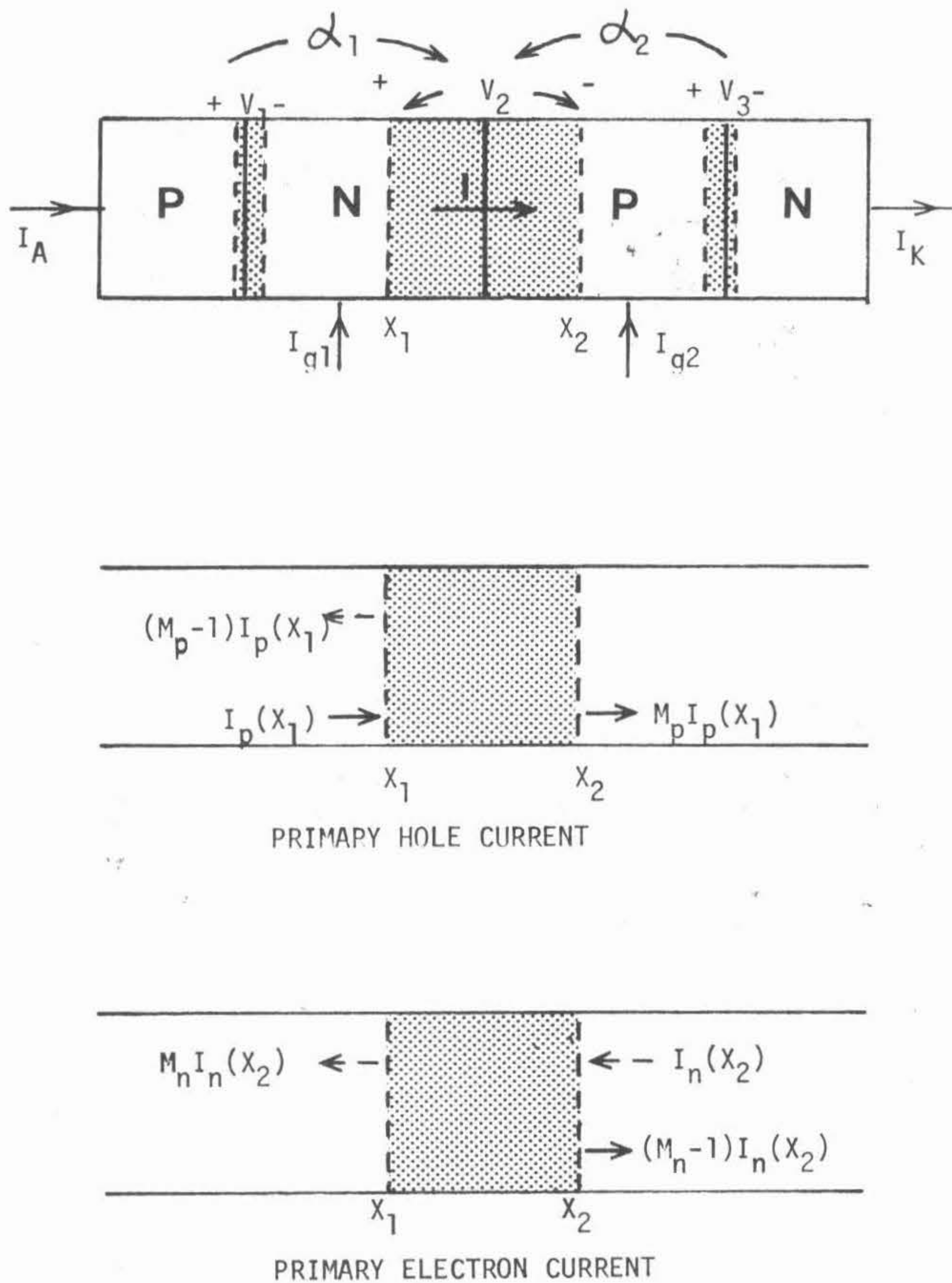

Fig. 3-3 Generalized PNPN device. Electron current I_n and hole current I_p generate M_nI_n and M_pI_p, respectively, under avalanche multiplication conditions.

obtains for electron current entering the depletion layer from the right at x_2. The collector current of the PNP transistor is primarily the hole current and can be expressed as

$$I_p(x_1) = \alpha_1 I_A + I_{CO1} \tag{3-6}$$

The collector current of the NPN transistor can be similarly expressed as

$$I_n(x_2) = \alpha_2 I_K + I_{CO2} \tag{3-7}$$

The total current flowing across any plane between x_1 and x_2 is then

$$I = M_p I_p(x_1) + M_n I_n(x_2) \tag{3-8}$$

For GaAs, the multiplication factor for electrons is the same as for holes. Therefore $M_p = M_n = M$, and

$$I = M(\alpha_1 I_A + I_{CO1} + \alpha_2 I_K + I_{CO2}) \tag{3-9}$$

From conservation of current we get

$$I = I_A + I_{g1} \quad \text{and} \quad I_K = I + I_{g2} \tag{3-10}$$

Upon substituting these two relations into eq.(3-9) we get

$$I_A = \frac{M(\alpha_2 I_{g2} - \alpha_1 I_{g1} + I_{CO1} + I_{CO2})}{1 - M(\alpha_1 + \alpha_2)} \tag{3-11}$$

The switching condition is obtained when

$$M(\alpha_1 + \alpha_2) = 1 \tag{3-12}$$

The multiplication factor M is a function of the reverse biased voltage V_2 of the middle collector junction. The relation is usually expressed

as

$$M = \frac{1}{1 - \left(\frac{V_2}{V_{BD}}\right)^n} \qquad (3\text{-}13)$$

where V_{BD} is the breakdown voltage and n is a parameter, which is a function of V_2/V_{BD}.[9] The common-base current gains α_1 and α_2 are functions of the current. They increase as the current increases.[3] Using equations (3-12) and (3-13) we get for the breakover voltage

$$V_{BO} = V_{BD}(1 - \alpha_1 - \alpha_2)^{1/n} \qquad (3\text{-}14)$$

If the breakdown voltage is fixed, the breakover voltage depends on the values of alphas, α_1 and α_2. If the alphas are large and increase very rapidly with voltage, breakover will occur at a voltage much less than V_{BD}. If the alphas are small and do not increase significantly with voltage, the breakover voltage will result from avalanche and be near the value of V_{BD}.

III.3 Design of the Barrier Controlled GaAs-GaAlAs PNPN Laser

As described in the introduction to this chapter, high breakover voltage is desirable if one wants to achieve a high "on" current after switching. In the previous section we have shown that the breakover voltage depends on the alpha parameters of the PNP and NPN transistors. Higher breakover voltage can be achieved if the alphas are small or do not increase with the voltage significantly. We are thus led to look for means of obtaining small alpha values. By definition, the common-base current gain α of a transistor is the product of the

injection efficiency γ of the emitter junction and the transport factor t

$$\alpha = \gamma t \tag{3-15}$$

The parameters γ and t are defined as follows:

$$\gamma \equiv \frac{\text{minority current injected from the emitter into the base}}{\text{total emitter current}} \tag{3-16}$$

$$t \equiv \frac{\text{minority current reaching the collector}}{\text{minority current injected into the base by the emitter}} \tag{3-17}$$

From simple calculations, for an ordinary transistor with base width w, we get

$$\gamma = \frac{1}{1 + \frac{N_E}{N_B} \frac{D_E}{D_B} \frac{L_B}{L_E} \tanh \frac{w}{L_B}} \tag{3-18}$$

$$t = \frac{1}{\cosh \frac{w}{L_B}} \tag{3-19}$$

where L is the diffusion length of minority carriers in the base, D is the diffusion constant, and N is the minority carrier concentration. The subscripts B and E denote the base and the emitter, respectively. It is clear from eq. (3-19) and eq. (3-15) that a larger w will result in a smaller α, and therefore a higher breakover voltage V_{BO}. Conventionally this approach has been used to achieve high V_{BO} for a PNPN device. However, as explained in the introduction to this chapter, wide bases are not suitable for laser structures because they result in high threshold currents. Another possibility of reducing the alphas is to decrease the injection efficiencies. This is also not desirable because it leads to a smaller density of injected minority carriers in the base

regions at a given total current and thus to a smaller laser gain. Lockwood et al.[10] have reported a GaAs PNPN laser diode which has both wide base and a small injection efficiency. The threshold current density of their laser was about 20 kA/cm^2. This value is approximately an order of magnitude higher than the threshold of conventional double heterostructure lasers.

In order to get low lasing threshold and high breakover voltage at the same time, we used a method of placing potential barriers in the base regions. The barriers reduce the minority carrier transport factors and hence reduce the alphas. In GaAs PNPN devices, potential barriers can be easily introduced by using $Ga_{1-x}Al_xAs$ layers. Since $Ga_{1-x}Al_xAs$ is almost perfectly lattice matched to GaAs and has a larger bandgap than GaAs, it serves as an effective potential barrier for the carriers flowing through it. Furthermore, the height of the barrier can be easily controlled by the Al content in the layer because the bandgap of $Ga_{1-x}Al_xAs$ changes with x (see Fig. 1-2). Figure 3-4a shows an example of a barrier controlled GaAs-GaAlAs PNPN device. In the P base region an additional layer of GaAlAs is added to serve as a potential barrier for the electrons diffusing through the base. The two emitters of this device are also made from GaAlAs because it provides electrical and optical confinement for the adjacent GaAs layers and improves the injection efficiencies of the emitter junctions. Figures 3-4b,c are the band diagrams of the device in the "off" state and "on" state, respectively. Due to the potential barrier in the conduction band of the P

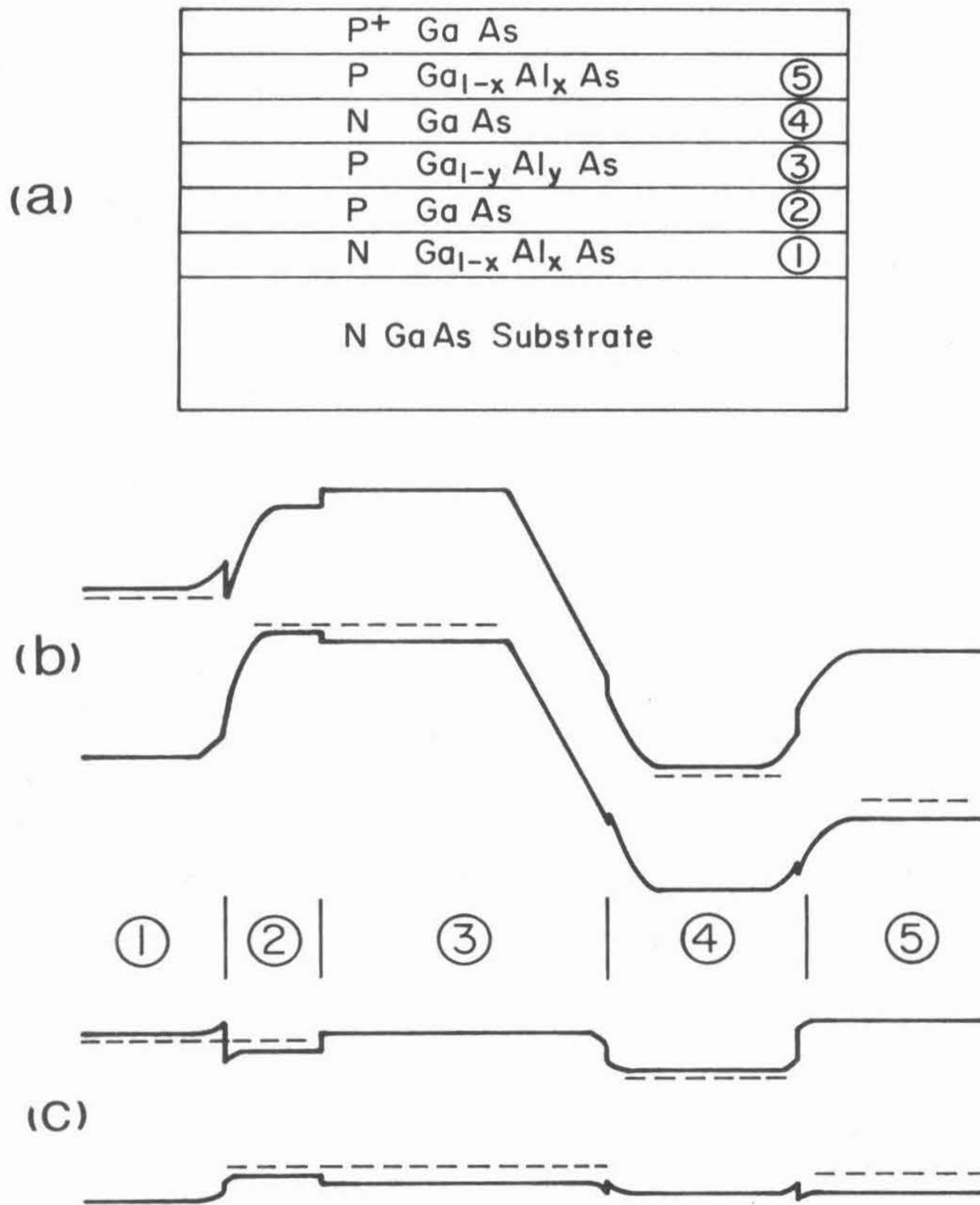

Fig. 3-4 (a) Schematic diagram of a GaAs-GaAlAs barrier controlled PNPN diode with a $Ga_{1-y}Al_yAs$ potential barrier in the P base. (b) Band diagram when the diode is in the forward blocking state. (c) Band diagram when the diode is "ON" and lasing.

base the number of electrons which can reach the collector junction (the P GaAlAs-N GaAs junction) from the left side is greatly reduced. Most of the electrons injected from the N GaAlAs emitter recombine with holes in the P GaAs region instead of diffusing through the P GaAlAs barrier region. The transport factor of electrons, and the current gain α of the NPN transistor are therefore reduced. When the device is switched to the "on" state and operated with a current above the lasing threshold, the GaAs region in the P base forms a potential well for the electrons, and the electrons trapped in this region recombine with the holes to generate stimulated emission. Besides the carrier confinement, this GaAs region also provides optical confinement for the light generated in this region, because the adjacent GaAlAs layers have refractive indices larger than that of GaAs. This GaAs layer is thus similar to the active layer of a regular double heterostructure laser. Since the P base of this device consists of a GaAs active layer and a GaAlAs barrier layer, and the current gain α can be controlled by the barrier, it is possible to make the GaAs layer very thin, and at the same time to keep the current gain of the device small. As a result, this barrier-controlled PNPN device is capable of lasing at a threshold comparable to that of a regular double heterostructure laser while still possessing a high breakover voltage.

In a barrier-controlled PNPN device, a GaAlAs barrier can be put in the P base as well as in the N base, or in both. Since the barrier layers are not lasing active regions, their thickness can be increased in order to alleviate the possible punch-through effect when the middle collector junction is reverse biased.

III.4. Current-Voltage Characteristics below the Holding Point

In this section we present the theoretical calculations of the I-V characteristics of a PNPN device having a GaAlAs layer in the P base region when the device is operated below the holding point. The holding point is the turning point where the I-V curve changes from a negative resistance region to a positive resistance region, or when the center collector junction changes from reverse bias to forward bias. The I-V characteristics below the holding point describe the behavior of the device in the forward blocking state and in the negative resistance state, and therefore provide information about the switching behavior of the device.

The particular structure used in the analysis is shown in Fig. 3-5a. This analysis can be easily extended to treat other similar structures, such as devices with a barrier in the N base or barriers in both base regions. The N $Ga_{1-x}Al_xAs$ and P $Ga_{1-x}Al_xAs$ layers serve as two emitters. Use of GaAlAs emitters provides high injection efficiencies and good electrical and optical confinement. Regions 1 and 2 form the base of the NPN transistor with the composition of region 2 being of $Ga_{1-y}Al_yAs$. Region 3 is an N GaAs layer which is the base of the PNP transistor. The doping concentration in region 3 is assumed much higher than that in region 2, so that most of the depletion region at junction C extends into region 2 and no punch-through occurs under reverse bias. Junctions under forward bias are assumed to have depletion layer widths that are negligible compared with the widths of the layers.

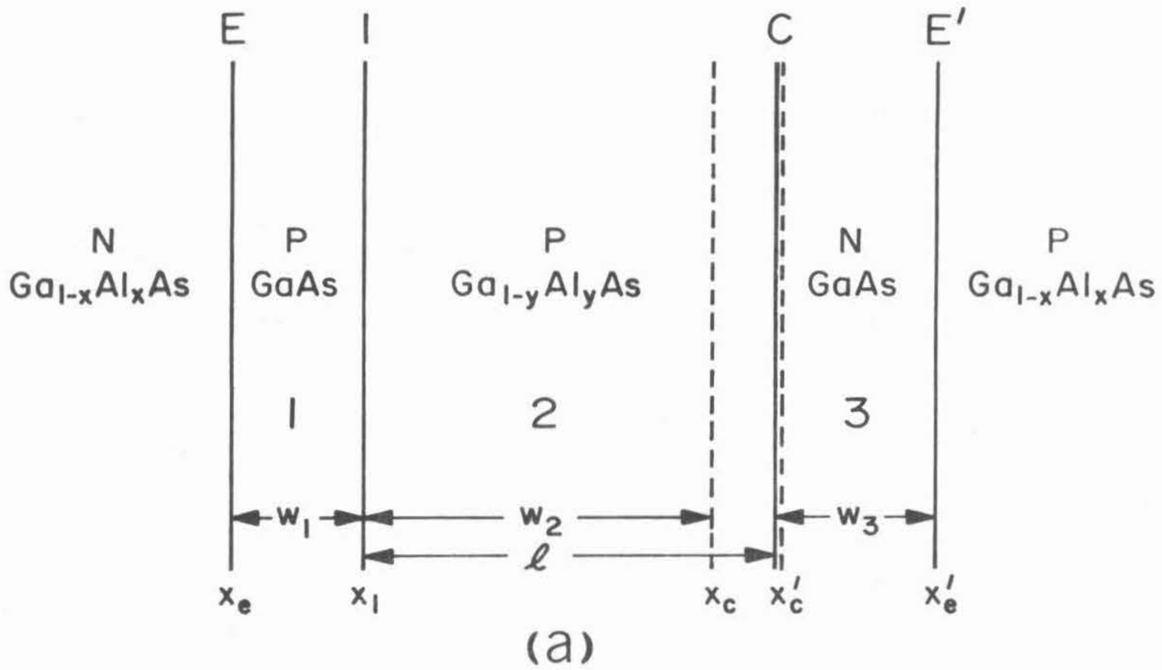

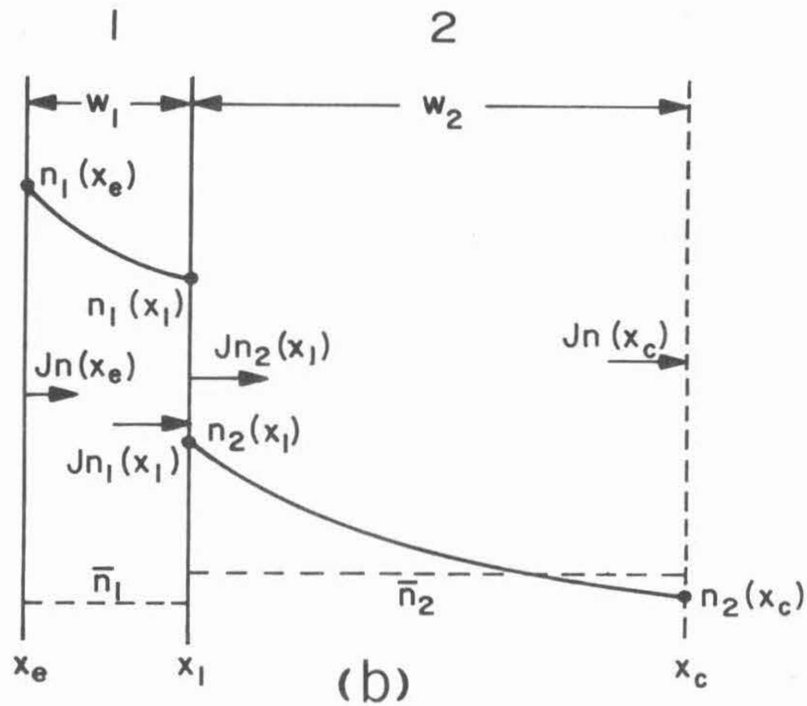

Fig. 3-5 (a) The structure of a PNPN device with a $Ga_{1-y}Al_yAs$ barrier layer in the p base. (b) The minority carrier distribution in the P base.

III.4.1 Boundary conditions

In solving for the I-V characteristics of the device, it is necessary to know the boundary conditions of the carrier concentrations at all the junctions. Since we are interested in the I-V curves below the holding point, low level injection conditions are assumed, i.e., the injected minority carrier densities are small compared with the majority carrier densities. In the structure of Fig. 3-5, E, E', and C are PN junctions, l is a PP hetero-junction. At the boundaries of the depletion regions of the PN junctions, the excess minority carrier densities follow the Shockley boundary conditions.(3) They are

$$n_1(x_e) = \overline{n}_1(e^{qV_E/kT} - 1) \quad (3\text{-}20)$$

$$n_2(x_c) = \overline{n}_2(e^{qV_C/kT} - 1) \quad (3\text{-}21)$$

$$p_3(x_c') = \overline{p}_3(e^{qV_C/kT} - 1) \quad (3\text{-}22)$$

$$p_3(x_e') = \overline{p}_3(e^{qV_{E'}/kT} - 1) \quad (3\text{-}23)$$

where n and p are the excess (or injected) electron and hole concentrations, respectively, $\overline{n}$ and $\overline{p}$ are the equilibrium values of the electron and hole densities, the subscripts 1, 2, and 3 denote the three different base regions, and V_E, V_C and $V_{E'}$ are the voltage drops across the three PN junctions E, C, E', respectively.

Since $Ga_{1-y}Al_yAs$ has a wider bandgap than GaAs, the conduction band edge at the P GaAs - P $Ga_{1-y}Al_yAs$ junction forms a potential barrier for the electrons and the valence band edge forms a potential barrier for

the holes in the GaAs region (see Fig. 3-6). From Boltzmann statistics, the electron densities on both sides of the boundary (x_1) are related by

$$\frac{n_1(x_1)}{n_2(x_1)} = \frac{N_{C1}}{N_{C2}} e^{\Delta E_C/kT} \tag{3-24}$$

where N_{C1} and N_{C2} are the effective densities of states of electrons in the conduction bands of GaAs and $Ga_{1-y}Al_yAs$, respectively, and ΔE_C is the barrier height in the conduction band. Similarly, the relation between the hole densities at the two sides of the boundary is

$$\frac{p_1(x_1)}{p_2(x_1)} = \frac{N_{V1}}{N_{V2}} e^{\Delta E_V/kT} \tag{3-25}$$

where N_{V1}, N_{V2} are the densities of states of holes in the valance bands of the two materials, and ΔE_V is the barrier height in the valence band. Multiplying eq. (3-24) by eq. (3-25) we obtain

$$\frac{n_1(x_1)}{n_2(x_1)} \cdot \frac{p_1(x_1)}{p_2(x_1)} = \frac{N_{C1}}{N_{C2}} \frac{N_{V1}}{N_{V2}} e^{(\Delta E_C + \Delta E_V)/kT} \tag{3-26}$$

Since these two regions are p type, under low-level injection conditions the hole concentrations are approximately the same as doping concentrations, i.e., $p_1(x_1) = N_{A1}$, $p_2(x_1) = N_{A2}$. $\Delta E_V + \Delta E_C$ in the exponent of eq.(3-26) is the energy difference, ΔEg, between the bandgaps of GaAs and $Ga_{1-y}Al_yAs$. Therefore, eq. (3-26) becomes

$$\frac{n_1(x_1)}{n_2(x_1)} = \frac{N_{C1}}{N_{C2}} \frac{N_{V1}}{N_{V2}} \frac{N_{A2}}{N_{A1}} e^{\Delta Eg/kT} \tag{3-27}$$

or

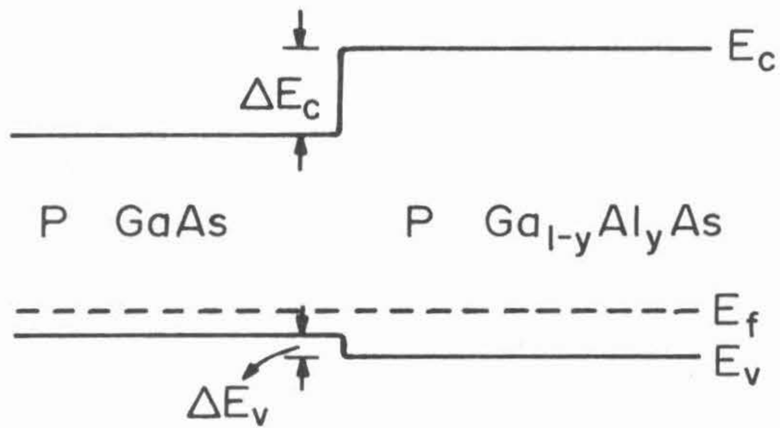

Fig. 3-6 The P GaAs - P $Ga_{1-y}Al_yAs$ junction

$$\frac{n_1(x_1)}{n_2(x_1)} = e^{\Delta E/kT} \tag{3-28}$$

where

$$\Delta E = \Delta Eg + kT(\ell n \frac{N_{A2}}{N_{A1}} + \ell n \frac{N_{C1}}{N_{V1}} \frac{N_{C2}}{N_{V2}}) \tag{3-29}$$

This ΔE is the effective height of the potential barrier for the electrons flowing from region 1 (GaAs) to region 2 ($Ga_{1-y}Al_yAs$).

III.4.2 Solution of the diffusion equation

In order to obtain the carrier and the current distributions in the p base of the device, it is necessary to solve the diffusion equations separately in the two materials which compose the base and match the boundary conditions at $x = x_1$ (see Fig. 3-5a). For convenience of illustration the p base region is drawn in Fig. 3-5b. In the absence of electric fields, the diffusion equation for the excess number of electrons is

$$\frac{d^2 n(x)}{dx^2} = \frac{n(x)}{L_n^2} \tag{3-30}$$

where L_n is the diffusion length of electrons. The solution of this equation is

$$n(x) = C_1 e^{x/L_n} + C_2 e^{-x/L_n} \tag{3-31}$$

where C_1 and C_2 are arbitrary constants to be determined by the boundary conditions. In region 1 the conditions for $n(x)$ at $x = x_e$ and x_1 are

$$n(x) = n_1(x_e) \qquad \text{at} \quad x = x_e$$

and

$$n(x) = n_1(x_1) \qquad \text{at} \quad x = x_1 \tag{3-32}$$

Applying these two relations to eq. (3-31) we can solve for the excess electron distribution in region 1

$$n_1(x) = \frac{1}{\sinh \frac{w_1}{L_{n1}}} [n_1(x_1) \sinh \frac{x-x_e}{L_{n1}} + n_1(x_e) \sinh \frac{x_1-x}{L_{n1}}] \tag{3-33}$$

where the subscript 1 indicates region 1, and w_1 is the distance between x_1 and x_e. Similarly, the distribution of excess electrons in region 2 is

$$n_2(x) = \frac{1}{\sinh \frac{w_2}{L_{n2}}} [n_2(x_c) \sinh \frac{x-x_1}{L_{n2}} + n_2(x_1) \sinh \frac{x_c-x}{L_{n2}}] \tag{3-34}$$

where w_2 is the distance between x_1 and x_c.

The diffusion current of electrons, $J_n(x)$, can be obtained by using the equation

$$J_n(x) = q\ D_n \frac{dn}{dx} \tag{3-35}$$

where D_n is the diffusion constant of electrons. Substituting eq. (3-33) and eq. (3-34) into eq. (3-35) we obtain

$$J_{n1}(x) = \frac{q\ D_{n1}}{L_{n1} \sinh \frac{w_1}{L_{n1}}} [n_1(x_e) \cosh \frac{x_1-x}{L_{n1}} - n_1(x_1) \cosh \frac{x-x_e}{L_{n1}}] \tag{3-36}$$

$$J_{n2}(x) = \frac{q\ D_{n2}}{L_{n2} \sinh \frac{w_2}{L_{n2}}} [n_2(x_1) \cosh \frac{x_c-x}{L_{n2}} - n_2(x_c) \cosh \frac{x-x_1}{L_{n2}}] \tag{3-37}$$

From the condition of continuity of electron current at $x = x_1$,

$$J_{n1}(x_1) = J_{n2}(x_1) \tag{3-38}$$

we obtain from eq. (3-36) and eq. (3-37) a relation between $n_1(x_1)$ and $n_2(x_1)$

$$\frac{D_{n1}}{L_{n1}\sinh\frac{w_1}{L_{n1}}}\left[\cosh\frac{w_1}{L_{n1}}\, n_1(x_1) - n_1(x_e)\right] = \frac{D_{n2}}{L_{n2}\sinh\frac{w_2}{L_{n2}}}\left[n_2(x_c) - n_2(x_1)\cosh\frac{w_2}{L_{n2}}\right] \quad (3\text{-}39)$$

Substituting the boundary condition

$$n_1(x_1) = n_2(x_1)\, e^{\Delta E/kT} \qquad \text{(from eq. (3-28))}$$

into eq. (3-20) we obtain the solutions for $n_1(x_1)$ and $n_2(x_1)$: they are

$$n_1(x_1) = \frac{\dfrac{D_{n2}\, n_2(x_c)}{L_{n2}\sinh\frac{w_2}{L_{n2}}} + \dfrac{D_{n1} n_1(x_e)}{L_{n1}\sinh\frac{w_1}{L_{n1}}}}{\dfrac{D_{n1}}{L_{n1}}\coth\dfrac{w_1}{L_{n1}} + \dfrac{D_{n2}}{L_{n2}}\coth\dfrac{w_2}{L_{n2}}\, e^{-\Delta E/kT}} \quad (3\text{-}40)$$

$$n_2(x_1) = \frac{\dfrac{D_{n2}\, n_2(x_c)}{L_{n2}\sinh\frac{w_2}{L_{n2}}} + \dfrac{D_{n1}\, n_1(x_e)}{L_{n1}\sinh\frac{w_1}{L_{n1}}}}{\dfrac{D_{n1}}{L_{n1}}\coth\dfrac{w_1}{L_{n1}}\, e^{\Delta E/kT} + \dfrac{D_{n2}}{L_{n2}}\coth\dfrac{w_2}{L_{n2}}} \quad (3\text{-}41)$$

Using the values of $n_1(x_e)$ and $n_2(x_c)$ from eq.(3-20) and eq.(3-21), the above two expressions become

$$n_1(x_1) = \frac{A_1}{C}\,\bar{n}_1(e^{qV_E/kT} - 1) + \frac{A_2}{C}\,\bar{n}_2(e^{qV_C/kT} - 1) \quad (3\text{-}42)$$

$$n_2(x_1) = e^{\Delta E/kT}\left[\frac{A_1}{C}\,\bar{n}_1(e^{qV_E/kT} - 1) + \frac{A_2}{C}\,\bar{n}_2(e^{qV_C/kT} - 1)\right] \quad (3\text{-}43)$$

where we have defined

$$A_1 \equiv \frac{qD_{n1}}{L_{n1}} \frac{1}{\sinh \frac{w_1}{L_{n1}}} , \qquad A_2 \equiv \frac{qD_{n2}}{L_{n2}} \frac{1}{\sinh \frac{w_2}{L_{n2}}}$$

and

$$C \equiv \frac{qD_{n1}}{L_{n1}} \coth \frac{w_1}{L_{n1}} + \frac{qD_{n2}}{L_{n2}} e^{-\Delta E/kT} \coth \frac{w_2}{L_{n2}} \qquad (3\text{-}44)$$

The distributions of the excess electron density and the electron diffusion current are obtained by substituting eq. (3-42) and eq. (3-43) into eqs. (3-33),(3-34) and eqs. (3-36),(3-37).

In the N base (region 3 in Fig. 3-5a) of the device, there is only one material, N GaAs. The diffusion equation for minority carriers can be easily solved. Using the conditions for holes at x_c' and x_e'

$$p_3(x_c') = \bar{p}_3(e^{qV_C/kT} - 1) \qquad \text{(from eq. (3-22))}$$

$$p_3(x_e') = \bar{p}_3(e^{qV_{E'}/kT} - 1) \qquad \text{(from eq. (3-23))}$$

we obtain the distribution for excess hole concentration

$$p_3(x) = \frac{1}{\sinh \frac{w_3}{L_{p3}}} \Big[\sinh \frac{x-x_c'}{L_{p3}} \bar{p}_3(e^{qV_C/kT} - 1) + \sinh \frac{x_e'-x}{L_{p3}} \bar{p}_3(e^{qV_{E'}/kT} - 1)\Big] \qquad (3\text{-}45)$$

and the diffusion current for holes

$$J_p(x) = \frac{qD_{p3}}{L_{p3} \sinh \frac{w_3}{L_{p3}}} \Big[\cosh \frac{x_e'-x}{L_{p3}} \bar{p}_3(e^{qV_{E'}/kT} - 1) - \cosh \frac{x-x_c'}{L_{p3}} \bar{p}_3(e^{qV_C/kT} - 1)\Big] \qquad (3\text{-}46)$$

where L_{p3} and D_{p3} are the diffusion length and diffusion constant for holes in region 3.

III.4.3 Transport factors

Using eqs. (3-36), (3-37) and eqs. (3-42), (3-43), one can show that the electron diffusion currents at $x = x_e$ and $x = x_c$ are

$$J_n(x_e) = a(e^{qV_E/kT} - 1) + b(e^{qV_C/kT} - 1) \tag{3-47}$$

$$J_n(x_c) = A(e^{qV_E/kT} - 1) + B(e^{qV_C/kT} - 1) \tag{3-48}$$

where

$$a = A_1\bar{n}_1(\cosh \frac{w_1}{L_{n1}} - \frac{A_1}{C}) , \quad b = -\frac{A_1A_2}{C}\bar{n}_2$$
$$A = \frac{A_1A_2}{C}\bar{n}_1 e^{-\Delta E/kT} , \quad B = -A_2\bar{n}_2(\cosh \frac{w_2}{L_{n2}} - \frac{A_2}{C} e^{-\Delta E/kT}) \tag{3-49}$$

and A_1, A_2 and C are defined in eq. (3-44). We now define

$$t_N \equiv A/a$$

$$= \frac{1}{\frac{D_{n1}}{D_{n2}}\frac{L_{n1}}{L_{n2}} e^{\Delta E/kT} \sinh \frac{w_1}{L_{n1}} \sinh \frac{w_2}{L_{n2}} + \cosh \frac{w_1}{L_{n1}} \cosh \frac{w_2}{L_{n2}}} \tag{3-50}$$

$$t_I \equiv b/B$$

$$= \frac{1}{\frac{D_{n2}}{D_{n1}}\frac{L_{n1}}{L_{n2}} e^{-\Delta E/kT} \sinh \frac{w_1}{L_{n1}} \sinh \frac{w_2}{L_{n2}} + \cosh \frac{w_1}{L_{n1}} \cosh \frac{w_2}{L_{n2}}} \tag{3-51}$$

From eq. (3-47) and eq. (3-48) and the definition of the transport factor (eq. (3-17)), t_N can be regarded as the transport factor for minority carriers flowing from the emitter to the collector when the emitter junc-

tion is forward biased and the collector junction is reversed biased. Similarly t_I can be regarded as the transport factor for minority carriers flowing from the collector to the emitter when the collector junction is forward biased and the emitter junction is reversed biased. We shall call t_N the normal transport factor and t_I the inverse transport factor.

The effect of the barrier height ΔE on the transport factors, t_N and t_I, can be seen very clearly from eq. (3-50) and eq. (3-51). A small barrier with a height of a few kT can reduce the normal transport factor, t_N, by a very large factor. If region 1 and region 2 have the same material and same doping (i.e., $N_{A1} = N_{A2}$, $\Delta E = 0$, $L_{n1} = L_{n2}$, $D_{n1} = D_{n2}$), the expressions for t_N and t_I reduce to the ordinary expressions of the transport factors.[3] They are

$$t_N = t_I = \frac{1}{\cosh \frac{w}{L_n}} \tag{3-52}$$

where $w = w_1 + w_2$ and $L_n = L_{n1} = L_{n2}$. For the case of $\Delta E \gg kT$, $L_{n1} \gg w_1$, and $L_{n2} \gg w_2$ the transport factors become approximately

$$t_N \simeq \frac{D_{n2}}{D_{n1}} \frac{L_{n1}^2}{w_1 w_2} e^{-\Delta E/kT} \tag{3-53}$$

$$t_I \simeq 1 \tag{3-54}$$

In the forward direction (the electrons being transported from the emitter to the collector) the transport factor is greatly reduced due to the potential barrier. But in the reverse direction the transport factor is

unity since no barrier exists. In the devices which we fabricated, eq. (3-53) and eq. (3-54) are nearly true because the widths of the base regions are usually on the order of 1 μm or less and the barrier height is usually much higher than kT.

In the PNP transistor part of the device, there is only one material (N GaAs) in the base. From eq. (3-46) the hole currents at the emitter and the collector junctions are

$$J_p(x_e') = a'(e^{qV_{E'}/kT} - 1) + b'(e^{qV_C/kT} - 1) \qquad (3\text{-}55)$$

$$J_p(x_c') = A'(e^{qV_{E'}/kT} - 1) + B'(e^{qV_C/kT} - 1) \qquad (3\text{-}56)$$

where

$$a' = -B' = \frac{qD_{p3}}{L_{p3}} \coth \frac{W_3}{L_{p3}} \bar{p}_3 \qquad (3\text{-}57)$$

$$A' = -b' = \frac{qD_{p3}}{L_{p3}} \frac{\bar{p}_3}{\sinh \frac{W_3}{L_{p3}}} \qquad (3\text{-}58)$$

The transport factors are therefore

$$t_N' \equiv \frac{A'}{a'} = \frac{1}{\cosh \frac{W_3}{L_{p3}}} \qquad (3\text{-}59)$$

and

$$t_I' \equiv \frac{b'}{B'} = \frac{1}{\cosh \frac{W_3}{L_{p3}}} \qquad (3\text{-}60)$$

III.4.4 I-V Characteristics

The total current flowing across the emitter junction E (see Figs. 3-5) is the sum of the electron diffusion current at x_e, the hole diffusion current at the edge of the depletion region in the emitter and the recombination current I_R in the depletion region. Since this junction is a heterojunction and the emitter has a larger band gap than the base, the hole current injected into the emitter is negligible compared with the electron current injected into the base. Therefore the total current J is

$$J = J_n(x_e) + I_R = a(e^{qV_E/kT} - 1) + t_I B(e^{qV_C/kT} - 1) + I_R \qquad (3\text{-}61)$$

where we have used the relation $b = t_I B$. At the other emitter junction E' we obtain a similar expression for the total current.

$$J = J_p(x_e') + I_R' = a'(e^{qV_{E'}/kT} - 1) + t_I' B'(e^{qV_C/kT} - 1) + I_R' \qquad (3\text{-}62)$$

where J_R' is the recombination current in the depletion region of the junction E'. When qV_E, $qV_{E'} >> kT$, I_R and I_R' are of the form[11]

$$I_R = I_o e^{qV_E/2kT} \quad , \; I_R' = I_o' e^{qV_{E'}/2kT} \qquad (3\text{-}63)$$

where I_o and I_o' are some constants.

At the collector, the junction is reverse biased because it is operated below the holding point. If this reverse biased voltage is sufficiently high, the electrons and the holes entering the junction and the

carriers thermally generated in the space charge region will be accelerated by the electric field in this region and collide with the valence electrons and the lattice, causing avalanche multiplication. The total current flowing across the collector junction is, therefore,

$$J = M[J_n(x_c) + J_p(x_c') + I_G] \tag{3-64}$$

where M is the multiplication factor, which is a function of V_c. I_G is the current generated in the space charge region, which can be due to thermogeneration, light activation or other means which can generate electron-hole pairs. It also has the effect of the leakage current or the gate current. Substituting eq. (3-56) and eq. (3-48) into eq. (3-64), we get

$$J = M[t_N a(e^{qV_E/kT} - 1) + t_N' a'(e^{qV_{E'}/kT} - 1) + (B + B')(e^{qV_C/kT} - 1) + I_G] \tag{3-65}$$

The total voltage drop across the device is the sum of the voltage drops in the three PN junctions, i.e.,

$$V = V_E + V_C + V_{E'} \tag{3-66}$$

Now, since there are five unknowns, V, J, V_E, V_C, and $V_{E'}$, in the four equations, eqs. (3-61),(3-62), (3-65), and (3-66), we can eliminate V_E, V_C, and $V_{E'}$ from these equations and get the relation between J and V. Some numerical calculations of the I-V characteristics will be given in the next section.

The injection efficiencies γ, γ' of the two emitter junctions can be calculated from eq. (3-61) and eq. (3-62). They are

$$\gamma \equiv \frac{J_n(x_e)}{J} = \frac{1}{J}\left[a(e^{qV_E/kT} - 1) + t_I B(e^{qV_C/kT} - 1)\right] \qquad (3\text{-}67)$$

$$\gamma' \equiv \frac{J_p(x_c')}{J} = \frac{1}{J}\left[a'(e^{qV_{E'}/kT} - 1) + t_I' B'(e^{qV_C/kT} - 1)\right] \qquad (3\text{-}68)$$

Combining these two equations with eq. (3-65), we get

$$J = \frac{M\, I_G + M[(1 - t_N t_I)B + (1 - t_N' t_I')B'](e^{qV_C/kT} - 1)}{1 - M(\alpha + \alpha')} \qquad (3\text{-}69)$$

where $\alpha \equiv \gamma t_N$ and $\alpha' \equiv \gamma' t_N'$ are the common base current gains of the NPN and PNP transistors, respectively. When the denominator on the right hand side of eq. (3-69) approaches zero, $J \to \infty$. Therefore, switching will result if

$$M(\alpha + \alpha') = 1 \qquad (3\text{-}70)$$

Since the alphas are proportional to the transport factors, which are controlled by the potential barrier in the base and can be made very small, the alphas can be reduced to small values by the barrier. The multiplication factor M is a function of the reverse bias voltage V_C, or approximately the total blocking voltage, and increase with V_C. Therefore, small alphas will result in a greater breakover voltage.

III.4.5 Numerical results

In this subsection we present the numerical solutions of the equations derived in the last subsection. The structure used in the calculations is shown in Fig. 3-5a. The parameters of the base regions are given in Table 3-1. The energy difference ΔEg in the band gaps of the two materials, $Ga_{1-y}Al_yAs$ and GaAs, in the P base region depends on the Al content y and is taken as a variable parameter. The two emitters are $Ga_{1-x}Al_xAs$ with Al content x = 0.4. I_o and I_o' for the two emitter junctions are taken to be 10^{-9} A/cm^2 and 3.33×10^{-10} A/cm^2, respectively. The multiplication factor, M, as a function V_C/V_{BD} is taken from the calculations of Leguerre et al.[9]

The I-V characteristics of the device are solved using eqs. (3-61), (3-62), (3-65), and (3-66). Fig. 3-7 shows the I-V curves with different I_G's when ΔEg = 8 kT (corresponding to y = 0.2 in the $Ga_{1-y}Al_yAs$ barrier layer). These curves are similar to the usual characteristics of a PNPN device with different triggering levels. Fig. 3-8 gives the I-V curves at I_G = 0.01 A/cm^2 with different ΔEg's. It is clear from this figure, that the breakover voltage increases with the height of the potential barrier. As explained before, this is because the transport factor decreases as the barrier height is increased. The holding current I_h (defined as the current at V_C = 0), which is the current at the upper limit of each curve, also increases with ΔEg. Fig. 3-9 is the plot of I_h as a function of ΔEg at I_G = 0. I_h increases very rapidly with increasing ΔEg and the larger the ΔEg, the greater is the rate of increase.

Region	Material	Width (μm)	Doping Concentration (cm^{-3})	Mobility (cm^2/V-sec)	Diffusion Length (μm)
1	P GaAs	0.4	10^{17}	$\mu_{n1} = 3000$	7
2	P $Ga_{1-y}Al_yAs$	1.7	3×10^{16}	$\mu_{n2} = 3000$	7
3	N GaAs	0.5	10^{18}	$\mu_{p3} = 300$	2

Table 3-1 Parameters of the base regions used in the numerical calculations

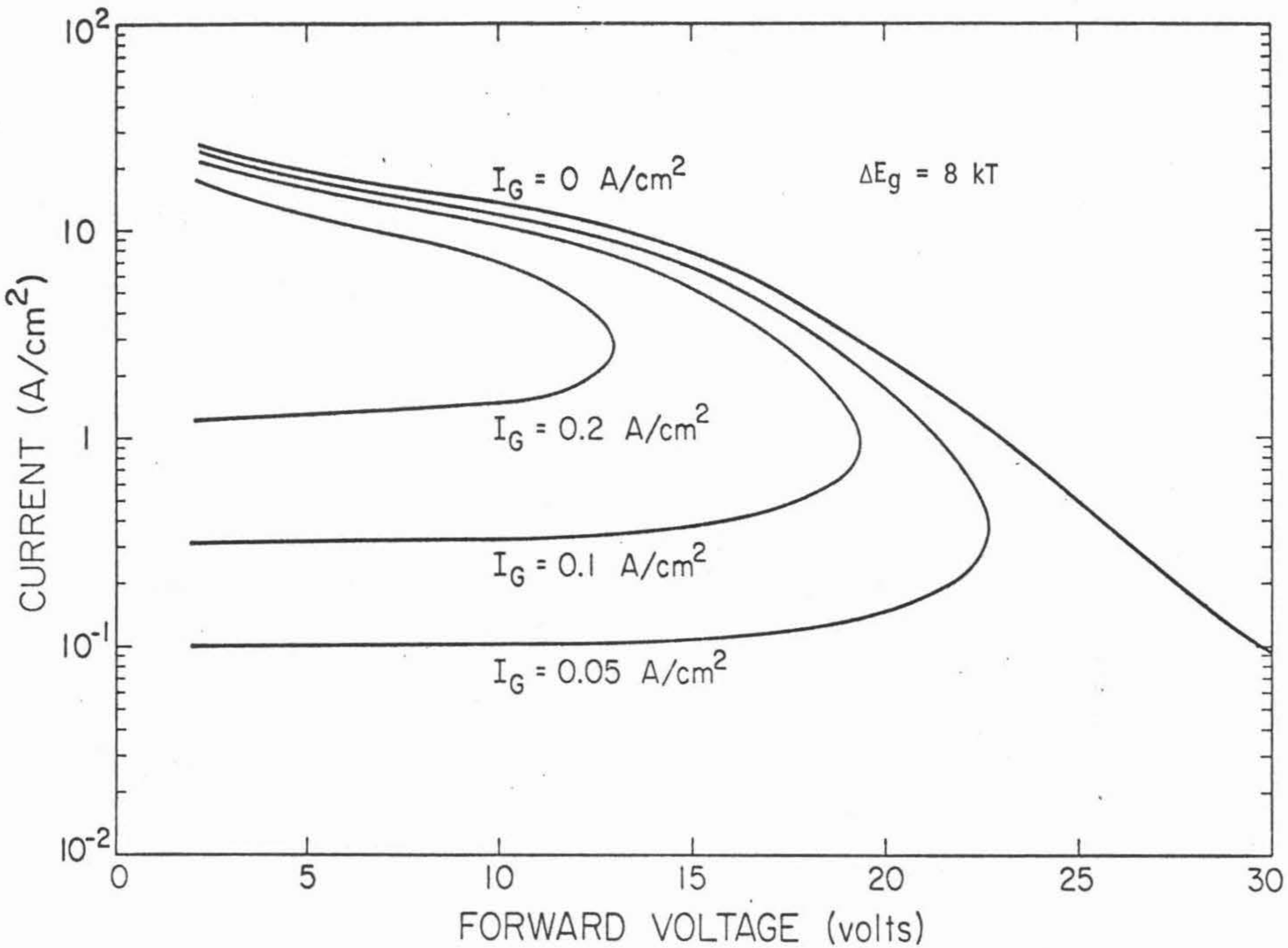

Fig. 3-7 Forward I-V characteristics (below holding point) when $\Delta Eg = 8$ kT. I_G is used as a parameter

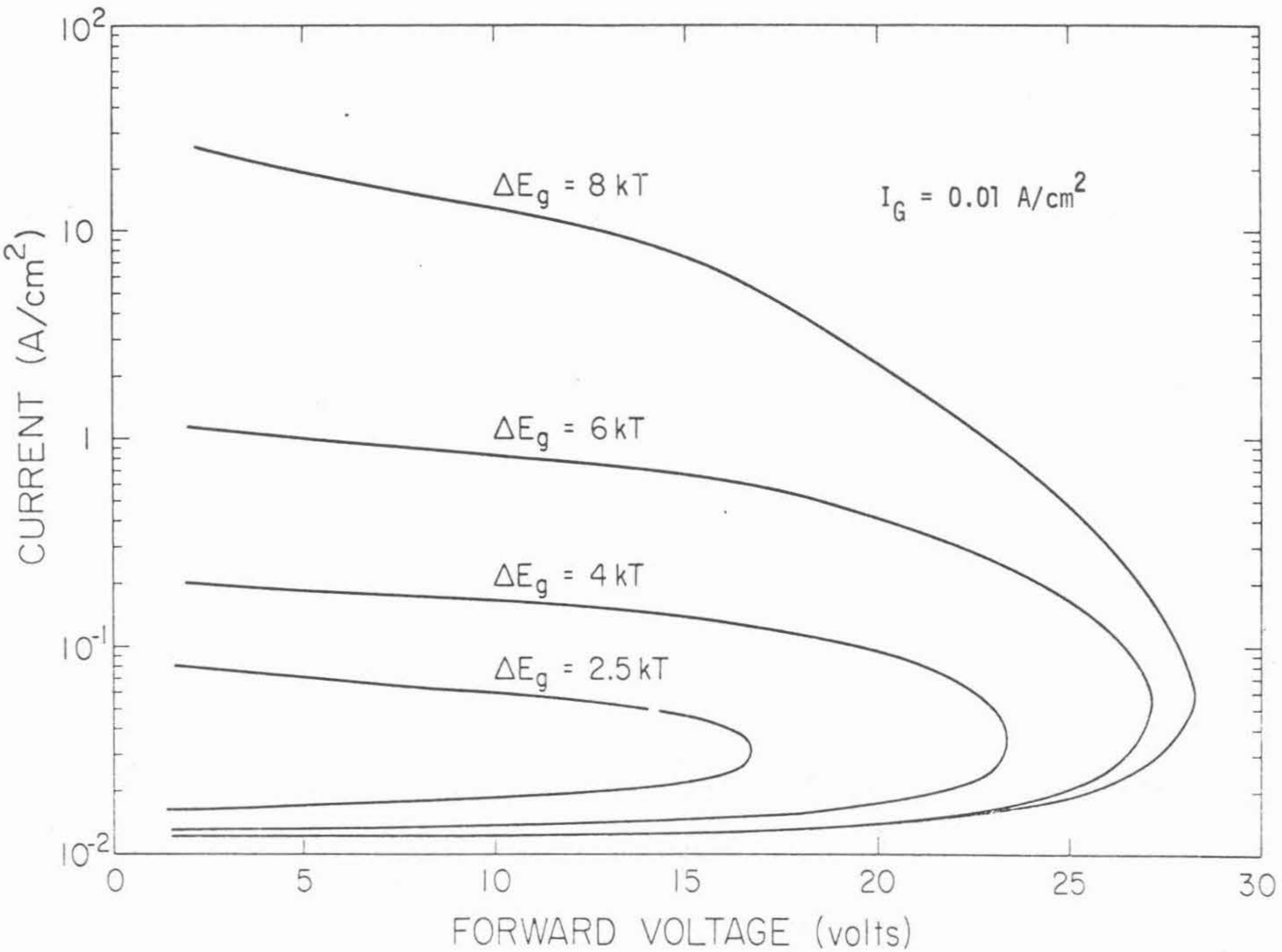

Fig. 3-8 I-V characteristics when $I_G = 0.01\ A/cm^2$. ΔEg is used as a parameter.

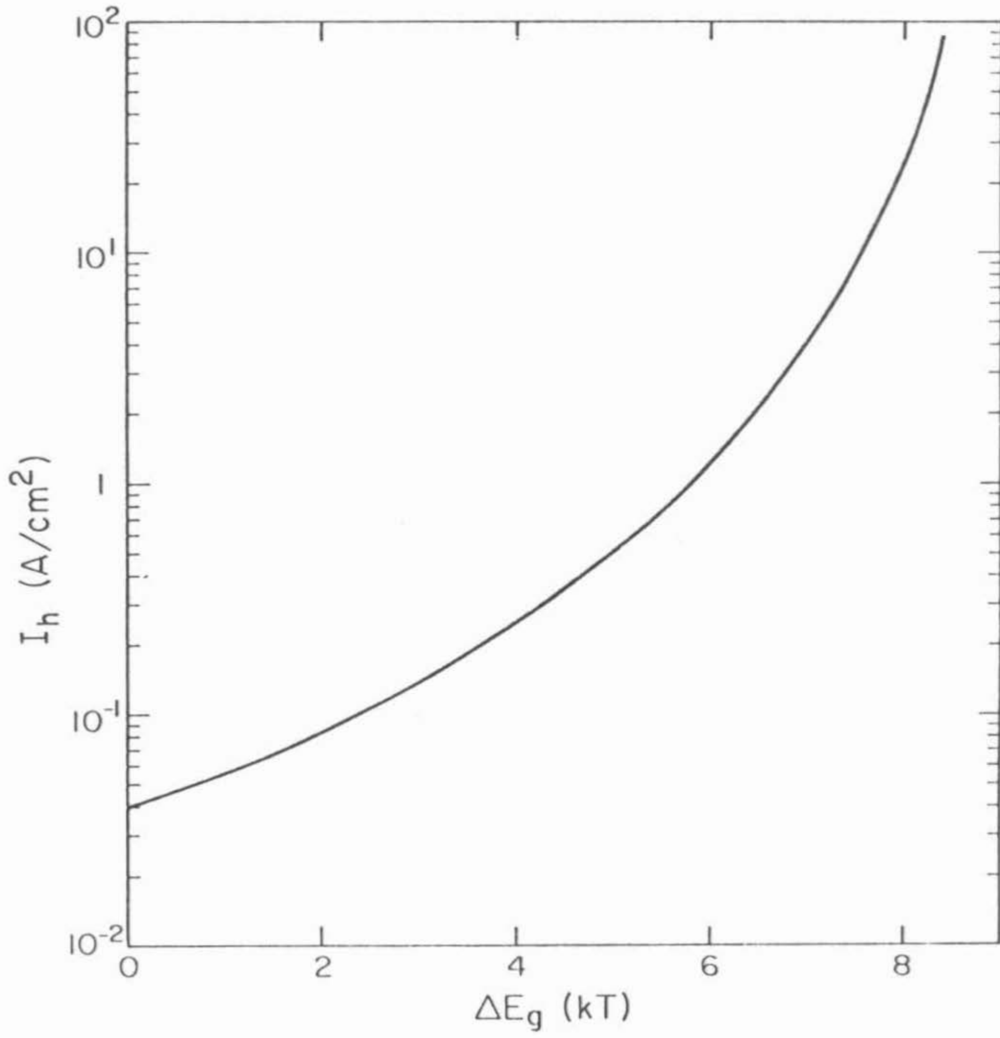

Fig. 3-9 Holding current as a function of ΔE_g.

The plot of the breakover voltage V_{BO} as a function of ΔEg with I_G as as parameter is shown in Fig. 3-10. For each $I_G \neq 0$ the breakover voltage increases with ΔEg and increases slowly when ΔEg is large and very quickly when ΔEg is small. This figure also shows that each curve (with a particular value of I_G) has some minimum value of ΔEg, where V_{BO} drops very sharply. If the band gap difference between the P GaAs and the P $Ga_{1-y}Al_yAs$ is smaller than this value there is no breakover, and therefore, no negative resistance region in the I-V curve. Physically, this is understandable because the alpha of the device becomes higher as the barrier height is reduced, and when ΔEg is smaller than a certain value the alphas, or the gain, will be too high for the device to sustain a negative resistance region. We have shown experimentally that a PNPN device having the same dimensions as we discussed here shows an I-V curve just like those of regular PN diodes if there is no potential barrier in the base regions.

The excess minority carrier distribution in the base regions has been calculated at the holding point (V_C = 0) for the case when ΔEg = 8 kT and I_G = 0. The curve is shown in Fig. 3-11. The discontinuity of the curve at the boundary of P GaAs and P $Ga_{1-y}Al_yAs$ shows the effect of the potential barrier.

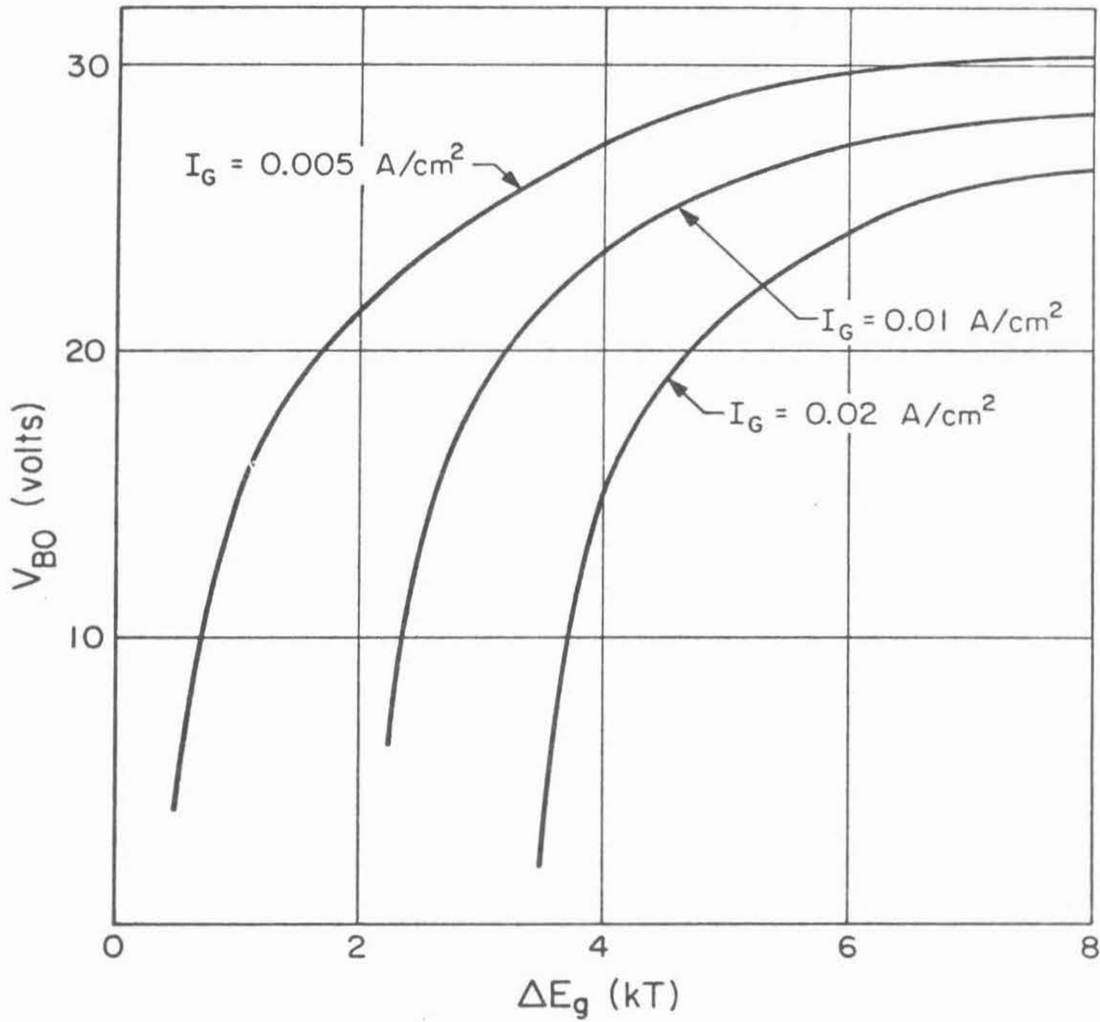

Fig. 3-10 Breakover voltage V_{BO} as a function of ΔE_g. I_G is used as a parameter

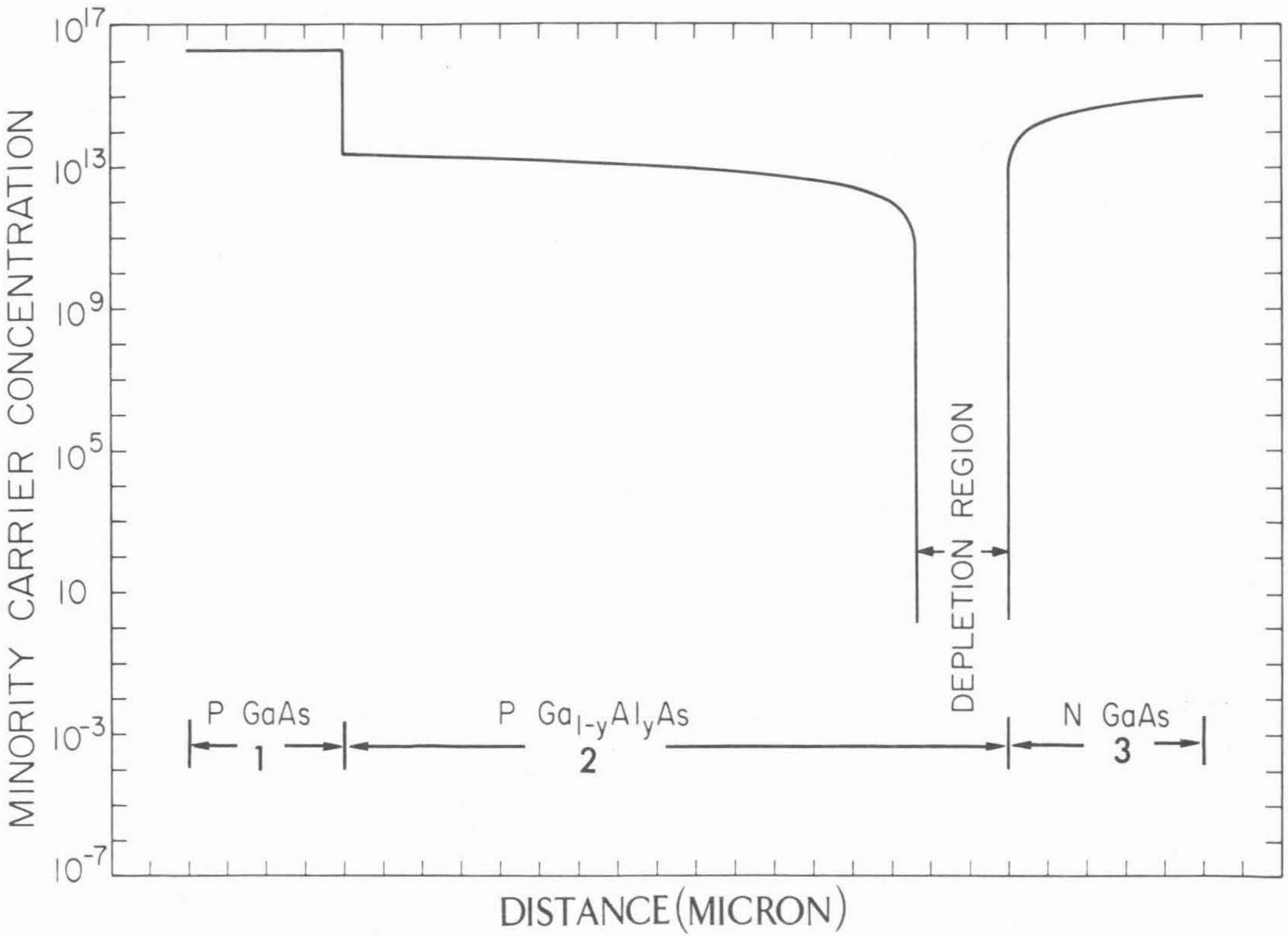

Fig. 3-11 The minority carrier distribution in the base region

III.5 Characteristics Near the Lasing Threshold

We have shown in Fig. 3-11, that when a $Ga_{1-y}Al_yAs$ barrier layer is present in the P base of the device, the number of injected carriers in region 1 (P GaAs) is higher than those in other regions of the bases. If we continue to increase the driving current and operate the device above the holding point, an increasing number of carriers will be injected into this region. When the number of injected carriers reaches some threshold value, lasing action, or stimulated recombination, will take place. The driving current at this point is the lasing threshold current and region 1 is the lasing active region.

Near lasing threshold, the carrier density in the active region is usually higher than the doping concentration. High level conditions ($n = p >> N_{p1}$) have to be used to solve for the carrier and current distributions in this region. Under high level conditions the carrier concentration in region 1 satisfies the ambipolar diffusion equation,[12] namely

$$\frac{d^2 n_1}{dx^2} = \frac{n_1}{{L_I}^2} \tag{3-71}$$

where L_I is the ambipolar diffusion length, defined by

$${L_I}^2 = \frac{2\ D_{n1}(\tau_{no} + \tau_{po})}{b + 1} \tag{3-72}$$

where $b = D_{n1}/D_{p1}$, τ_{no} and τ_{po} are the lifetimes of electrons and holes, respectively. Subject to the conditions $n_1(x) = n_1(x_e)$ at $x = x_e$ and

$n_1(x) = n_1(x_1)$ at $x = x_1$, the solution of eq. (3-71) is

$$n_1(x) = \frac{1}{\sinh \frac{w_1}{L_I}} [n_1(x_e) \sinh \frac{x_1 - x}{L_I} + n_1(x_1) \sinh \frac{x - x_e}{L_I}] \quad (3\text{-}73)$$

In regions 2 and 3 we assume the low level conditions are still valid. The distributions of the minority carrier densities are the same as shown in equations (3-34) and (3-45).

To solve for the carrier distribution in the base regions, we need to know the boundary condition for electron densities (the relation between $n_1(x_1)$ and $n_2(x_1)$) at the boundary of P GaAs and P $Ga_{1-y}Al_yAs$. Let us refer again to Fig. 3-4c, the band diagram of the device near the lasing threshold. The electron quasi-Fermi level in the P GaAs active region is higher than the edge of the conduction band because of population inversion. In order to know the electron concentration in this region we have to use the more accurate Fermi-Dirac function instead of the Boltzmann function. If ξ is the quasi-Fermi level measured from the bottom of the conduction band of P GaAs at $x = x_1$, the electron density at this point is

$$n_1(x_1) + \bar{n}_1 = N_{C1} \frac{2}{\sqrt{\pi}} F_{1/2}(\frac{\xi}{kT}) \quad (3\text{-}74)$$

where $F_{1/2}$ is the Fermi-Dirac integral.[3] In the P $Ga_{1-y}Al_yAs$ barrier region, we assume that the barrier is high enough so that the quasi-Fermi level is lower than the conduction band edge. The electron density in this region at $x = x_1$ is, therefore,

$$n_2(x_1) + \bar{n}_2 = N_{C2} e^{-(E_{C2} - E_f)/kT} \tag{3-75}$$

where E_{C2} is the energy at the bottom of the conduction band of region 2 (P $Ga_{1-y}Al_yAs$) and E_f is the Fermi level at $x = x_1$. The equilibrium values of the electron densities in region 1 and region 2 are related by

$$\frac{\bar{n}_2}{\bar{n}_1} = \frac{N_{C2}}{N_{C1}} e^{(E_{C1} - E_{C2})/kT} \tag{3-76}$$

Substituting this relation into eq. (3-75) we get

$$n_2(x_1) + \bar{n}_2 = \frac{\bar{n}_2}{\bar{n}_1} N_{C1} e^{\xi/kT} \tag{3-77}$$

The boundary condition for electron density at $x = x_1$ is thus obtained by eliminating ξ from eq. (3-74) and eq. (3-77).

The electron current in region 1, under high level conditions, satisfies[12]

$$J_{n1}(x) = \frac{bJ - 2qD_{n1} \frac{dn_1}{dx}}{b + 1} \tag{3-78}$$

where J is the total current density flowing through the device. In the other two regions of the bases (P $Ga_{1-y}Al_yAs$ and N GaAs) since low level conditions are still valid, eq. (3-37) and eq. (3-46) are used to calculate the diffusion currents. At the two emitter junctions, since the total current is high when the device is near lasing threshold, the recombination currents in the depletion regions can be neglected.

The minority currents injected into the emitters are also negligible because the $Ga_{1-x}Al_xAs$ emitters have wider band gaps than GaAs. At $x = x_e$ the total current is, therefore, equal to the electron current injected into the base. Thus

$$J = J_n(x_e) \tag{3-79}$$

Using this relation with eq. (3-78), we obtain for the total current

$$J = J_n(x_e) = -\ 2qD_{n1} \left.\frac{dn_1}{dx}\right|_{x=x_e} \tag{3-80}$$

At the other emitter, $x = x_e'$, we get similarly

$$J = J_p(x_e') \tag{3-81}$$

At the collector junction, since it is now forward biased, the multiplication factor M is equal to one. I_G is negligible compared with the total current. So

$$J = J_n(x_e) + J_p(x_e') \tag{3-82}$$

$J_n(x_c)$ and $J_p(x_c')$ are the same as shown in equations (3-48), (3-56). The continuity of electron current at $x = x_1$ requires

$$J_{n1}(x_1) = J_{n2}(x_1) \tag{3-83}$$

Substituting eq. (3-78) into eq. (3-83) we get

$$\frac{b}{1+b} J - \frac{2qD_{n1}}{1+b} \left.\frac{dn_1}{dx}\right|_{x=x_1} = J_{n2}(x_1) \tag{3-84}$$

Equations (3-80), (3-81), (3-82), (3-84) and the boundary condition of the electron densities at $x = x_1$ are the necessary conditions one needs to solve for the carrier distribution in the base regions.

The ambipolar diffusion equation (eq. (3-71)), which we used to solve for the electron distribution in region 1 holds true when the device is operated at or below lasing threshold. Above threshold, however, this equation is only an approximation because it does not include the stimulated process. Stimulated recombination of carriers in the active region is related to the optical power density of the laser light and is very important when the device is lasing. If one wants to know exactly the carrier distribution in the active region, one has to solve the diffusion equation (eq. (3-71)) with an added term of stimulated recombination. However, even without solving the equation, it is still possible to know approximately the carrier concentration. Below lasing threshold, the number of carriers in the active region increases with the driving current. When the carrier density reaches some threshold value, stimulated recombination begins. Because of the stimulated recombination, the number of carriers in the active region will not increase with the current, but will be clamped at the threshold value. This phenomenon is the so-called gain saturation.(13) Therefore, above threshold, the carrier concentration in the active region can be taken to be the same as the threshold value, and does not change with current.

The threshold carrier concentration depends on the thickness of the active region and the loss of the laser cavity. In our PNPN device the active layer (region 1) is 0.4 μm thick. If the optical and the

electrical confinement provided by the confining layers is sufficient the threshold carrier concentration for lasing can be estimated to be about 1.5×10^{18} cm^{-3}.[14] Using this value as $n_1(x_1)$ and substituting it into the equations derived earlier in this section, which are assumed to be valid at the threshold, one can easily calculate the minority carrier distribution in the bases and the threshold current density. When the device is driven above threshold, the number of carriers in region 1 is clamped. Since this active region is much narrower than the carrier diffusion length it is reasonable to assume that the carriers are clamped uniformly. In this way the carrier density is assumed constant at the threshold value, and we don't need to solve the equations exactly. In regions 2 and 3, since they are not the lasing regions, the carrier distribution can be still calculated using the diffusion equations derived earlier.

We have made calculations on a structure having dimensions the same as those given in Table 3-1 and a band gap difference between the barrier and the active regions of 8 kT. The minority carrier distributions in the base at different currents are shown in Fig. 3-12. It can be seen very clearly that the P $Ga_{1-y}Al_yAs$ potential barrier confines the carriers in the P GaAs active region. Because of this confinement the lasing threshold can be made as small as the threshold of a regular double heterostructure laser. The threshold current density calculated in our example is 3.64 kA/cm^2, which is very close to what we achieved experimentally.

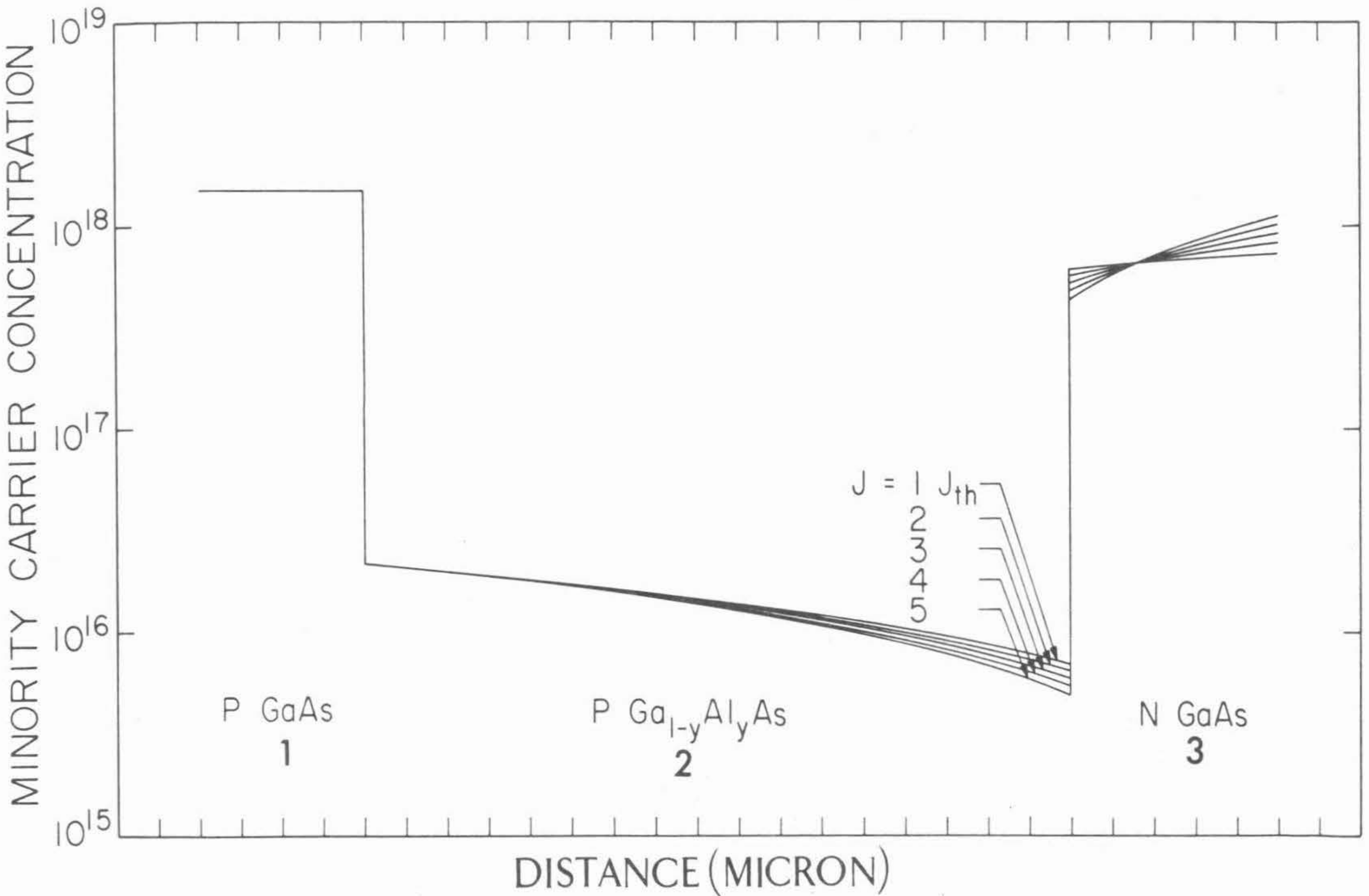

Fig. 3-12 Minority carrier distribution in the base regions at different currents above lasing threshold

III.6 Experimental Results

The barrier controlled PNPN devices were fabricated using our horizontal liquid phase epitaxial growth system. The epitaxial layers were grown on a (100) oriented N type GaAs substrate with doping concentration $n = 3 \times 10^{18}$ cm^{-3}. The layers included, from the bottom, N $Ga_{1-x}Al_xAs$ emitter, P type base, N type base, P $Ga_{1-x}Al_xAs$ emitter, and last a P^+ GaAs layer. The two emitters had Al content $x = 0.4$, and were doped in excess of 10^{18} cm^{-3}. The base layers were doped to about 5×10^{16} cm^{-3}. The last layer, P^+ GaAs, was used to achieve a better ohmic contact.

We have fabricated three types of devices: (1) with no potential barriers, (2) with a single barrier in the P base, (3) with double barriers, one in the P base and one in the N base. Some of the parameters and the measured results of these three kinds of devices are listed in Table 3-2. The devices with no barriers, which have only GaAs in the bases, had I-V curves just like those of ordinary PN diodes and showed no negative resistance regions when the base widths were about 0.5 μm. The diodes with single barrier and double barriers had breakover voltages varying from 10 to 35 volts. The holding currents were about 10 A/cm^2 and 150 A/cm^2 for the single barrier and the double barrier devices, respectively. The results show that when the bases are thin and contain no potential barriers, the devices have too much gain and, therefore, cannot function as normal PNPN devices. The gain in the devices with barriers is greatly reduced. The double barrier devices have the lowest gain and this is clearly indicated by the high value of the holding current.

		N Emitter	P Base		N Base		P Emitter	P^+			
		$Ga_{1-x}Al_xAs$	GaAs	$Ga_{1-y}Al_yAs$	$Ga_{1-y}Al_yAs$	GaAs	$Ga_{1-x}Al_xAs$	GaAs	$J_h(\frac{A}{cm^2})$	V_{BO}(volt)	$J_{th}(\frac{KA}{cm^2})$
No Barrier	1	x = 0.3 2 μm	2 μm	—	—	2 μm	x = 0.3 1.8 μm	1 μm	1 - 3	5 - 10	no lasing
	2	x = 0.3 2 μm	0.5μm	—	—	0.5μm	x = 0.3 2 μm	1 μm	—	—	no lasing
Single Barrier	1	x = 0.4 2 μm	0.3μm	y = 0.2 1 μm	—	0.5μm	x = 0.4 2 μm	1 μm	~10	~10	~5
	2	x = 0.4 1.8 μm	0.2μm	y = 0.2 1.4 μm	—	0.6μm	x = 0.4 2 μm	0.8μm	~9	~10	~4
Double Barrier	1	x = 0.4 2 μm	0.3μm	y = 0.2 1 μm	y = 0.2 1 μm	0.5μm	x = 0.4 2 μm	0.8μm	~150	~15	~3
	2	x = 0.4 2 μm	0.2μm	y = 0.2 1 μm	y = 0.2 1.6 μm	0.5μm	x = 0.4 2 μm	1 μm	~200	~35	~3

J_h: Holding current, V_{BO}: Breakover voltage, J_{th}: Lasing threshold current density

Table 3-2 Layer thicknesses and experimental results of some barrier controlled PNPN devices.

Fig. 3-13a shows a scanning electron micrograph (SEM) of a single barrier device. The P base of this device contains a GaAs layer and a $Ga_{0.8}Al_{0.2}As$ barrier layer. The 20% Al content in the barrier corresponds to a band gap difference, ΔEg, of about 8 kT. The I-V curve obtained for this device is shown in Fig. 3-13b. Since the active region of the barrier controlled PNPN laser can be made very thin, low threshold lasing operation can be achieved. We have measured threshold current density $\sim$ 3 kA/cm^2 at room temperature, which is comparable to our conventional double heterostructure lasers with the same active region thickness.

Because of their negative resistance characteristics, the PNPN devices can be operated in a (current) relaxation oscillation mode using a circuit arrangement shown in Fig. 3-14. If the current pulses passing through the diodes exceed the lasing threshold current, repetitive laser pulses will be obtained. The repetition rate and the pulse duration time can be adjusted by the external resistors and capacitor. This circuit is, therefore, very useful for a PNPN laser because it produces laser pulses without the need for external drives. If we neglect the parasitic inductance and the junction capacitance of the diode, the characteristic times associated with the device in this circuit can be easily shown to be

$$\tau_c = RC \ \ell n \frac{V - V_h}{V - V_{BO}} \qquad (3\text{-}69)$$

Fig. 3-13 (a) An scanning electron micrograph of the cross section of a single barrier PNPN device. (b) The I-V curve of this device.

(a)

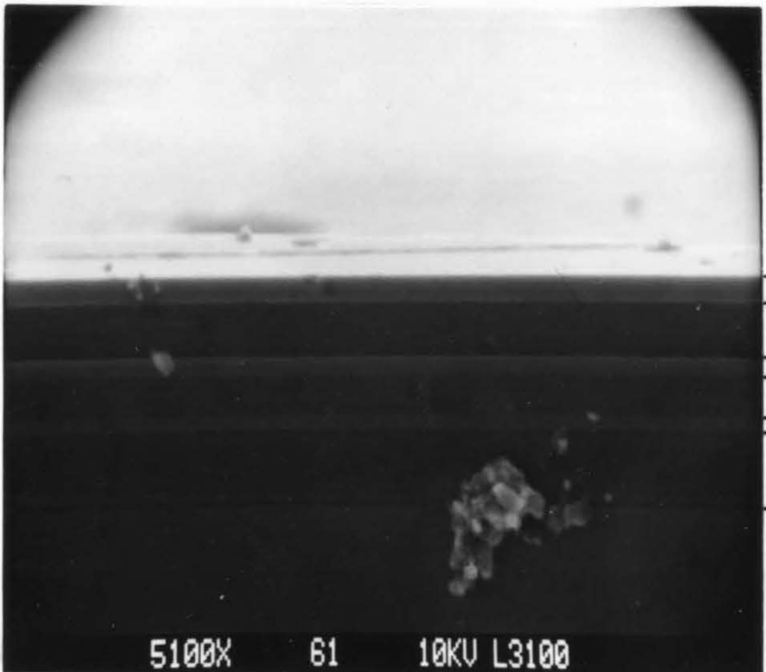

(b)

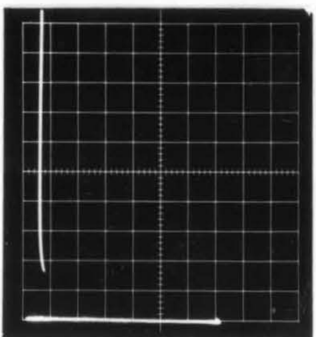

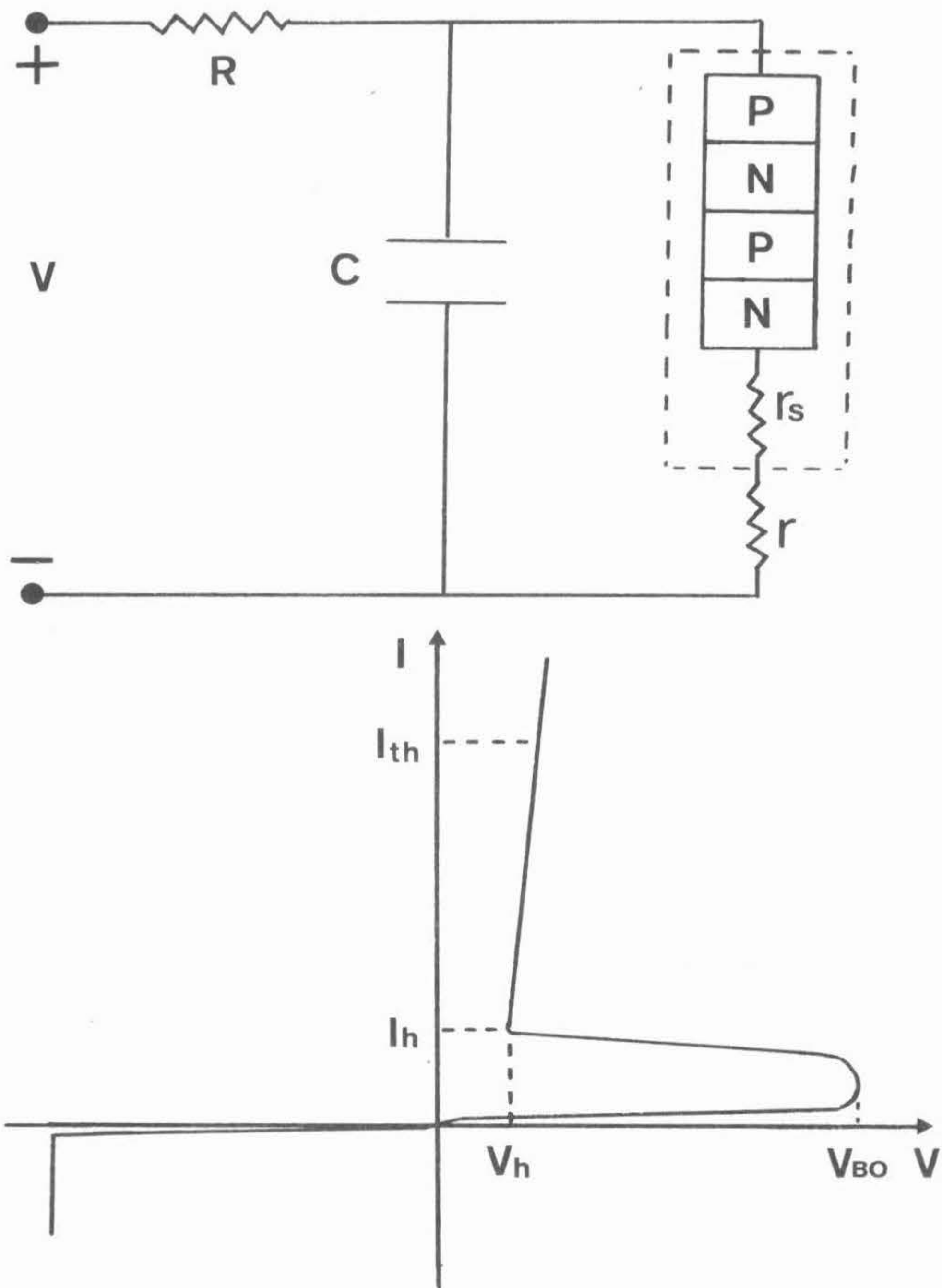

Fig. 3-14 An oscillation circuit for a PNPN laser diode, and the I-V characteristic of the diode. r_S is the series resistance of the diode.

$$\tau_d = (r + r_s)C \, \ell n \frac{V_{BO}}{I_h \, (r + r_s)} \tag{3-70}$$

$$\tau_L = (r + r_s)C \, \ell n \frac{V_{BO}}{I_{th} \, (r + r_s)} \tag{3-71}$$

where τ_c is the time to charge the capacitor C through R from the holding voltage V_h to the breakover voltage V_{BO}, τ_d is the time to discharge C through the diode's resistance r_s and the resistance r, and τ_L is the total on time of the lasing pulse during the discharge of C. The frequency of relaxation oscillation is determined by $(\tau_c + \tau_d)^{-1}$, but since $\tau_d << \tau_c$, it is τ_c that determines the laser pulse repetition rate.

Fig. 3-15a,b are oscillograms of the current and light output of a double barrier device whose I-V curve trace is shown in Fig. 3-15c. The circuit was operated with a bias voltage of 25 V, a charging resistor R = 420 Ω, and a capacitor C = 0.2 μF. The current pulse level was changed by adjusting the 10 Ω trimpot resistor r. The lasing threshold current of this device was I_{th} = 3.3 A. Note that as the current increases from below threshold (Fig. 3-15a) to above threshold (Fig. 3-15b) the light pulse (measured from a S1 photomultiplier) increases in a nonlinear way and also narrows! A plot of the device emission spectrum 10% above threshold is shown in Fig. 3-16.

In conclusion, we have found a new way of controlling the characteristics of a PNPN device. It is achieved by incorporating potential barriers into the base regions. We have realized this concept with GaAs - GaAlAs PNPN heterostructure laser diodes. The barriers are provided by the wider band gap material $Ga_{1-y}Al_yAs$, and the height

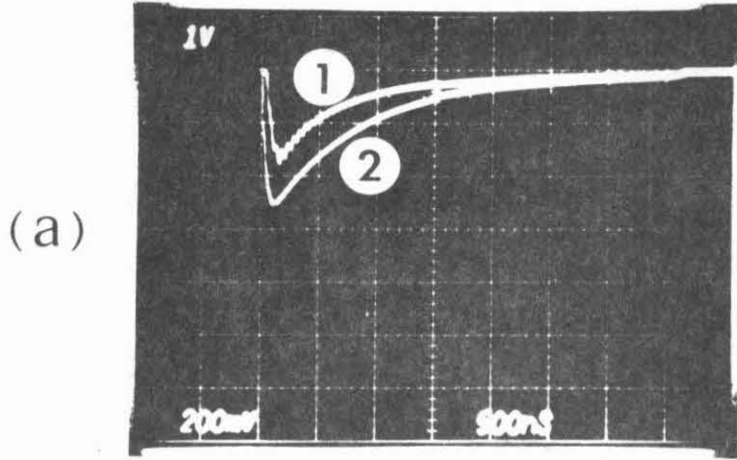

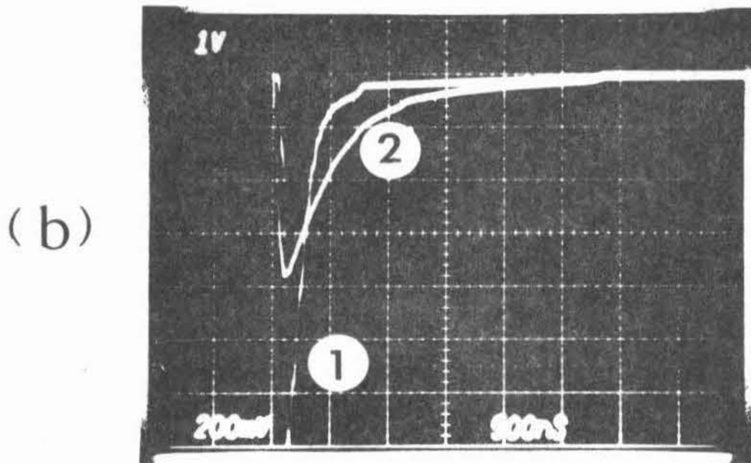

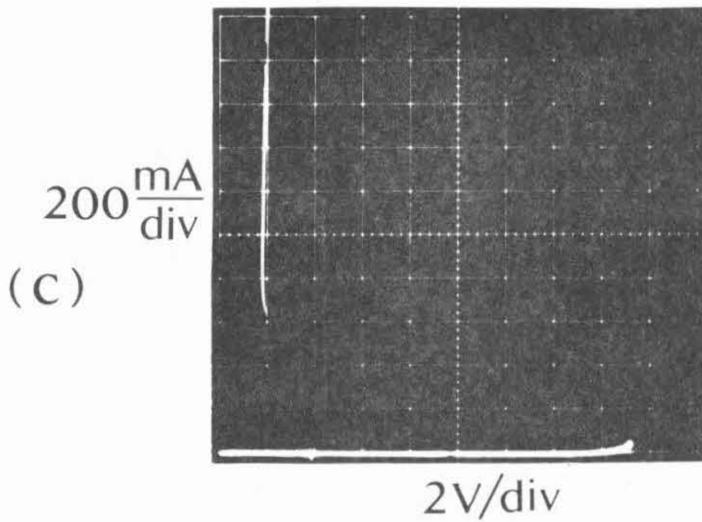

Fig. 3-15 The current and light output oscilloscope traces of a PNPN laser connected in an electronic circuit shown in Fig. 3-14. (a) Below threshold: 1 - light pulse, 2 - current pulse; (b) above threshold: note the narrowing and nonlinear increase of the lasing light pulse relative to the current pulse. (c) is the I-V curve of this laser.

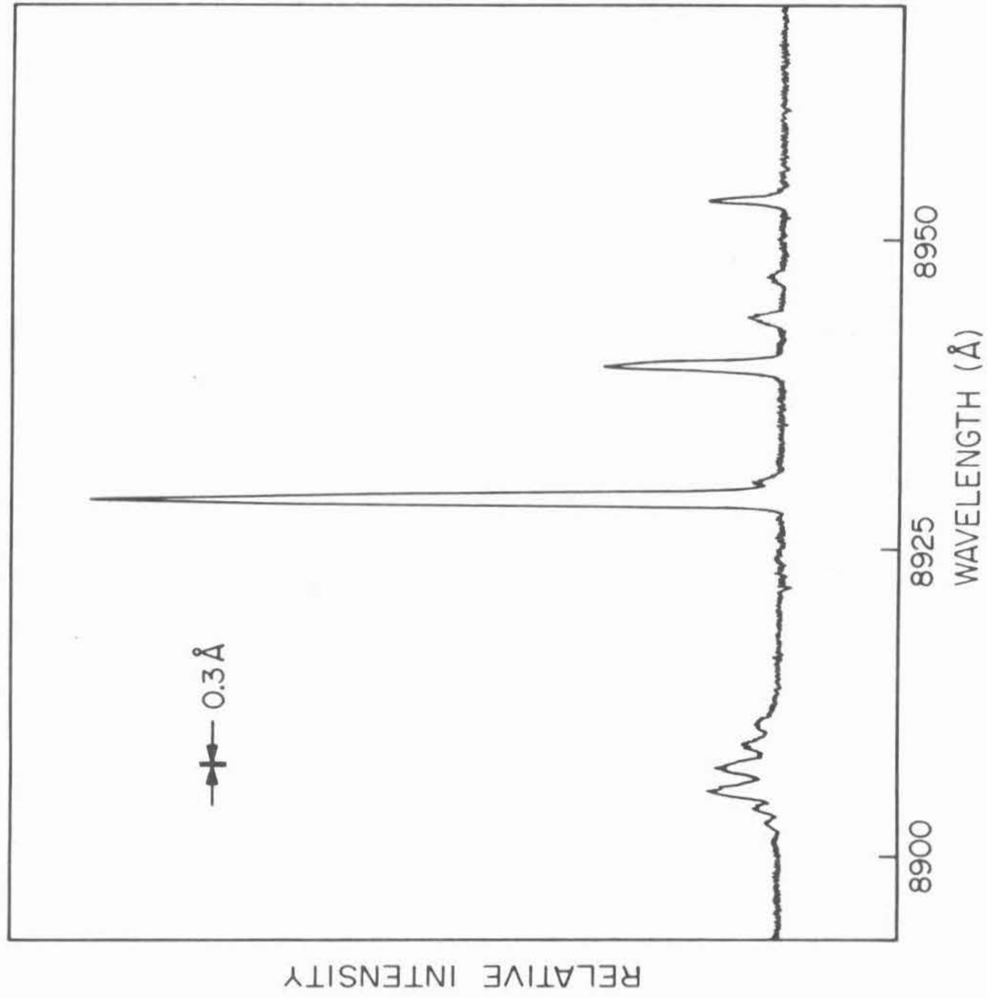

Fig. 3-16 Lasing spectrum of a barrier controlled PNPN laser

of the barriers can be controlled by the Al content y. This $Ga_{1-y}Al_yAs$ barrier not only controls the I-V characteristics of the PNPN operation but also provides the electrical and optical confinement which is necessary for low threshold laser operation. Barrier controlled PNPN lasers with threshold current densities comparable to those of conventional double heterostructure lasers have been achieved.

REFERENCES FOR CHAPTER III

(1) W. Shockley, Electrons and Holes in Semiconductors, D. Van Nostrand Inc. (1950)

(2) J. L. Moll, M. Tanenbaum, J. M. Goldley, and N. Holonyak, "p-n-p-n transistor switches", Proc. IRE, 44, 1174 (1956)

(3) S. M. Sze, Physics of Semiconductor Devices, John Wiley & Sons, Inc., New York (1969)

(4) W. V. Muench, "Gallium arsenide four-layer devices", Solid State Electron. 8, 827 (1965)

(5) C. R. Wronski, C. J. Nuese, and H. F. Gossenberger, "GaAs vapor grown Shockley diodes and semiconductor-controlled rectifiers", IEEE Trans. Electron Device. ED-19, 691 (1972)

(6) C. J. Nuese, J. J. Gannon, M. F. Gossenberger, and C. R. Wronski, "Electroluminescent Shockley diodes of GaAs and $GaAs_{1-x}P_x$", J. Elec. Mater. 2, 571 (1973)

(7) C. P. Lee, A. Gover, S. Margalit, I. Samid, and A. Yariv, "Barrier-controlled low-threshold PNPN GaAs heterostructure laser", Appl. Phys. Lett. 30, 535 (1977)

(8) J. J. Ebers, "Four-terminal p-n-p-n transistors", Proc. IRE, 40, 1365 (1952)

(9) R. Leguerre and J. Urgell, "Approximate values of the multiplication coefficient in one-sided abrupt junctions", Solid State Electron. 19, 857 (1976)

(10) H. F. Lockwood, K. F. Etzold, T. E. Stockton, and D. P. Marinelli, "The GaAs PNPN laser diode", IEEE J. Quantum Electron. QE-10, 567 (1974)

(11) A. S. Grove, Physics and Technology of Semiconductor Devices, John Wiley & Sons, Inc., New york (1967)

(12) R. Kokosa, "The potential and carrier distributions of a PNPN device in the ON state", Proc. IEEE 55, 1389 (1967)

(13) A. Yariv, Quantum Electronics, 2nd edition, John Wiley & Sons, Inc., New York (1975)

(14) M. B. Panish, "Heterostructure injection lasers", Proc. IEEE 64, 1512 (1976)

CHAPTER IV

GaAs-GaAlAs HETEROSTRUCTURE LASERS ON SEMI-INSULATING SUBSTRATES

IV.1 Introduction

During the last ten years or so GaAs technology has evolved along two main directions. One is that of optical devices, the other in the area of electronic devices. As described in the previous chapters, the interest in GaAs as a basic material for optical devices is due to the following facts: (1) It is a direct bandgap semiconductor suitable for laser operation. (2) The $Ga_{1-x}Al_xAs$ ternary system, which is lattice matched to GaAs, has optical characteristics which are strongly dependent on x and can be easily grown epitaxially. (3) It has high electro-optic, acousto-optic and optical nonlinear coefficients making it applicable to a variety of switching, modulation and frequency conversion devices. Using GaAs-GaAlAs heterostructures, it became possible to fabricate optical devices such as low threshold single mode lasers,[1-3] waveguides,[4,5] modulators and couplers,[6,7] etc. In parallel, a great amount of progress has been made on the development of GaAs electronic devices. The major reasons for the development are: (1) In GaAs the conduction electrons have mobilities which are six times larger and a peak drift velocity which is bigger by a factor of two than in Si.[8] This causes the parasitic resistance to be smaller, the transconductance to be larger, and a shorter transit time of electrons in the high field region. (2) The existence of semi-insulating GaAs substrates makes it possible to fabricate monolithic integrated circuits with low parasitic

capacitance, low loss interconnections, and high packing density. (3) Bulk effects in GaAs makes it suitable for fabricating Gunn oscillators.[9] Due to the rapidly increasing needs for high speed communication systems and the saturation of low frequency communication bands there is an increasing demand for microwave devices capable of operation at high frequencies ($>$ 1 GHz). The severe limitations of most devices at the high microwave frequencies make GaAs the most promising material to operate in this regime. Today, GaAs field-effect-transistors (FET) capable of operating at frequencies higher than 10 GHz, for example, can be easily fabricated on epitaxial layers or on ion-implanted layers.[10]

Although progress has been made in both the optical devices and the electronic devices, the integration of these two kinds of devices has not been achieved. The difficulty of integration is due to the fact that most of the optical devices at present are fabricated on highly conductive substrates. For example, conventional GaAs lasers use heavily doped N type substrates. The P type contact is applied on the top of the P type epilayers and the N type contact is made on the bottom of the substrate. Current flows from one side to the other across the junction. Monolithic integration of this type of lasers with electronic devices is almost impossible. One way of solving this problem is to fabricate the optical devices on semi-insulating substrates and to confine the current flow to the thin epilayers on the substrate. By so doing one is able not only to achieve the electrical isolation which is needed for integration, but also to apply conventional planar technology in the device fabrication.

In this chapter we describe two different laser structures fabricated on semi- insulating GaAs substrates. They are the first injection lasers reported on semi-insulating substrates. Because of the non-conductive substrate, current flows laterally along the epilayers. Instead of a two-dimensional design which is needed for ordinary stripe geometry lasers, we need to employ a three-dimensional design for lasers on semi-insulating substrates. The laser which is described in section IV.2 is called the crowding effect laser.[11] The laser action is based on carrier confinement via the crowding effect. The second laser, which is described in section IV.3,is called the lateral injection laser.[12] The PN junction of this laser is not parallel to the epilayers. Current flows laterally across the junction.

These newly developed lasers are natural candidates for monolithic integration with other devices sharing the same crystalline layers. Section IV.5 describes an experimentally demonstrated device - a laser with a Gunn oscillator on a single chip of semi-insulating GaAs.[13] Other types of integration are suggested.

Fabricating GaAs-GaAlAs injection lasers on semi-insulating substrates not only revolutionizes the design of conventional injection lasers but also opens up a new field for integrated optics.

Before we discuss the laser structures it is necessary to describe briefly what semi-insulating GaAs is. Semi-insulating GaAs is obtained by adding chromium (Cr) atoms (deep acceptors) to GaAs. The first successful preparation of Cr doped high resistivity GaAs was made by Cronin and Haisty.[14] The high resistivity of the material is due

to the compensation of residual shallow donors and deep donors associated with oxygen impurities by deep Cr acceptors.[15] In this way it is possible to make "semi-insulating" GaAs with resistivity in the range of 10^8 ohm-cm. This resistivity is sufficient to assure good isolation between devices in an integrated circuit. The semi-insulating GaAs substrates used in our experiments were purchased from Laser Diode Laboratory. The resistivity of the wafers is $>10^7$ ohm-cm, and the etched pit density is about 3000 cm^{-2}. The wafers are about 400 μm thick, and the surfaces are oriented in the [100] direction.

IV.2 GaAs-GaAlAs Heterostructure Lasers on Semi-Insulating Substrates using Carrier Crowding

As a first step, ordinary GaAs-GaAlAs heterostructures are prepared by epitaxial growth. The layers are parallel to the surface of the substrate and so is the PN junction. If we want to maintain this structure and use the semi-insulating substrate instead of the N type substrate we have to face the problem of putting metal contacts on the P type and the N type layers on the same side of the wafer. One natural way of solving this problem is to make a structure as the one shown in Fig. 4-1. On the semi-insulating GaAs substrate there are five epitaxially grown layers forming the double heterostructure. On the left hand side the upper four layers are selectively etched away so that we can put the P type contact on the first layer. The current injected through the P type contact flows through the P GaAs layer into the mesa region. Due to the sheet resistance of the P GaAs and P GaAlAs layer,

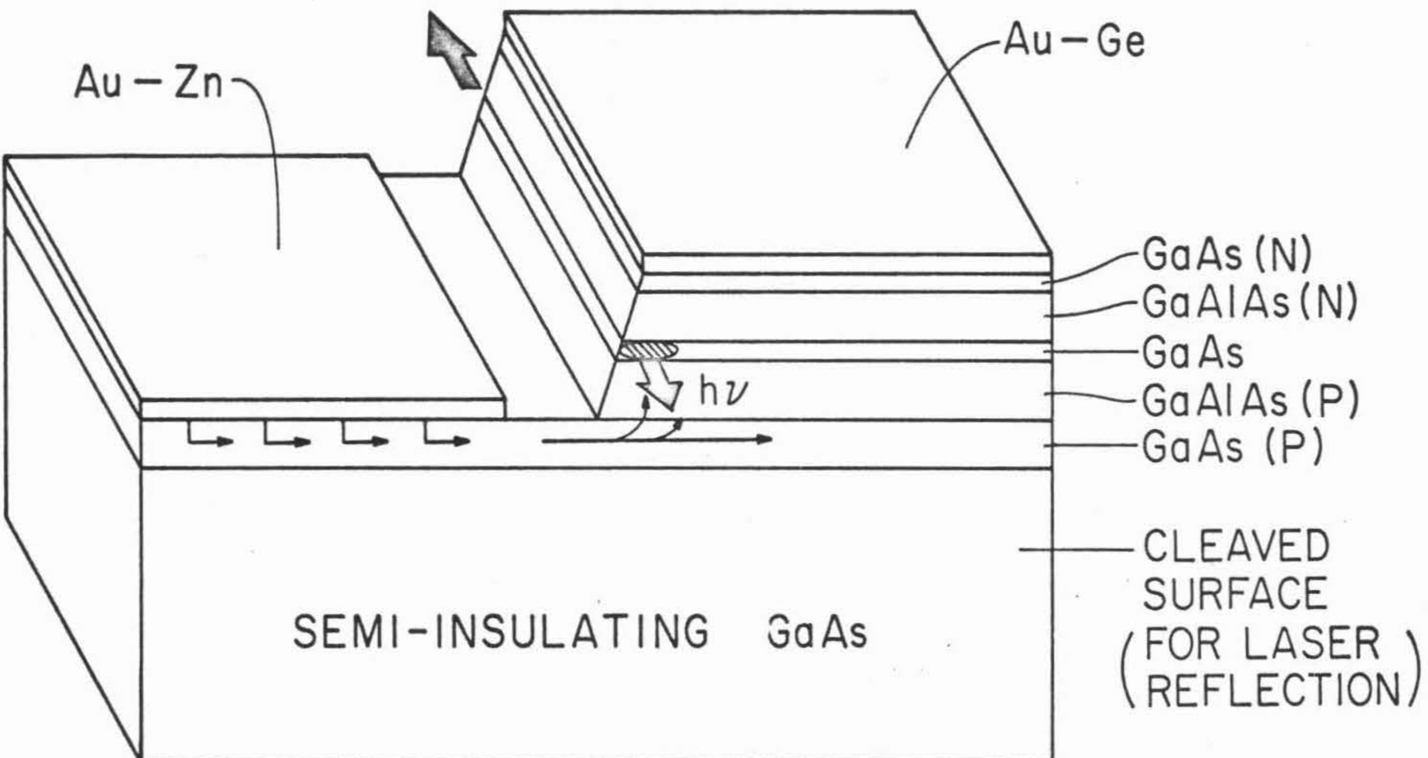

Fig. 4-1 A schematic drawing of the crowding effect laser.

the potential drop across the PN junction decreases with distance from the edge of the mesa. This causes the injected current to cross the PN junction in a narrow stripe adjacent to the edge of the mesa. This current crowding yields a narrow effective gain region near the mesa edge when the diode is operated with currents above the lasing threshold. Consequently, in the transverse direction the lasing action takes place in a small region just as in the case of stripe geometry lasers. However, for conventional stripe geometry lasers, two boundaries are needed to define the lasing active region. In the case of crowding effect lasers only one boundary is needed. The electrical confinement on the other side is automatically provided by the current crowding effect.

IV.2.1 Crowding effect

The crowding effect, or edge crowding, is a term used in bipolar transistors.[16] This phenomenon exists in any transistor to some degree at high currents. Because of the transverse IR drop resulting from the base current flowing through the base resistance, a non-uniform emitter-base voltage distribution occurs. The polarity of the voltage is such that the emitter-base junction voltage is largest on the portions of the junction nearest the base terminal. Consequently most of the injection occurs in these outer portions of the emitter. With increasing current, the IR drop increases, the effect becomes more pronounced, and the active emitter region is crowded closer and closer to the external base contact.

The crowding effect which occurs in our lasers can be understood

via Fig. 4-2. The structure is simplified to include only the important layers. The first two layers in the mesa region are assumed to be very thin compared to the distance over which the current density falls off and have a composite sheet resistance R. Total current I injected from the contact flows through the first layer into the mesa region. At $x > 0$ the current divides into two parts. Part of it, $i(x)$ goes forward and part of it flows up across the PN junction with current density $j_y(x)$. Because of the sheet resistance of the first two layers both $i(x)$ and $j_y(x)$ decrease with x. If ℓ is the length of the laser, the changes in the potential V of the first two layers, and the current $i(x)$ in a small distance dx are

$$dV(x) = -i(x)\frac{R}{\ell}\,dx \tag{4-1}$$

$$di(x) = -j_y(x)\ell dx \tag{4-2}$$

From these two equations we get the following differential equations

$$\frac{dV(x)}{dx} = -i(x)\frac{R}{\ell} \tag{4-3}$$

and

$$\frac{di(x)}{dx} = -j_y(x)\ell \tag{4-4}$$

Differentiating eq. (4-3) with x and substituting eq.(4-4) into it we get

$$\frac{d^2V}{dx^2} = j_y(x)R \tag{4-5}$$

Since the contact covers the whole mesa, we assume that the potential

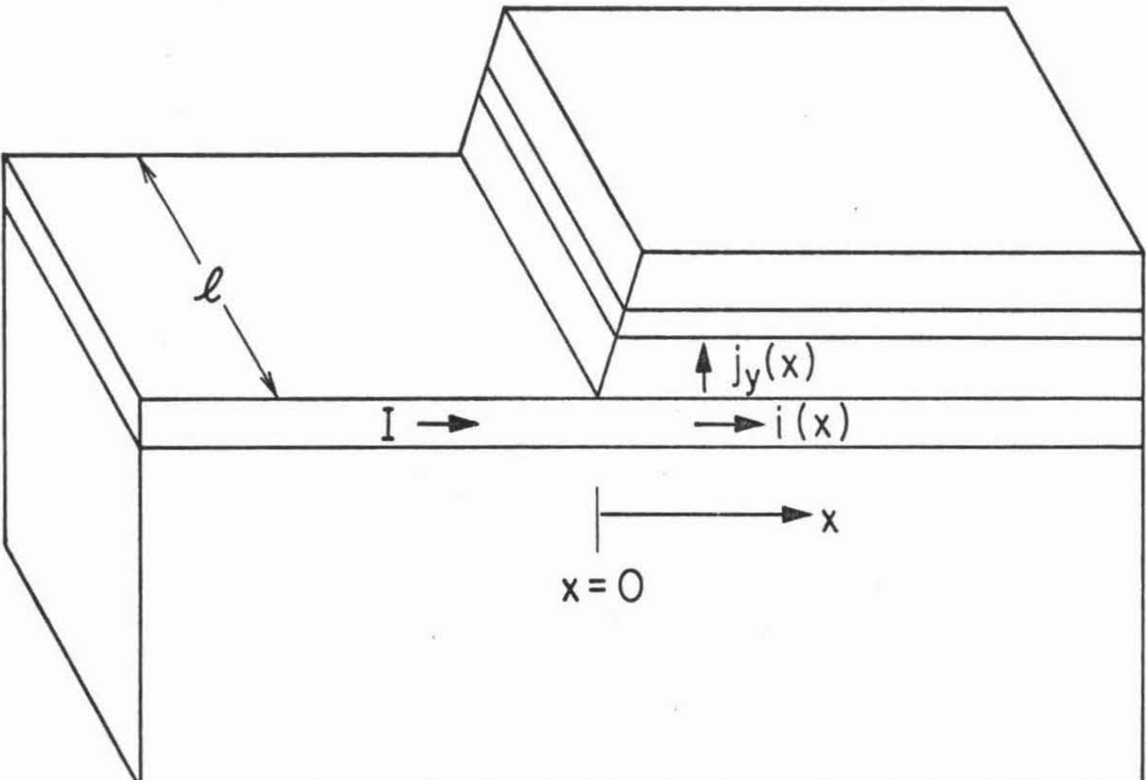

Fig. 4-2 This figure shows that the total current I decomposes into two components after it enters the mesa region ($x>0$). $i(x)$ is the component which flows forward in the x direction while $j_y(x)$ is the current density which flows upward in the y direction.

is uniform along x in the layers above the PN junction. The junction equation which determines the current density is then

$$j_y(x) = j_y(0)\, e^{qV/mkT} \tag{4-6}$$

Where q is the electronic charge, k is the Boltzmann's constant, m is a constant, and T is the absolute temperature. Here we have taken $V = 0$ at $x = 0$. Substituting eq.(4-6) into eq.(4-5) we get the equation for $V(x)$

$$\frac{d^2V}{dx^2} = Rj_y(0)\, e^{qV/mkT} \tag{4-7}$$

The solution of this equation is

$$V(x) = \frac{mkT}{q} \ln \frac{2}{(\frac{x}{x_o} + \sqrt{2}\,)^2} \tag{4-8}$$

Where

$$x_o = (\frac{mkT}{Rj_y(0)q})^{1/2} \tag{4-9}$$

Substituting eq. (4-8) into eq. (4-3) we get

$$i(x) = \frac{2mkT\ell}{Rqx_o} \frac{1}{\frac{x}{x_o} + \sqrt{2}} \tag{4-10}$$

The current density $j_y(x)$ is obtained by substituting eq. (4-8) into eq. (4-6)

$$j_y(x) = \frac{2j_y(0)}{(\frac{x}{x_o} + \sqrt{2}\,)^2} \tag{4-11}$$

Using the condition $i(0) = I$ we obtain for the parameter x_o and the current $i(x)$

$$x_o = \frac{\sqrt{2}\ mkT}{qRI} \cdot \ell \tag{4-12}$$

$$i(x) = \frac{\sqrt{2}\ I}{\frac{x}{x_o} + \sqrt{2}} \tag{4-13}$$

From equations (4-11) and (4-13) one can see clearly that both $j_y(x)$ and $i(x)$ decrease with x and the rates of decrease depend on x_o. The smaller the x_o the faster are the rates of decrease. $j_y(x)$ decays to half of $j_y(0)$ at $x = (2 - \sqrt{2})x_o$ and $i(x)$ decays to half of I at $x = \sqrt{2}\ x_o$.

The carrier distribution in the active region can be determined by solving the diffusion equation

$$D \frac{d^2n}{dx^2} - \frac{n}{\tau} + G = 0 \tag{4-14}$$

where

$$G = \frac{j_y(x)}{qt} \tag{4-15}$$

is the generation current provided by the injected current density $j_y(x)$. Here D is the effective diffusion constant, τ is the recombination time and t is the thickness of the active layer. Using eq. (4-11) and defining the diffusion length $L \equiv D\tau$ we can write eq. (4-14) as

$$\frac{d^2n}{dx^2} - \frac{n}{L^2} + \frac{2j_y(0)}{qDt\ (\frac{x}{x_o} + \sqrt{2})^2} = 0 \tag{4-16}$$

The general solution of this equation is

$$n(x) = C_1 \exp(\frac{x}{L}) + C_2 \exp(-\frac{x}{L}) + \frac{A}{2} \exp(\frac{x}{L}) \int \frac{\exp(-\frac{x}{L})}{B + x} dx$$

$$+ \frac{A}{2} \exp(-\frac{x}{L}) \int \frac{\exp(\frac{x}{L})}{B + x} dx \qquad (4\text{-}17)$$

where $A = \frac{2j_y(0)x_o^2}{qDt} = \frac{2\ mkT}{q^2 DtR}$ (4-18)

$$B = \sqrt{2}\ x_o \qquad (4\text{-}19)$$

The two integrals on the right hand side of eq. (4-17) are exponential integral functions defined by[17]

$$E_i(x) \equiv \int \frac{e^x}{x} dx = \gamma + \ln(x) + \sum_{k=1}^{\infty} \frac{x^k}{k \cdot k!} \qquad (4\text{-}20)$$

$$E_1(x) \equiv \int \frac{e^{-x}}{x} dx = -\gamma - \ln(x) - \sum_{k=1}^{\infty} \frac{(-1)^k x^k}{k \cdot k!} \qquad (4\text{-}21)$$

Therefore eq. (4-17) becomes

$$n(x) = C_1 \exp(\frac{x}{L}) + C_2 \exp(-\frac{x}{L}) - \frac{A}{2} \exp(\frac{B+x}{L})\ E_1(\frac{B+x}{L})$$

$$+ \frac{A}{2} \exp(-\frac{B+x}{L})\ E_i(\frac{B+x}{L}) \qquad (4\text{-}22)$$

At $x \to \infty$ the current injected into the active layer is zero. The excess number of carriers $n(x) \to 0$. At the boundary $x = 0$, because of the air-semiconductor interface, there is surface recombination. If we take S to be the surface recombination velocity, the boundary condition for $n(x)$ at $x = 0$ is

$$qD \left. \frac{dn}{dx} \right|_{x=0} = qSn(0) \qquad (4\text{-}23)$$

Applying these two boundary conditions to eq. (4-22) we obtain the constants C_1 and C_2. They are

$$C_1 = 0 \tag{4-24}$$

$$C_2 = \frac{A}{2}\exp\left(\frac{B}{L}\right) E_1\left(\frac{B}{L}\right) \frac{SL-D}{SL+D} - \frac{A}{2}\exp\left(-\frac{B}{L}\right) E_i\left(\frac{B}{L}\right) + \frac{A}{B}\frac{LD}{SL+D} \tag{4-25}$$

Taking $\alpha = \frac{B}{L}$ and $g = \frac{SL}{D}$ we get for $n(x)$ and C_2

$$n(x) = C_2 \exp\left(-\frac{x}{L}\right) - \frac{A}{2}\exp\left(\alpha+\frac{x}{L}\right) E_1\left(\alpha+\frac{x}{L}\right) + \frac{A}{2}\exp\left(-\alpha-\frac{x}{L}\right) E_i\left(\alpha+\frac{x}{L}\right) \tag{4-26}$$

$$C_2 = \frac{A}{2} e^{\alpha} E_1(\alpha) \frac{g-1}{g+1} - \frac{A}{2} e^{-\alpha} E_i(\alpha) + \frac{A}{\alpha}\frac{1}{g+1} \tag{4-27}$$

Using α as a parameter we can convert equations (4-11) and (4-13) into

$$j_y(x) = \frac{j_y(0)}{\left(\frac{x}{L}\frac{1}{\alpha} + 1\right)^2} \tag{4-28}$$

$$i(x) = \frac{I}{\frac{x}{L}\frac{1}{\alpha} + 1} \tag{4-29}$$

where $$\alpha = \frac{B}{L} = \frac{\sqrt{2}\, x_o}{L} = \frac{2\, mkT}{qRI}\frac{\ell}{L} \tag{4-30}$$

Plots of $i(x)$ and $j_y(x)$ as functions of distance using α as a parameter are shown in Fig. 4-3 and Fig. 4-4. When α is small, or the product RI is large, both $i(x)$ and $j_y(x)$ are very much crowded near the edge of the mesa. When α is large or RI is small the effect of crowding is weak and currents spread out more, away from $x = 0$. If we take $R = 60$ ohm, $I = 100$ mA and $L = 5\ \mu m$, α, from eq. (4-30), is equal to 1.

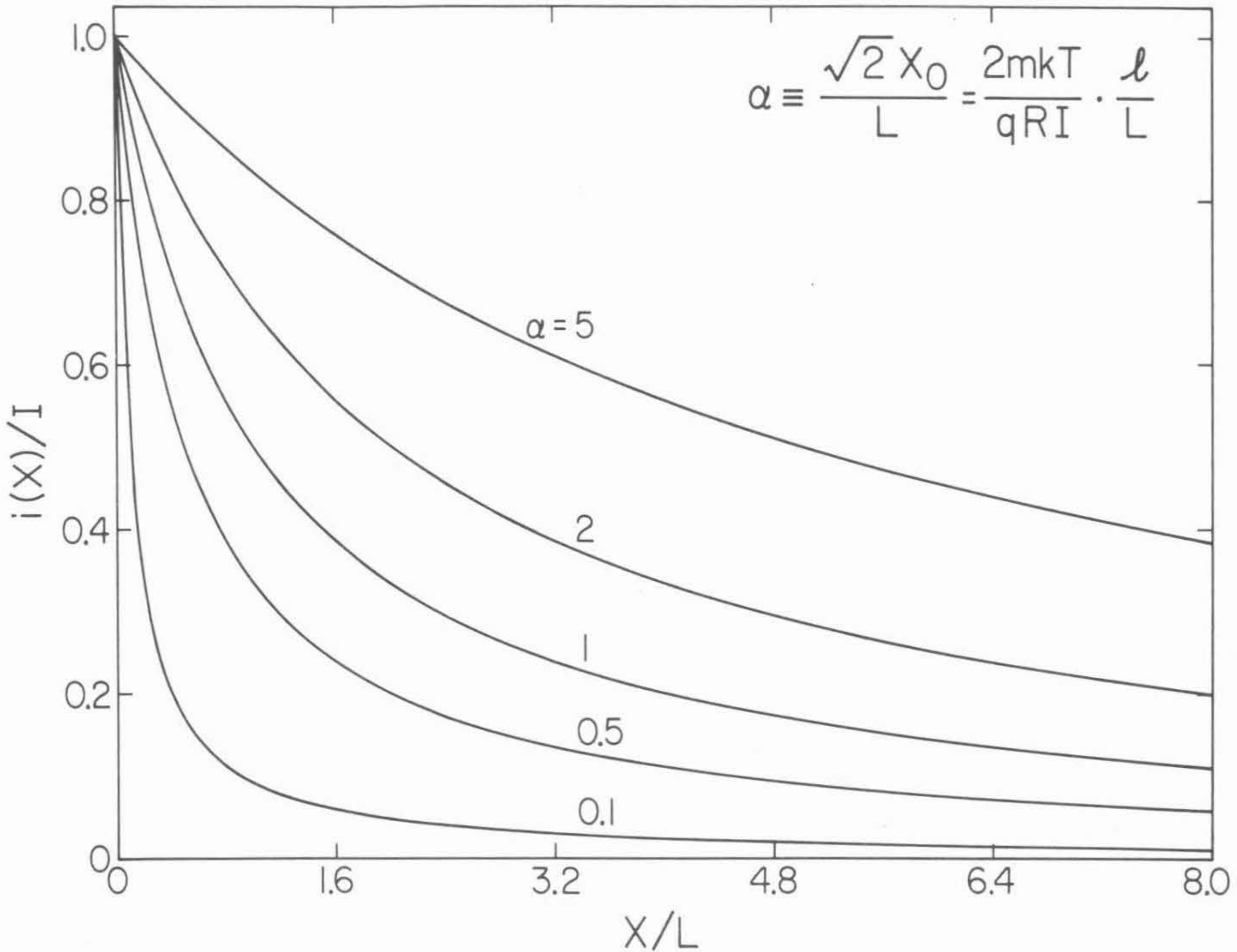

Fig. 4-3 Distribution of the current $i(x)$ as a function of distance. α is used as a parameter.

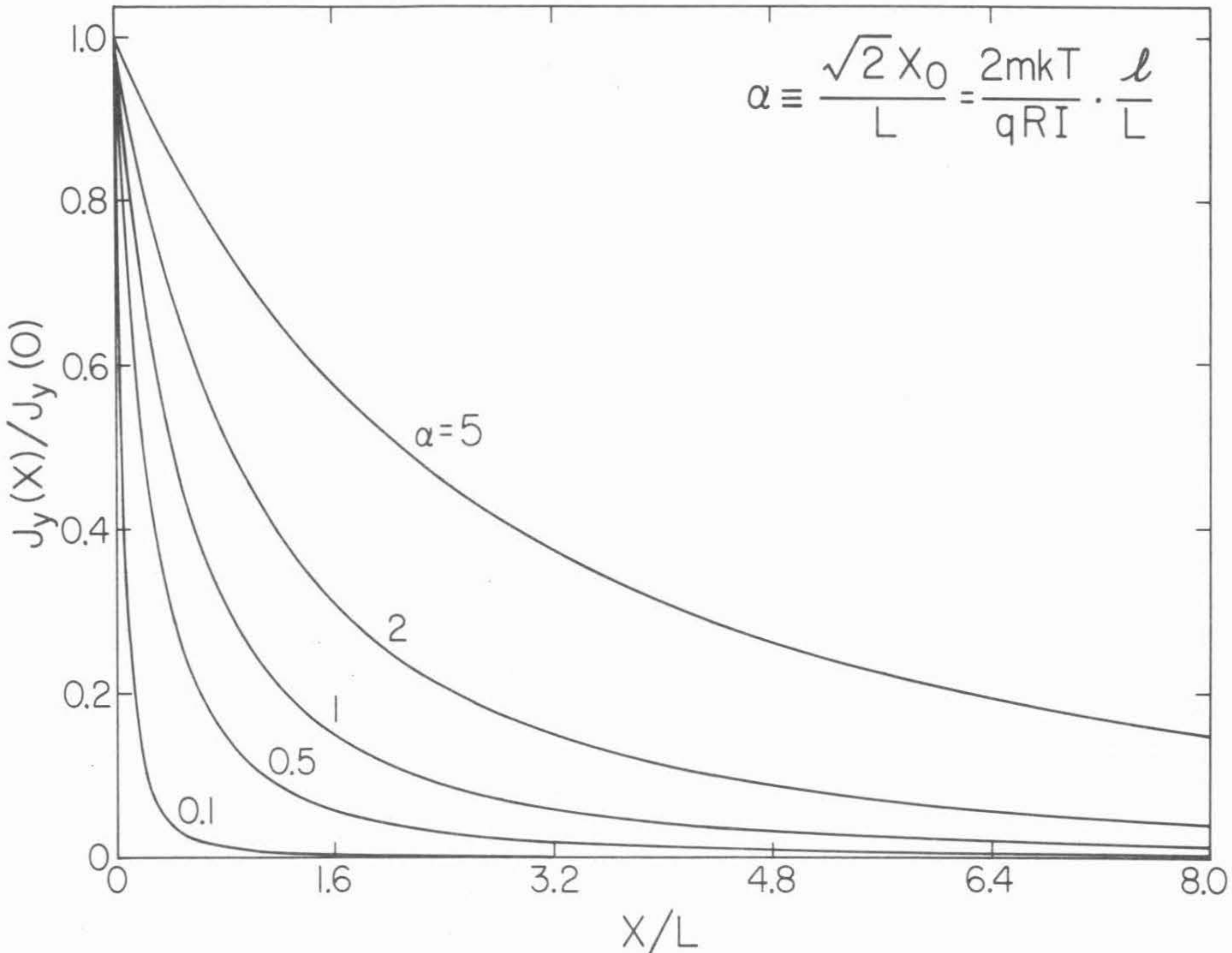

Fig. 4-4 Distribution of the current density $j_y(x)$, which flows upward across the junction, as a function of distance. α is used as a parameter.

We can see from Fig. 4-3 that half of the total current flows across the junction in a small area, within 5 μm of the mesa edge.

The distributions of the carriers n(x) at different α's are shown in Fig.4-5. The effect of crowding on n(x) is similar to that on i(x) and $j_y(x)$. The smaller the α, or the larger the RI, the stronger the crowding. In Fig. 4-5 we have taken g = 10, which corresponds to a surface recombination velocity $S = 1.5 \times 10^6$ cm/sec.

Since the crowding effect in our structure depends on the value RI, one can control this effect by changing the sheet resistance R. This can be achieved by adjusting either the thickness or the doping concentrations of the first two layers. But larger R or stronger crowding does not mean that the laser is better, because as more carriers are crowded near the edge of the mesa the larger the effects of surface recombination and light scattering due to the proximity of the air interface.

IV.2.2 Device structure and fabrication

The fabrication procedure for a crowding effect laser is shown in Fig. 4-6. On the semi-insulating substrate five layers of GaAs and GaAlAs layers are grown by liquid phase epitaxy. The layer sequence and the parameters for each layer are shown in table 4-1. The layers form a double heterostructure in the direction perpendicular to the surface of the substrate. After the growth the N type contact Au-Ge is first evaporated over the whole surface of the wafer. A part of this layer is removed photolithographically. The remaining

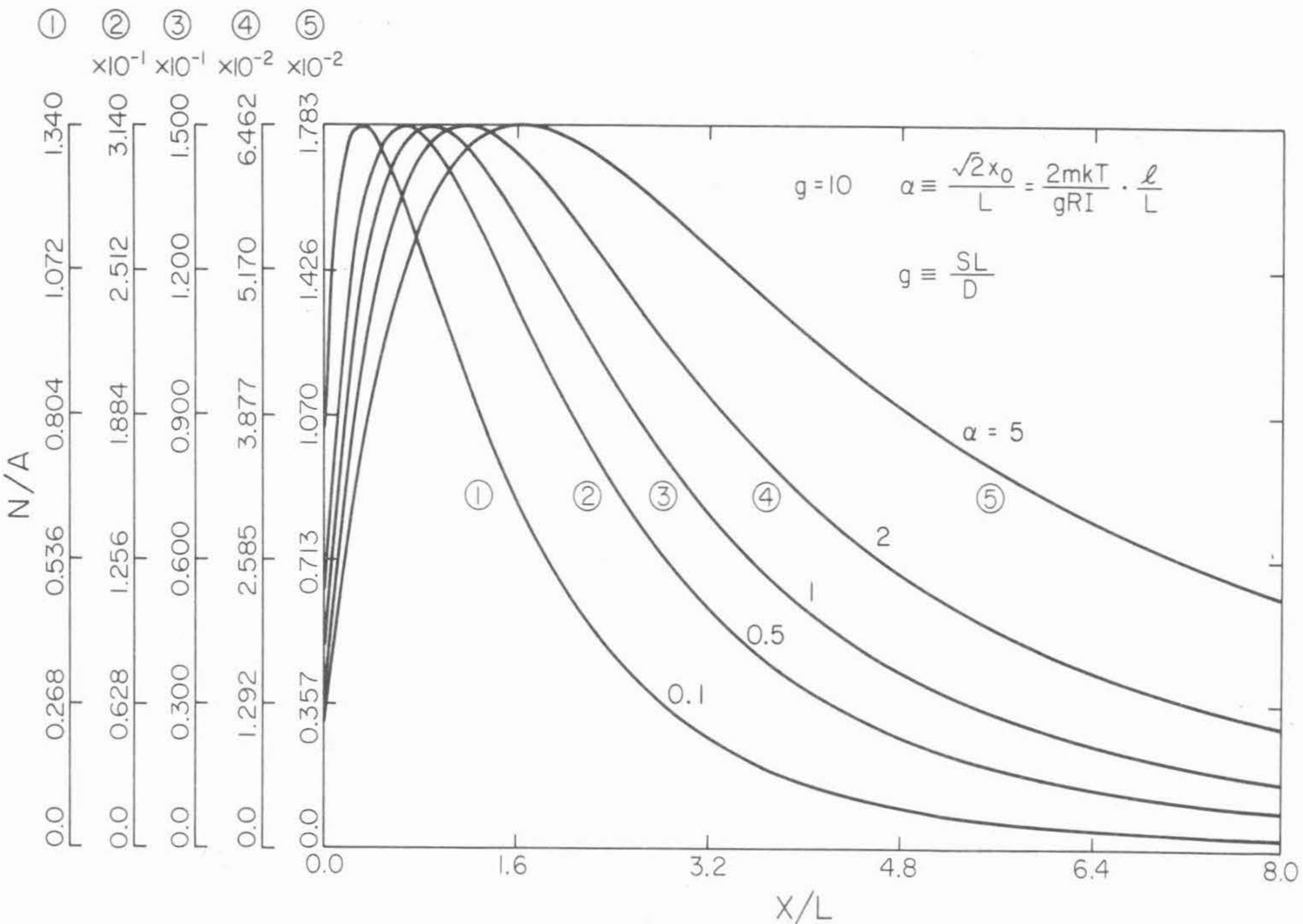

Fig. 4-5 Carrier distribution in the active region as a function of x, α is used as a parameter.

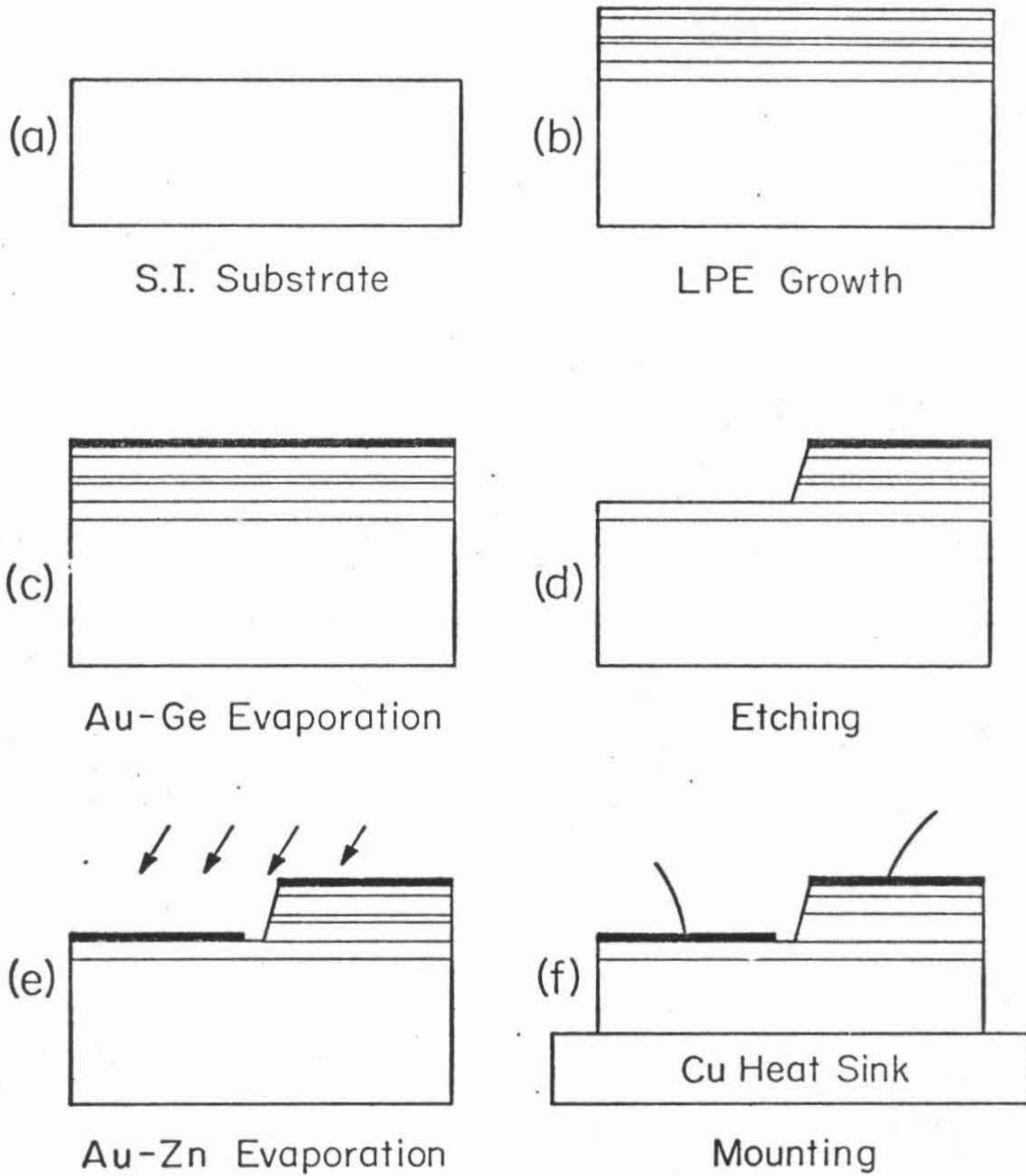

Fig. 4-6 Fabrication steps for a crowding effect laser.

Layer	Material	Thickness (μm)	Al Content	Carrier Concentration (cm^{-3})	Dopant
1st	P GaAs	3	-	2×10^{18}	Ge
2nd	P GaAlAs	2	0.4	10^{17}	Ge
3rd	GaAs (undoped)	0.3	-	5×10^{15}	-
4th	N GaAlAs	2	0.4	10^{17}	Sn
5th	N GaAs	1	-	10^{18}	Sn

Table 4-1

Parameters for each grown layer of a crowding effect laser

metal serves as the mask for the selective etching of the layers. Etching results in a steplike structure with the edge parallel to [110] direction. The etching must be deep enough to reach the P type GaAs layer since ohmic contact to P GaAlAs is poor. The etchants we used are H_2SO_4:H_2O_2:H_2O (4:1:1) and HF. The first solution etches the layers down to the P GaAlAs region and the second solution removes the remaining P GaAlAs selectively without attacking the P GaAs layer. After the etching, a second evaporation is performed , in which Au-Zn is used for the P type contact. During evaporation, the sample is tilted at an angle to the metal source so that the edge of the step acts as a mask to the evaporation and the metal contacts on the first layer and on top of the mesa are separated.

The contact alloying was carried out in H_2 atmosphere at 440°C after the evaporation. The sample was then thinned down to about 100 μm thick and diced into laser chips. Each laser has a cavity about 300 μm long. The cross section of the final structure is shown in Fig. 4-1. The laser chips were mounted on a copper heat sink with two contact leads up. (see Fig. 4-7) Since the size of the active region is not determined by the area of the contact, one can cut a wide chip and use a broad top contact for the purpose of smaller resistance and ease of handling.

IV.2.3 Experimental results

Experimental measurements of the crowding effect lasers were carried out under pulsed operation. The current pulses which drove

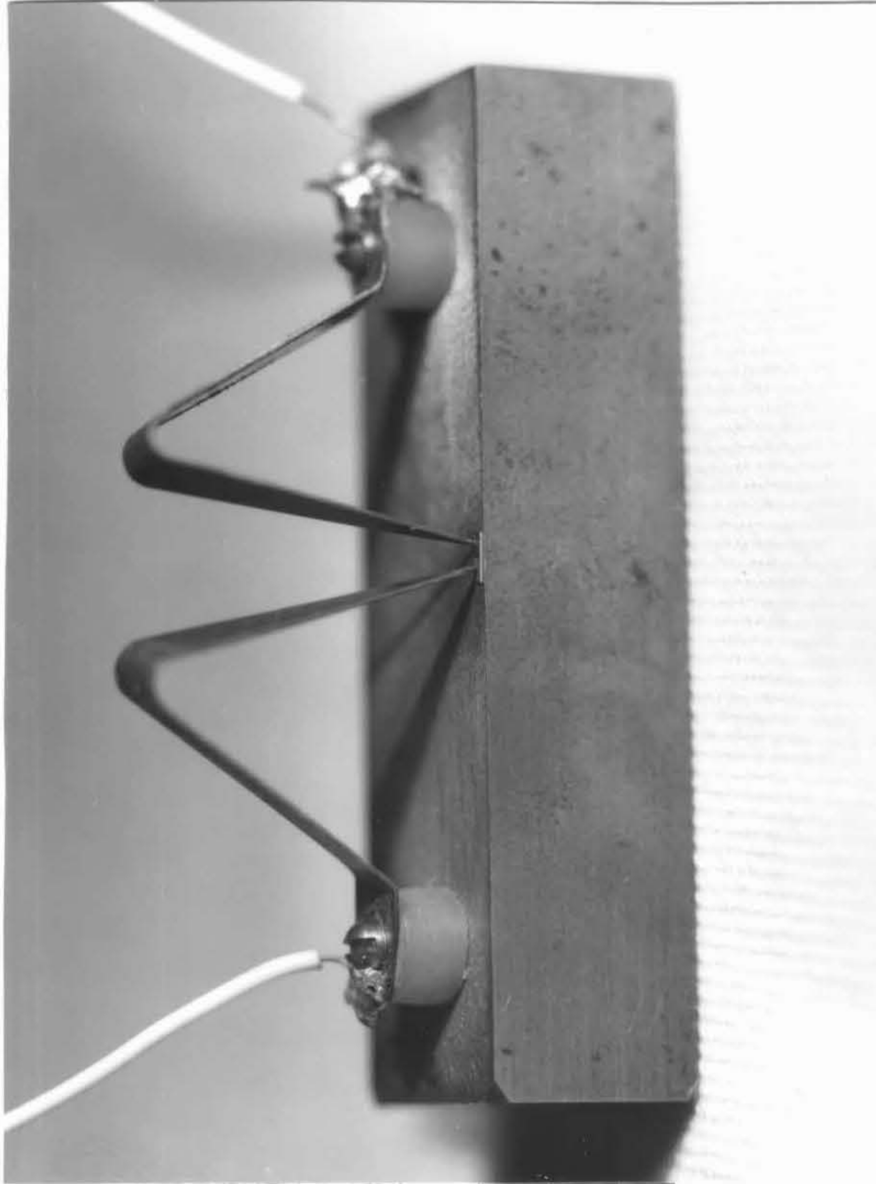

Fig. 4-7 Photograph of a copper heat sink used to mount the crowding effect lasers and the lateral injection lasers.

the laser diodes were 100 nsec wide with a repetition rate of 1KHz.

The threshold currents of the crowding effect lasers are comparable to those of conventional stripe geometry lasers. The typical value for a 300 μm long laser diode is 150 mA. The differential quantum efficiency, defined as the ratio of the increase in the photon output rate to the increase in the carrier injection rate, is about 30%. These lasers can be driven to very high current and deliver high output power without breakdown. Fig. 4-8 is an example of a typical laser's light versus current curve. The threshold current of this laser is 120 mA. The differential quantum efficiency is 32%. At 800 mA, which is almost seven times the threshold current, the laser delivers 130 mW output power from one mirror.

The light distribution at the cavity mirror, i.e. the near field, can be viewed with a microscope equipped with an infrared image converter. Fig. 4-9 shows two photographs of the light distribution of a crowding effect laser at two different currents: Fig. 4-9a, at a current of 10 mA, far below threshold, shows a light distribution extending a long distance ($\sim$ 100 μm) under the mesa; and Fig. 4-9b, at a current above threshold, shows a much narrower light distribution. Most of the laser light emanates from a region some 10 - 15 μm wide near the edge of the mesa. These two pictures provide a direct evidence for the crowding effect.

More detailed measurements of the near fields were made by scanning the cavity mirror with a rotating mirror. (The set-up will be described in chapter V.) Using this method we were able to record

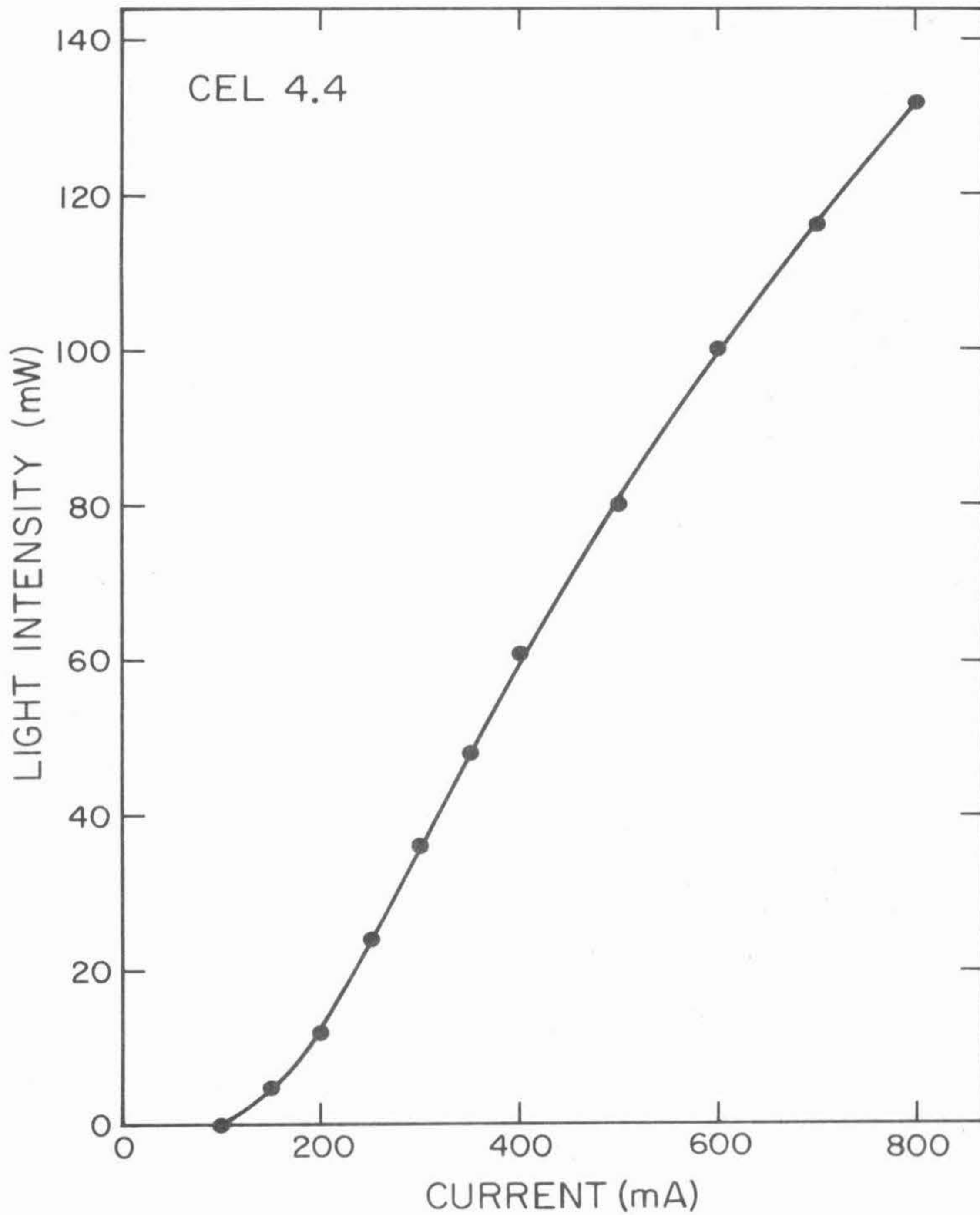

Fig. 4-8 Light intensity vs. driving current curve of a crowding effect laser. The threshold current is 120 mA.

Fig. 4-9 The photographs of the near field radiation patterns of a crowding effect laser. (a), with a current of 10 mA, way below threshold, shows a light distribution extending a long distance ($\sim$100 μm) under the mesa. (b), with a current 250 mA, which above threshold (240 mA) shows much narrower light distribution. Most of the laser light is due to a narrow region near the edge of the mesa.

(a)

20μ

(b)

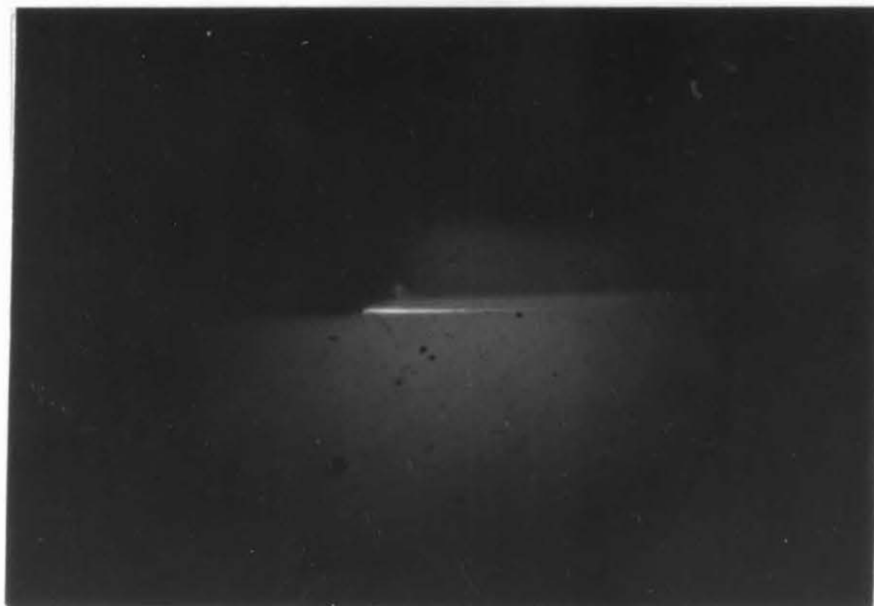

the light distributions on an X-Y recorder and obtain much better resolution. Fig. 4-10 and Fig. 4-11 show the measured near fields of a crowding effect laser at two different current levels. The angular distributions of the emitted laser light in the junction plane, i.e. the far fields, are shown along with the near fields. In Fig. 4-10, at a lower current, the near field indicates that there is only one transverse mode. The distance between the half power points is about 5 μm. In Fig.4-11, at a higher current, the width of the light profile becomes wider and more modes begin to develop.

The modes of the crowding effect lasers are guided along the cavity with a mechanism different from those of regular dielectric waveguides. The transverse confinement of the laser modes is not due to the refractive index change but,rather, to the monotonic decrease of the gain as a function of distance from the mesa edge. This decrease of gain is due to the carrier crowding effect which we discussed before. The gain-induced guiding also influences the lasers' far field radiation patterns. As shown in Fig. 4-10 and Fig. 4-11, the far field patterns are not symmetric with respect to 0°, which is normal to the laser mirror, but instead display peaks at about 10° toward the mesa side. This gain-induced guiding phenomenon has been analyzed, and will be discussed in detail in section IV.4.

The spectrum of a typical crowding effect laser is shown in Fig. 4-12. The laser light is polarized with the electric field parallel to the junction plane. This polarization is similar to that of a regular heterostructure laser.

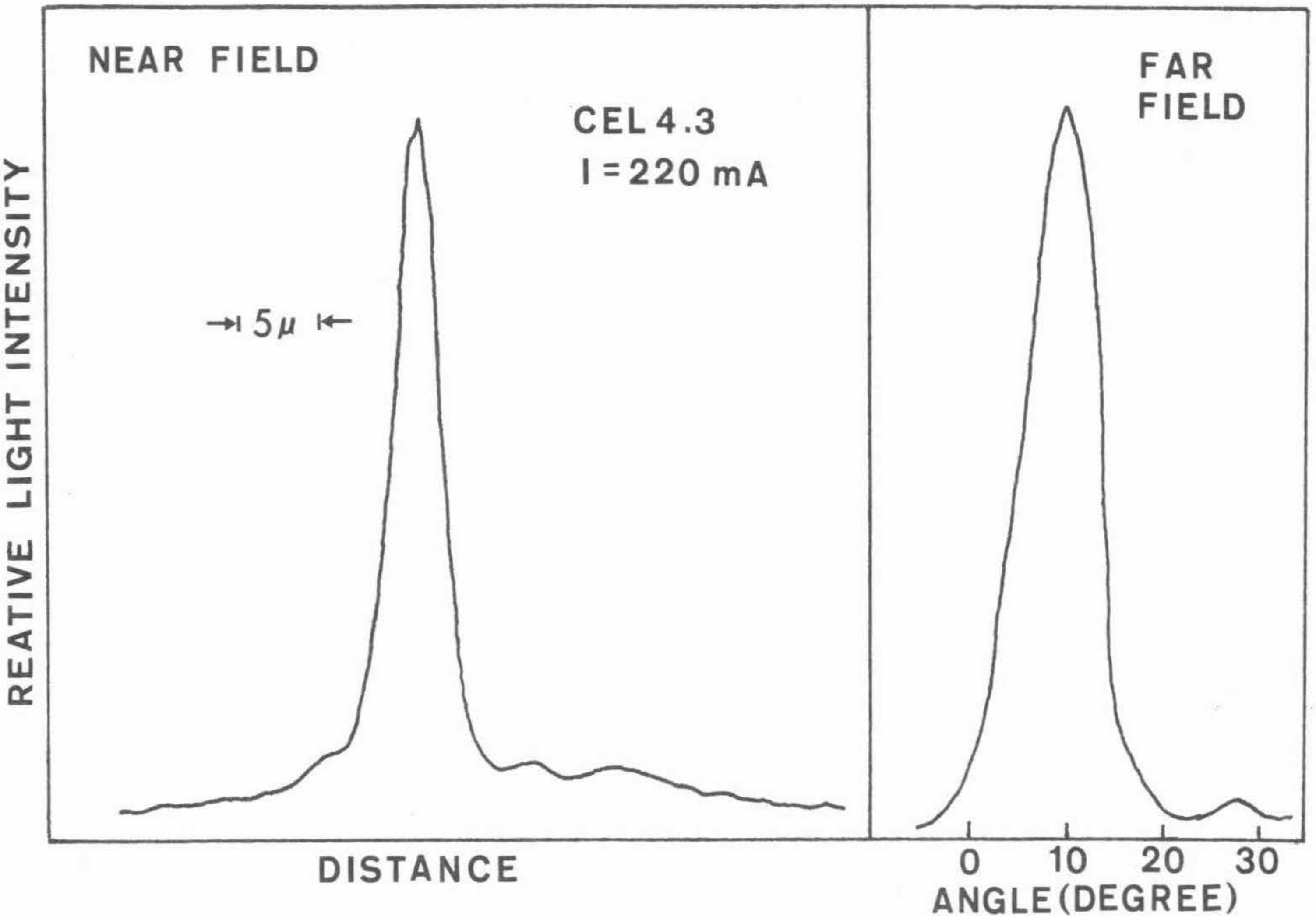

Fig. 4-10 The recorder traces of the near field and the far field of a crowding effect laser at a current of 220 mA. The threshold current of this laser is 180 mA. The right hand side of each curve is the mesa side.

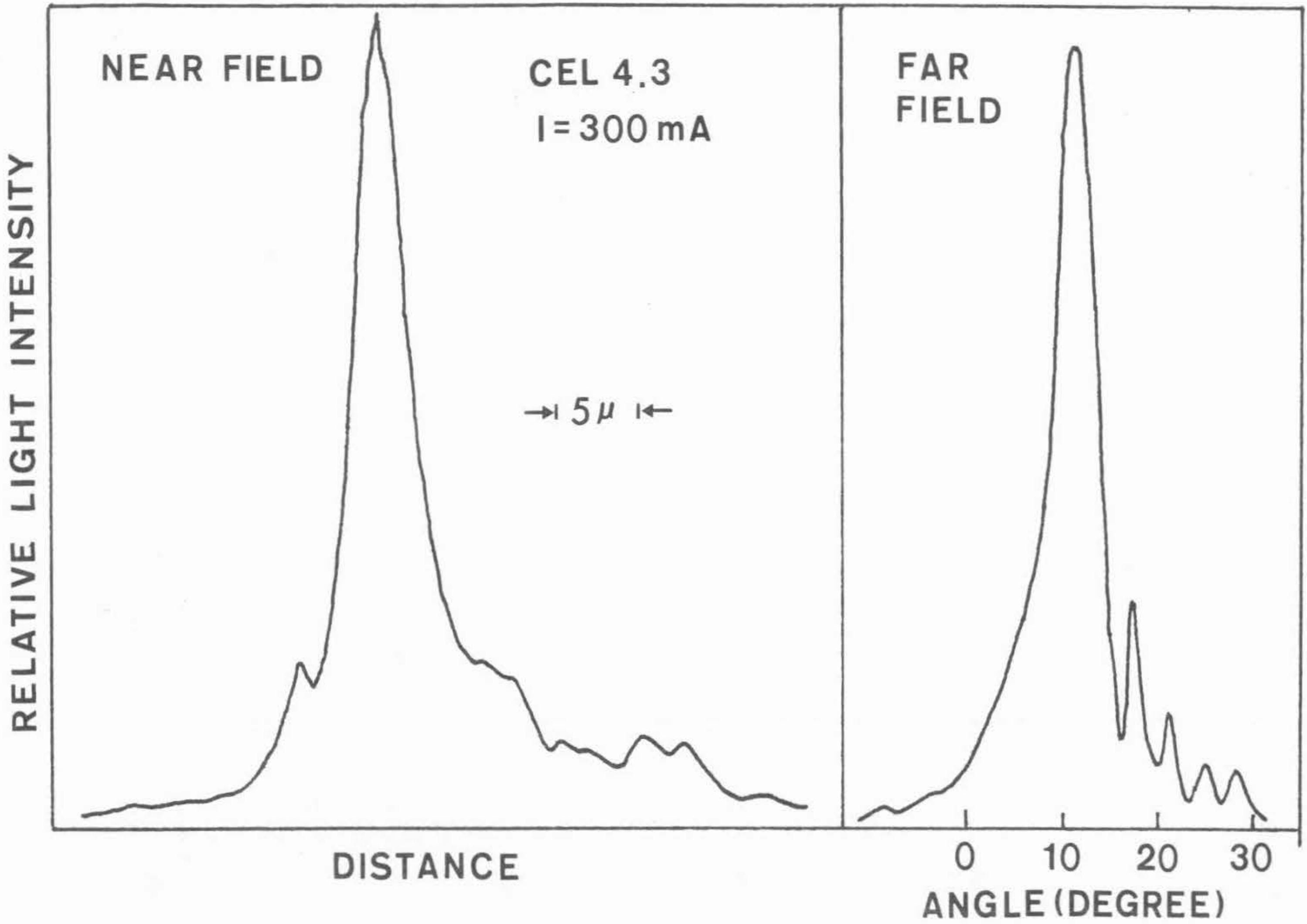

Fig. 4-11 The near field and far field of the same laser as in Fig. 4-10 when the current is increased to 300 mA.

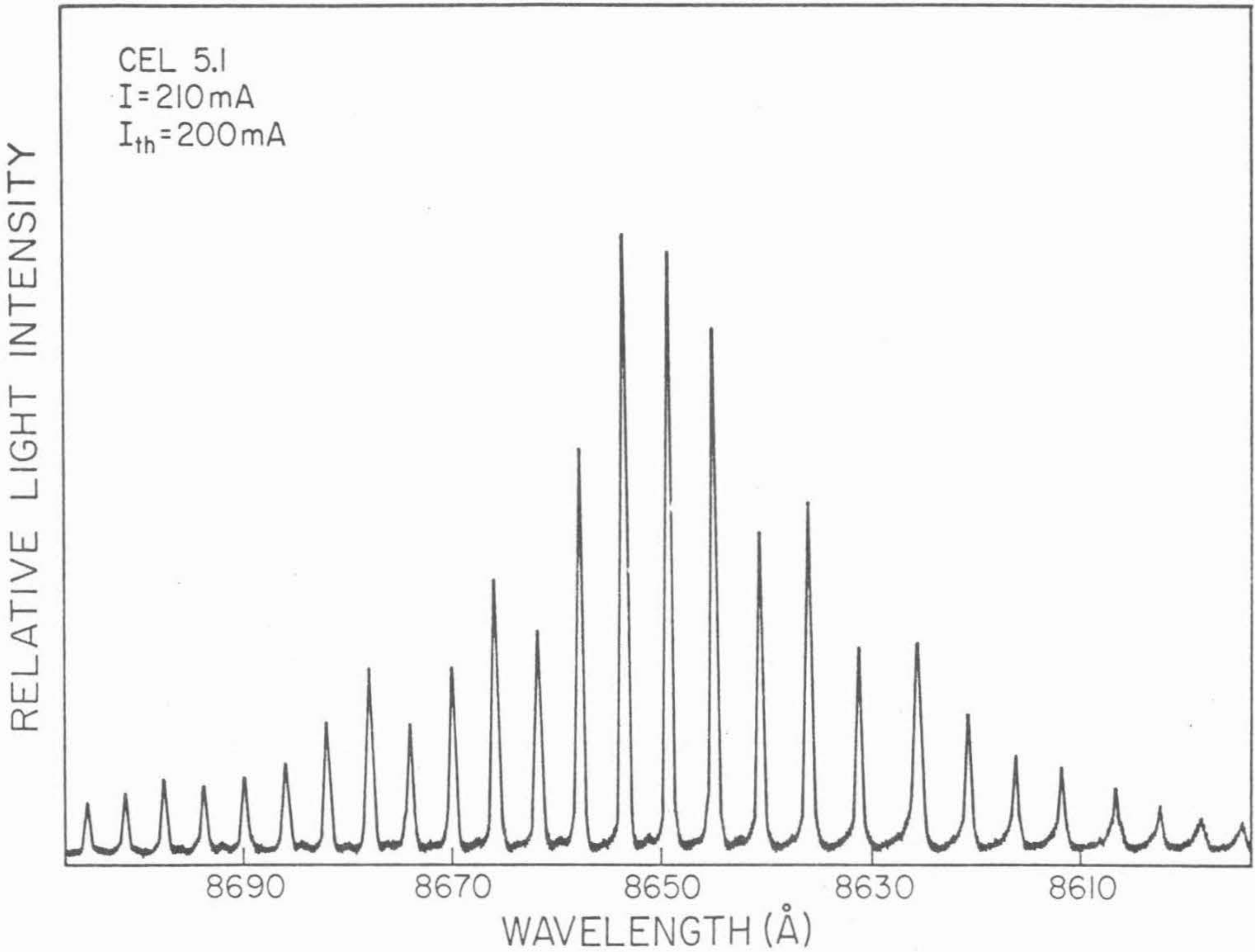

Fig. 4-12 The spectrum of a crowding effect laser.

Since the crowding effect depends on the sheet resistance of the first two layers, it is possible to control the width of the injection region (the active region) by varying the thickness and the doping concentration of these layers. We have used a carrier concentration of $\sim 2 \times 10^{18} cm^{-3}$ in the first layer with a thickness $\sim 3\ \mu m$. The second P GaAlAs layer is more lightly doped. The crowding effect in this case is thus controlled by the first layer. The crowding effect lasers can also be made with N type layers under the P type layers, but the doping concentration of the first two layers have to be much lower in order to get proper crowding effect, because in GaAs the electron mobility is about an order of magnitude higher than the hole mobility.

IV.3 GaAs-GaAlAs Heterostructure Lasers on Semi-Insulating Substrates using Lateral Injection

The structure of the crowding effect laser is similar to the conventional double heterostructure lasers, in that the PN junction is parallel to the epilayers. The current crowding effect provides the lateral confinement of the carriers near the edge of the mesa. However, at the air-semiconductor boundary the carriers in the active region undergo a nonradiative surface recombination loss which increases the threshold. The lasing characteristics also suffer from scattering loss due to the etched surface. Owing to these reasons it is difficult to achieve very low threshold crowding effect lasers. The lateral injection laser, which is described in this section, was

conceived with the aim of solving these problems.

The structure of the lateral injection laser, shown in Fig.4-13b, consists of three double-heterostructure epilayers on a semi-insulating substrate. The layers are doped with N type dopants, while the P type region is obtained by Zn diffusion. The current flows laterally across the junction from the P type contact to the N type contact. Since GaAlAs has a wider bandgap than that of GaAs, carriers are injected predominantly across the GaAs PN junction. The effective area of the current injection is therefore determined by the thickness of the GaAs layer. Since very thin GaAs layers can be easily obtained by liquid phase epitaxy (LPE), very low threshold lasers can be achieved.

The technique of transverse injection was first used by Namizaki et al.[18, 19] to make transverse-junction-stripe (TJS) lasers on N^+ GaAs substrates. However, their structure suffered from current leakage across the (diffused) P GaAlAs-N GaAlAs junction which made for a rapid increase of the threshold current at higher temperatures. Recently Susaki et al. developed a new TJS structure to eliminate this current leakage problem.[20] However, it requires five epitaxial layers. In our structure only three layers are needed and the current leakage is eliminated because the substrate is semi-insulating.

As shown in Fig. 4-13b, the PN junction in the three different layers have different junction areas. In the first GaAlAs layer the junction lies within the layer and hence has a very large area. However, owing to the crowding effect, the current which flows into this layer can not proceed very far to the right. As a result, most

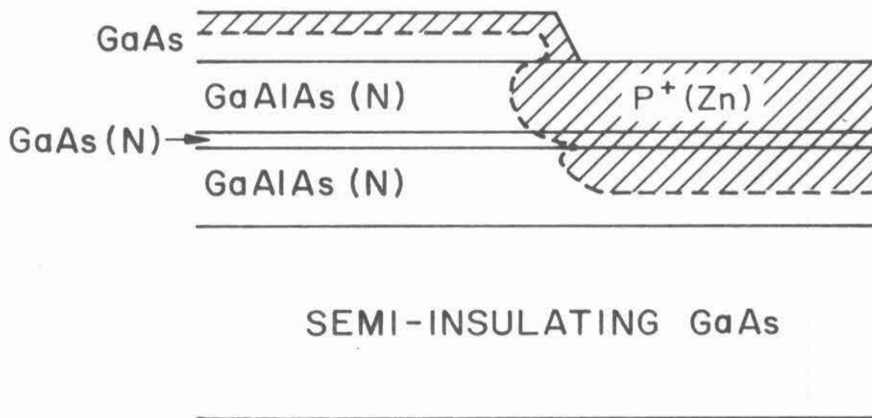

Fig. 4-13 (a) The cross section of a lateral injection laser after Zn diffusion. Right hand side of the top layer is etched away. The remaining part (on the left) serves as the diffusion mask.

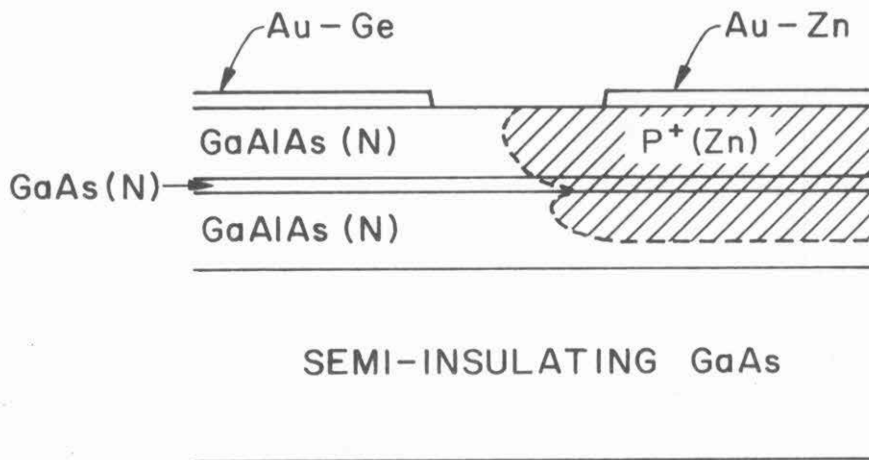

Fig. 4-13 (b) The cross section of the final structure of a lateral injection laser.

of the current flows across the junction in a small area at the left corner of the junction. If we take the first GaAlAs layer and the top GaAlAs layer to be one layer with effective junction area A_1, the ratio of the currents flowing through the GaAs and GaAlAs junction can be roughly estimated with a method similar to that used to calculate the leakage current in II.3. The current which flows through the GaAlAs junction, according to the junction equation, is

$$I_1 = A_1 J_{o1} \exp(qV_1/mkT) \tag{4-31}$$

where J_{o1} is the saturation current density, m is a constant, and V_1 is the voltage across the junction. Similarly, the current flowing through the GaAs junction is

$$I_2 = A_2 J_{o2} \exp(qV_2/mkT) \tag{4-32}$$

where A_2 is the junction area, and J_{o2} and V_2 are defined in the same way as those for the GaAlAs junction. The ratio of I_1 and I_2 is

$$\frac{I_1}{I_2} = \frac{A_1 J_{o1}}{A_2 J_{o2}} \exp[q(V_1 - V_2)/mkT] \tag{4-33}$$

The saturation current densities J_{o1} and J_{o2} depend on the bandgaps of GaAlAs and GaAs, respectively. The ratio is approximately given by[8]

$$\frac{J_{o1}}{J_{02}} \approx \exp(-\Delta E_g/kT) \tag{4-34}$$

Substituting eq. (4-34) into eq. (4-33), we get

$$\frac{I_1}{I_2} = \frac{A_1}{A_2} \exp \left[- \frac{\Delta E_g}{kT} + \frac{q(V_1 - V_2)}{mkT} \right] \tag{4-35}$$

Since the layers are very thin and adjacent to each other, the difference between V_1 and V_2 is very small. If we take $\Delta E_g = 0.5$ eV (which corresponds to $x \simeq 0.4$ in the $Ga_{1-x}Al_xAs$ confining layers) and neglect $V_1 - V_2$, eq. (4-35) becomes

$$\frac{I_1}{I_2} = \frac{A_1}{A_2} \exp(-20) \tag{4-36}$$

For a typical lateral injection laser $A_1/A_2 \simeq 10$. The ratio of the currents is then

$$\frac{I_1}{I_2} = 10 \exp(-20) \tag{4-37}$$

Thus, nearly all the current passes through the GaAs junction and no current leaks through the GaAlAs junction.

IV.3.1 Zn diffusion in $Ga_{1-x}Al_xAs$

Zn diffusion is a very common method for obtaining P type regions in the $Ga_{1-x}Al_xAs$ system. Zn has a high diffusion rate in GaAlAs and produces sharp diffusion fronts.[21] In our lateral injection lasers the P type region is obtained by selective Zn diffusion into the epilayers. In the experiments we found that the diffusion rates

in $Ga_{1-x}Al_xAs$ depend strongly on the Al content x.[22] The diffusion rates in the Al containing layers are much larger than in the GaAs region (the difference increasing with x). Taking advantage of this difference, we used the GaAs layer as a diffusion mask in fabricating our lasers. (see Fig. 4-13a)

The GaAs mask has many advantages over the conventionally used masks. In an ordinary mask such as SiO_2 (doped with P) or Si_3N_4, there always exists an interfacial stress between the mask and the underlying crystal because of the nature of the deposition process and the different thermal expansion rates in $Ga_{1-x}Al_xAs$ and the mask. This stress contributes to problems such as crystal surface damage, unstable masks at high temperatures, and lateral diffusion under the masks.[23] In the GaAs mask, due to the near perfect lattice match to GaAlAs, these problems are largely alleviated. Futhermore, the GaAs mask is grown during the same sequence with the other epilayers so that no additional step of mask deposition is needed.

For determining the diffusion rates in $Ga_{1-x}Al_xAs$ regions with differing x we have measured the diffusion depth as a function of the Al content. We first prepared seven samples each containing a $Ga_{1-x}Al_xAs$ epilayer. The Al content x ranges from 0 to 0.71. Each epilayer has a thickness of about 12 μm. The samples were subsequently sealed in an evacuated quartz ampoule containing $ZnAs_2$ as the diffusion source. The diffusions were carried out under several conditions with varying temperatures and durations. After the diffusion the samples were cleaved and stained with $HF:HNO_3:H_2O$ (1:3:4) to reveal

the diffusion fronts. The diffusion depths were measured with a scanning electron microscope. Fig. 4-14 shows the diffusion depth as a function of Al content x in $Ga_{1-x}Al_xAs$ layer for three diffusion conditions: 670^oC, 70 min; 701^oC, 55 min; and 639^oC, 150 min. All three groups of data show that the diffusion depth increases with Al content when x is less than about 0.5. The depths at x = 0.47 are about three times the depths in GaAs (x = 0). When x is higher (x = 0.62, 0.71) the diffusion fronts become nonuniform and the data indicate a "slowing down", if not a reversal, in the rate of increase. The error bars in Fig. 4-14 indicate the variations of the diffusion depths.

It is well known that Zn diffusion in GaAs is based on the mechanism of interstitial-substitutional equilibrium in which the interstitial Zn atoms react with neutral Ga vacancies to form substitutional acceptors and holes.[24] The diffusion constant of the interstitial mode is much greater than that of the substitutional mode. Based on this mechanism, we can explain our experimental result as follows: The use of $ZnAs_2$ as the diffusion source results in a high As pressure which induces Ga vacancies in GaAs. As the concentration of the Ga vacancies increases, the Zn atoms are shifted to the substitutional sites and the fast interstitial diffusion is suppressed.[25] However, the sitution is different in $Ga_{1-x}Al_xAs$. The melting temperature of $Ga_{1-x}Al_xAs$ increases with Al content x, so it is natural to expect a higher binding energy and therefore less

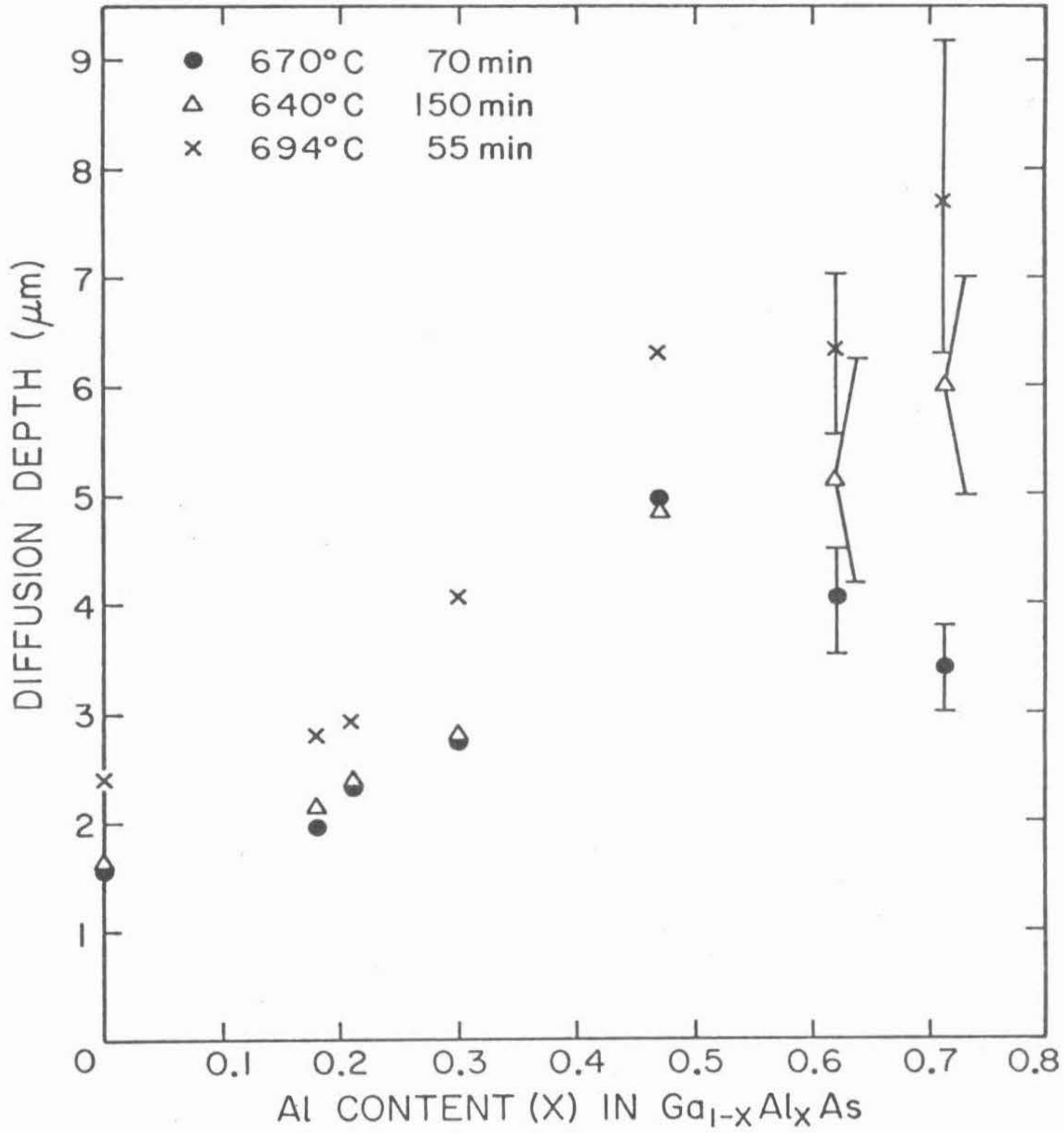

Fig. 4-14 Zn diffusion depth as a function of Al content in $Ga_{1-x}Al_xAs$.

lattice vacancies as x increases for a given As pressure. As the number of Ga vacancies becomes smaller, the fast interstitial diffusion becomes more favorable and results in a larger diffusion depth. This explanation seems to be satisfactory, at least when $x < 0.5$. When the Al content is higher ($x = 0.62$, 0.71) the diffusion fronts are not uniform. This might be due to irregular interstitial diffusion,[26] or more likely, to other reasons yet to be understood.

IV.3.2 Device structure and fabrication

The fabrication procedure of the lateral injection laser is shown in Fig. 4-15. Four layers are first grown by liquid phase epitaxy on a semi-insulating substrate. They are, starting from the bottom, $Ga_{1-x}Al_xAs$, GaAs, $Ga_{1-y}Al_yAs$, and GaAs ($x \sim 0.5$, $y \sim 0.4$) with thicknesses 4, 0.3,2, and 2.5 μm, respectively. The first three layers are N type and form a double heterostucture in the direction perpendicular to the plane of the epilayers. The last GaAs layer is used as the diffusion mask.

After growth, a straight line parallel to [110] direction was defined using photolithographic methods. The GaAs layer on one side of the line was then etched away using the standard etching solution $H_2SO_4:H_2O_2:H_2O$ (1:8:1). The Zn diffusion was performed using $ZnAs_2$ as the diffusion source in an evacuated quartz ampoule ($\sim 10^{-6}$ torr at room temperature) at 660^oC for one hour. The cross

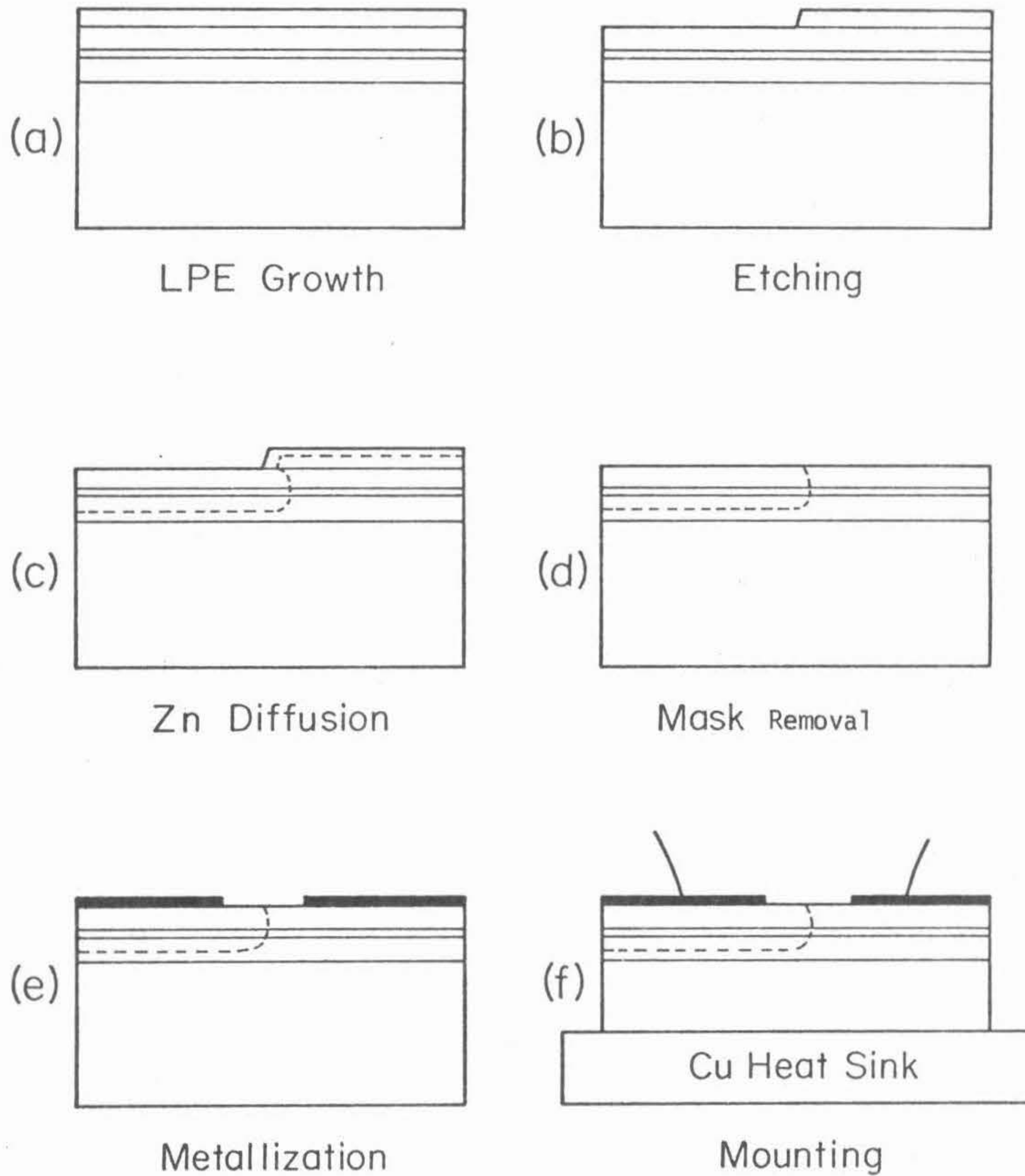

Fig. 4-15 Fabrication steps for a lateral injection laser.

section of the layers after diffusion is shown in Fig. 4-13a. Owing to the different Zn diffusion rates in GaAs and GaAlAs, the diffusion depth is much deeper in the unmasked region than in the GaAs mask. Following diffusion, the GaAs mask was etched away selectively using the solution H_2O_2 + NH_4OH at pH = 7.05.[27] The etchant removed GaAs only and stopped at the GaAlAs surface. Heat treatment was subsequently performed at 860°C for 1.5 hours in an H_2 atmosphere. Following that, metal contact of Au-Zn on the P side and Au-Ge on the N side were applied separately. The laser chip was mounted on a Cu heat sink with the two contact leads pointing up. The final structure is schematically shown in Fig. 4-13b.

In conventional stripe geometry lasers, two lines are required to define the active region. In our lateral injection lasers only one line is necessary because the active region is automatically defined by the carrier diffusion length. Therefore it requires no structural fineness in the lateral direction, which leads to easy fabrication and excellent reproducibility.

Fig. 4-16a is a scanning electron micrograph of the cross section of the layers. Two diffusion fronts can be seen, which are due to the two-step diffusion. The shallower one is from the first step diffusion, the deeper one is from the heat treatment. The enlarged portion of the PN junction near the GaAs region is shown in Fig. 4-16b. It shows very clearly that the slope of the diffusion

Fig. 4-16 (a) The SEM micrograph of the cross section of a lateral injection laser. The right hand side is the Zn diffused region. The left hand side was masked by a GaAs layer during the diffusion.

(b) The magnified picture of the diffusion front at the boundaries of the three epilayers. The shape of the diffusion front indicates different diffusion rates in different layers.

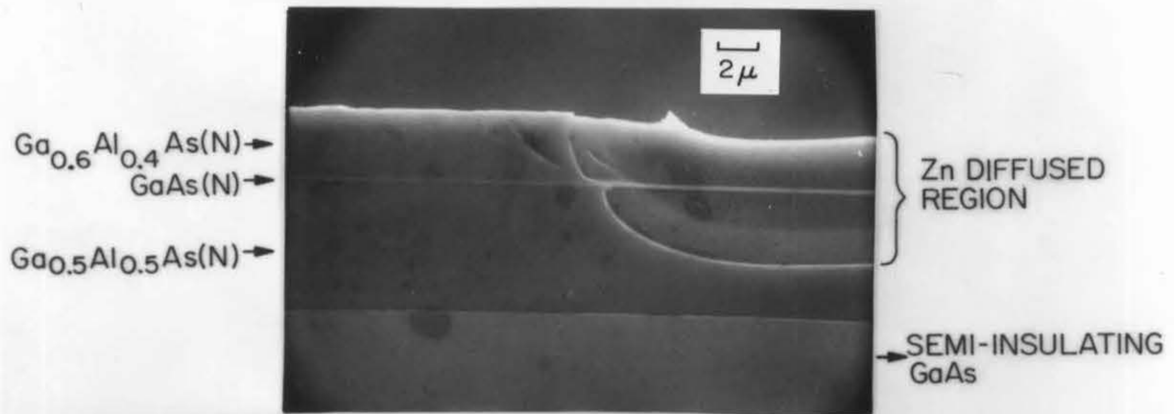

(a)

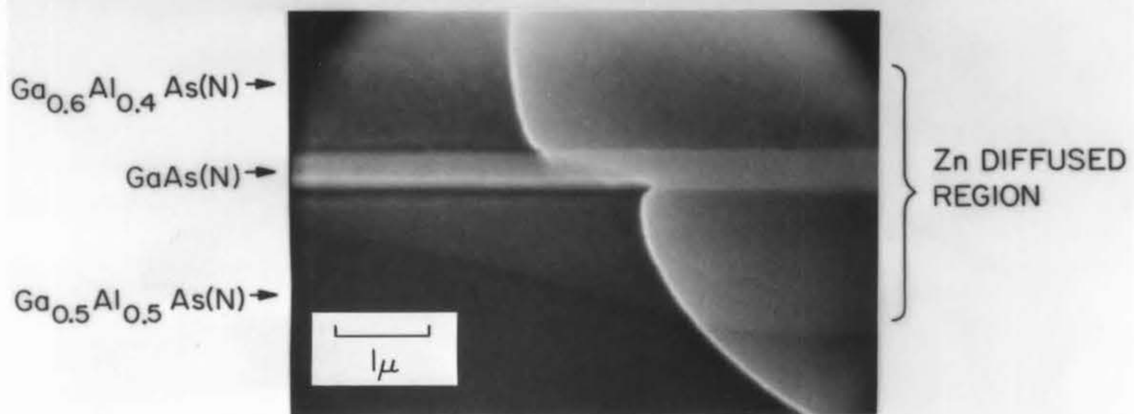

(b)

front changes at the GaAs and the GaAlAs boundaries. This indicates that Zn diffuses faster in GaAlAs than in GaAs. As shown in the micrograph the diffusion front in the GaAs region is not perpendicular but tilted at an angle to the plane of the epilayers. The width of the PN junction in this region is wider than the thickness of the GaAs layer. Because of this, the laser is not a pure homostructure laser as described in references 18,19 and 20, but a combination of homostructure and heterostructure.

IV.3.3 Experimental results

After fabrication the sample was thinned down to a thickness of about 100 μm and diced into individual laser bars. Each laser had a cavity length of about 300 μm. The lasers were mounted on Cu heat sinks similar to the one shown in Fig. 4-7. The measurements were carried out with the diodes driven by square current pulses having 100 nsec widths and a 1 KHz repetition rate.

The properties of lasers having different doping concentrations in the GaAs active layer were studied. We found that this concentration strongly affects the lasing characteristics. Fig. 4-17 shows the near field and the far field of a laser when the doping concentration is low ($\sim 10^{17}$ cm^{-3}, Sn doped). The near field has a half width (distance between the half power points) of about 5 μm. It has a small tail penetrating into the N side. As the current increases ($> 1.5\ I_{th}$) more modes appear on the N side. The far field distribution is similar to that of crowding effect lasers.

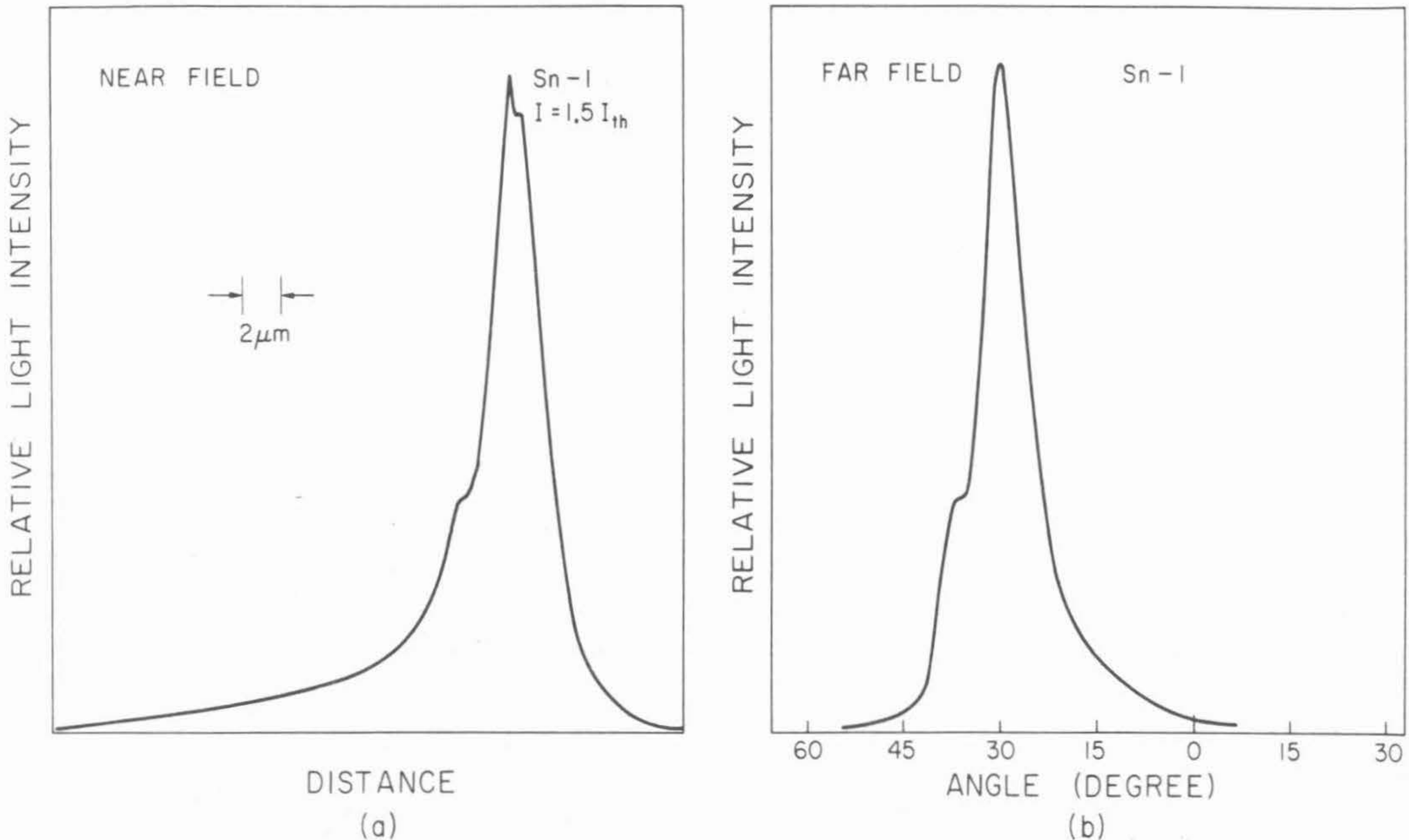

Fig. 4-17 (a) The near field, and (b) the far field of a lateral injection laser with a lightly doped ($\sim 1\times10^{17} cm^{-3}$, Sn doped) GaAs layer. The left hand side of each picture is the N side while the right hand side is the P side.

The light is emitted at an angle with respect to the normal direction to the N side. The maximum intensity appears at about 30°. This phenomenon can be explained by gain induced guiding and will be discussed in the next section. When the N type doping concentration of the GaAs layer is increased above 10^{18} cm^{-3} the near field becomes narrower and the peak of the far field moves to the center. Fig. 4-18, for example, shows the near field and the far field of a laser with a highly doped GaAs layer ($\sim 7 \times 10^{18}$ cm^{-3}, Te doped). The near field is very narrow with a half width of less than 2 μm. It corresponds to a single transverse mode and stays stable as the current increases. In most of the diodes the near field patterns remain unchanged as the driving current increases up to the point of catastrophic breakdown. The tail in the near field which appears on the N side at low doping concentration is absent. The far field pattern which is symmetric and centered at 0° resembles the usual far field of conventional stripe geometry lasers.

The difference in the mode characteristics between lasers having low doping concentration in the N GaAs region and lasers having high doping concentration is due to a difference in wave guiding mechanism. When the doping concentration of the N side of the GaAs junction is much lower than that of the P side ($\sim 10^{19}$ cm^{-3}, Zn doped), most of the recombination is due to hole injection. The laser light generated in

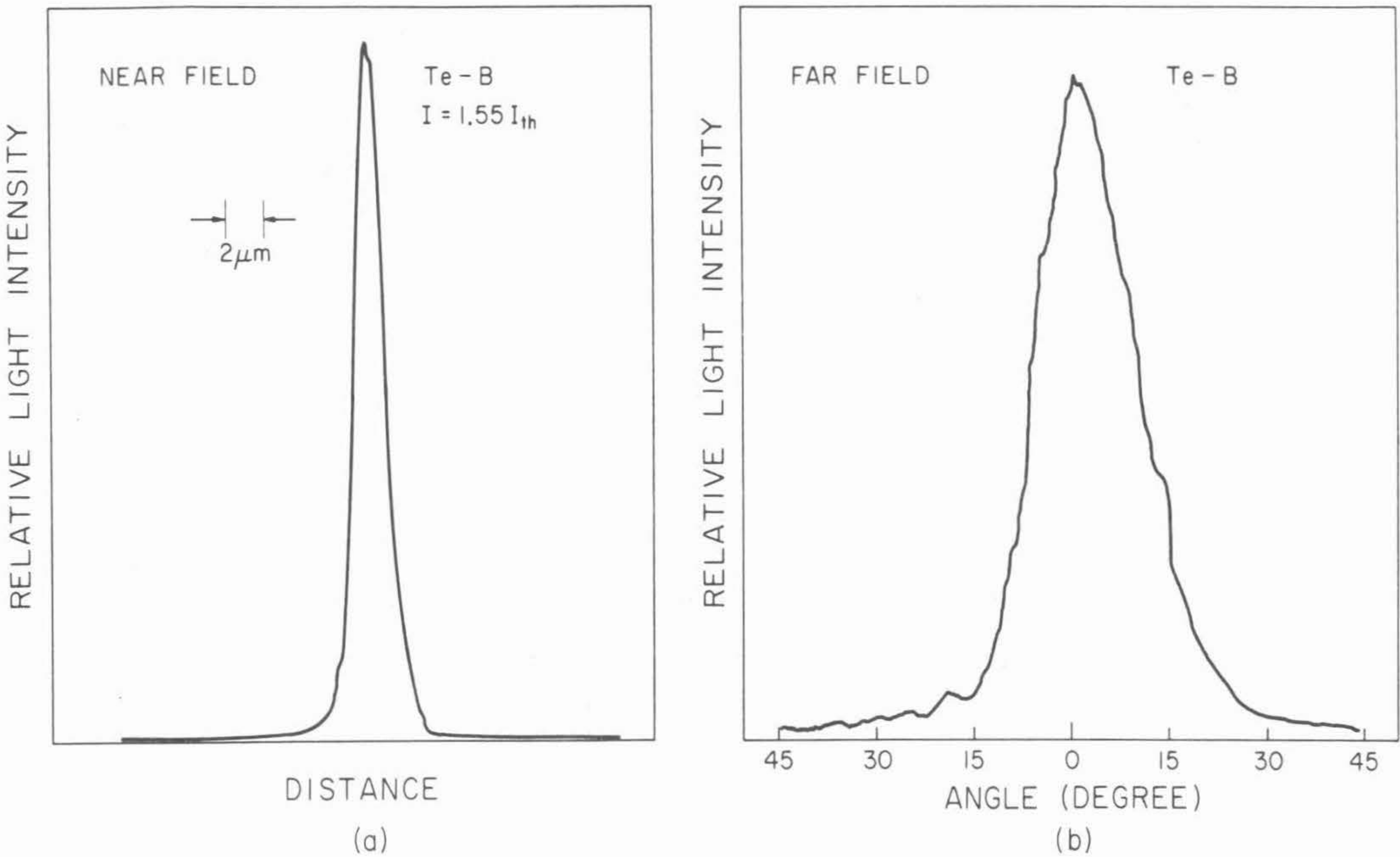

Fig. 4-18 (a) The near field, and (b) The far field of a lateral injection laser with a heavily doped GaAs layer ($\sim 7 \times 10^{18} cm^{-3}$, Te doped)

the active region is guided along the junction by the mechanism of gain-loss guiding. The gain-loss profile in the N side decays with distance away from the junction. As will be shown in the next section, the laser modes guided in such a medium have wavefronts tilted at an angle to the surface of the cavity mirror. The normal directions of the wavefronts point toward the N side. Consequently, as the laser light exits from the mirror surface, it propagates toward the N side. When the doping concentration is increased above 10^{18} cm^{-3} the increased electron injection to the P side causes the gain-loss profile to become symmetric about the junction plane. Furthermore, at the junction region, because of compensation, the effective doping concentration is lower and therefore the index of refraction is higher than those of the regions away from the junction.(28) The laser modes are guided along the junction by a combination of gain-loss guiding and real refractive index guiding. This results in symmetric far field patterns centered at 0°.

The N type dopant we used for the GaAs layer was Sn for low doping and Te for high doping. The lasers with the lowest threshold currents have doping concentrations of about 4×10^{18} cm^{-3} (Sn doped). The lasing threshold of a 300 μm long diode is about 40 mA. Fig. 4-19 shows the measured light intensity curve as a function of the driving current. The threshold current is 36 mA. The curve shows no kinks, or undesired nonlinearity, as the current is increased up to two times the threshold value. The differential quantum efficiency is about 35%. The near field and the far field are similar to those shown in Fig. 4-18.

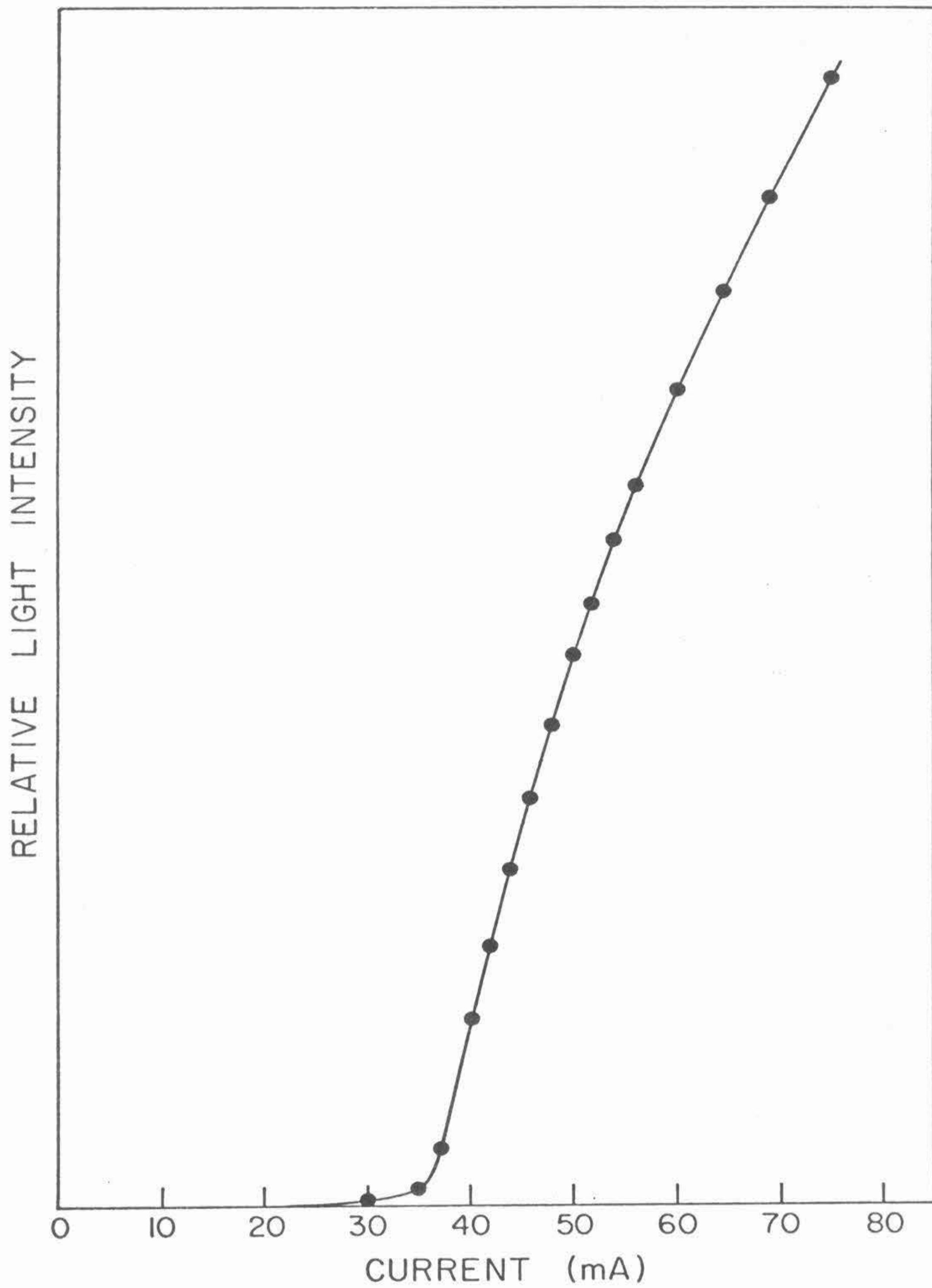

Fig. 4-19 The light output versus driving current curve of a lateral injection laser. The threshold is 36 mA.

The spectrum of the emitted light also varies as the N type doping concentration in the GaAs layer is changed. At low doping concentrations the spectrum shows the existence of a number of longitudinal modes. When the concentration is higher than about 5×10^{18} cm^{-3} (obtained by Te doping) a single longitudinal mode is observed. Fig. 4-20, for example, is the spectrum of one of these lasers. The oscillation wavelength is longer than that of one with lower doping concentration, which might be due to band tailing at high concentrations.

IV.4 Gain Induced Guiding

In this section we will develop the theory for explaining the nature of optical modes in a region with a gain profile. It is well known that confined Gaussian beams can be supported by a medium with a quadratic gain profile.(29) Unlike the case of refractive index guiding, the wavefronts of such modes are concave, as observed in the direction of wave propagation.(30) Gain induced guiding phenomenon has been found to be operative in several stripe geometry lasers.(31) The transverse laser modes are determined by the gain-loss profile in the active region. All the gain guided modes studied, however, involve only symmetric gain profiles. The observed near field and far field in such cases are not very different from those of the regular index guided modes. In the cases of crowding effect lasers and lateral injection lasers, described earlier in this chapter, the far field distributions are very different from those of regular lasers. The angular distributions of the light output of these lasers are asymmetric with respect to the normal direction of the cavity mirror (see Fig. 4-10

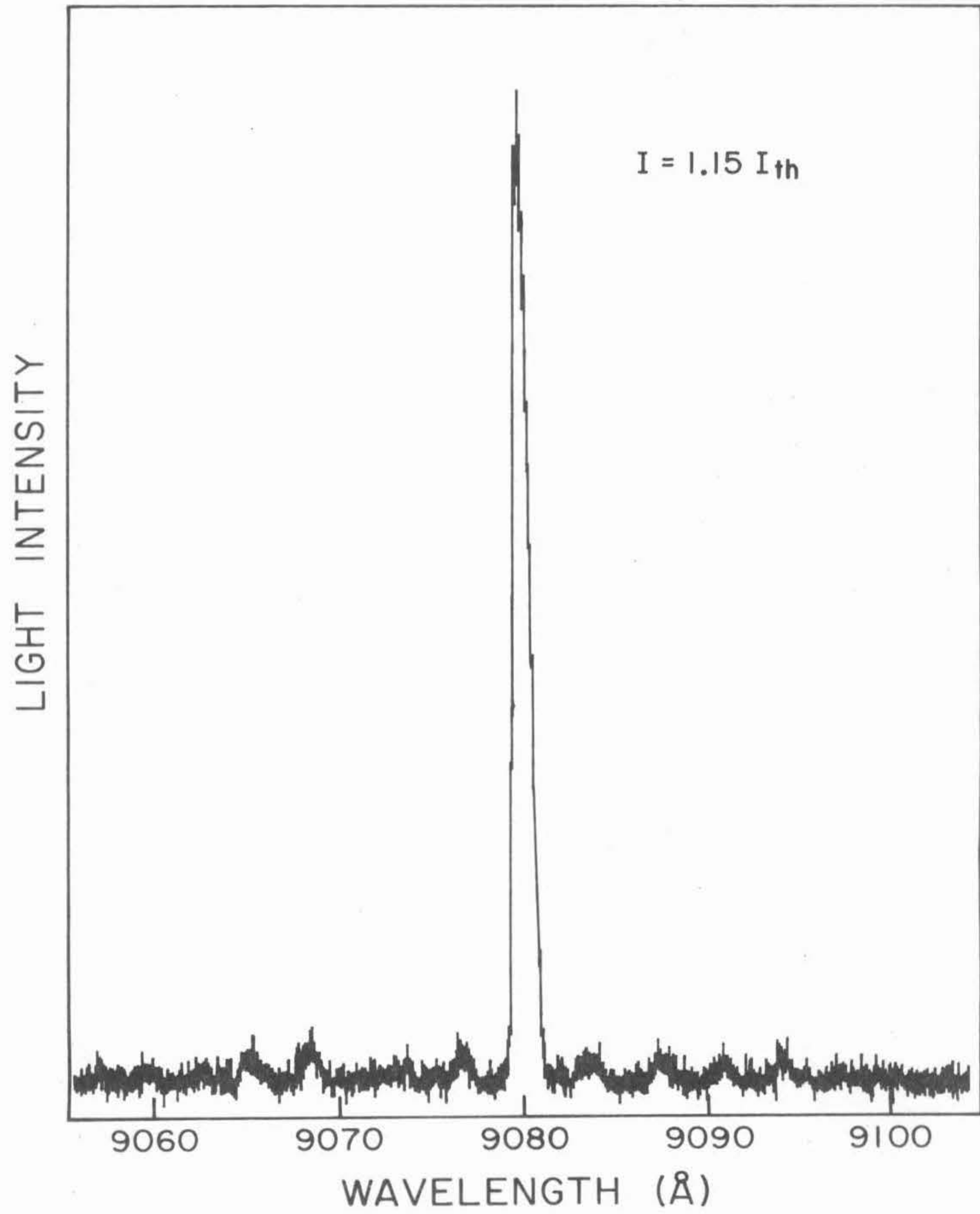

Fig. 4-20 The single mode spectrum of a lateral injection laser.

and Fig. 4-17). This feature can be explained in terms of gain-induced guiding but with an asymmetric gain-loss profile.[32]

For the convenience of illustration we redraw the crowding effect laser and the lateral injection laser in Fig. 4-21. In the crowding effect lasers the gain in the active region is highest near the edge of the step and decreases with distance away from the edge due to the injected carrier crowding near the step edge. In the case of lateral injection lasers, when the doping concentration of the N GaAs region is much lower than the Zn diffused P GaAs region, most of the recombination is due to hole injection. The injected carrier (hole) concentration and the gain profile, when lasing, decay exponentially with distance away from the junction into the N region.

In solving the wave equation in these two structures we assume the complex dielectric constant in the guiding region at $x > 0$ to be

$$\varepsilon(x) = \varepsilon_r + i(Ae^{-x/d} - B) \tag{4-38}$$

where ε_r is the real part of the dielectric constant. It is taken to be constant since for $x > 0$ the medium is homogeneous. The imaginary part of eq. (4-38) corresponds to the gain or the loss in the medium. The gain is assumed to be an exponentially decaying function with d as the characteristic length. The constant B accounts for the loss in the medium. Taking the electric field as $E(x)e^{i(\beta z-\omega t)}$ we can write the wave equation $\nabla^2 E + (\omega^2/c^2)\mu\varepsilon(r) = 0$ as

$$\frac{d^2E}{dx^2} + \left\{\frac{\omega^2}{c^2}\left[\varepsilon_r + i(Ae^{-x/d} - B)\right] - \beta^2\right\}E = 0 \tag{4-39}$$

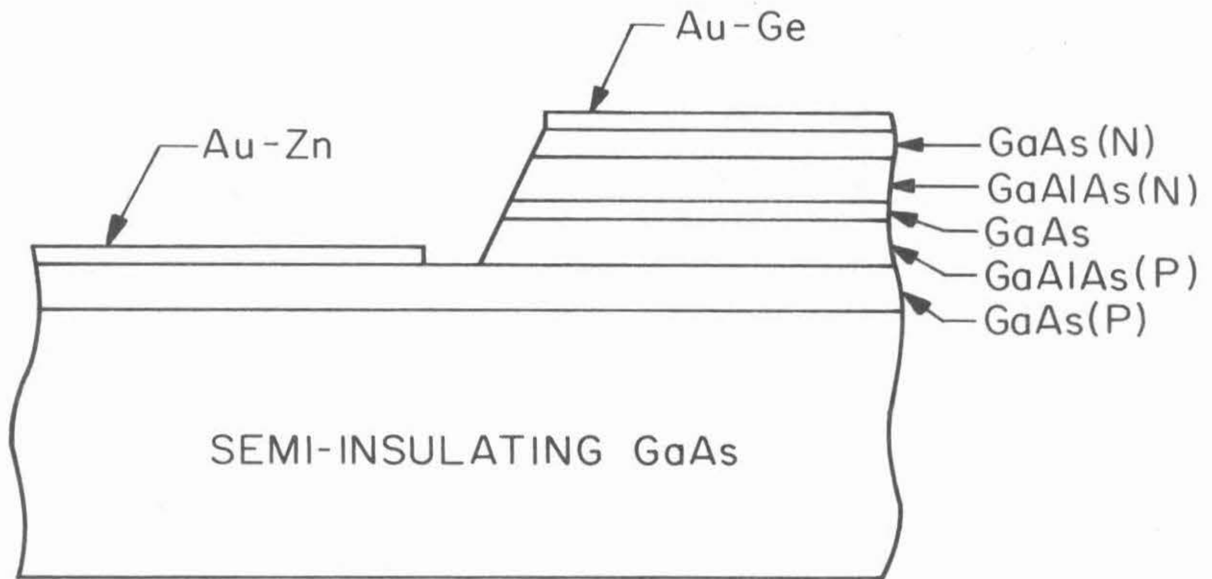

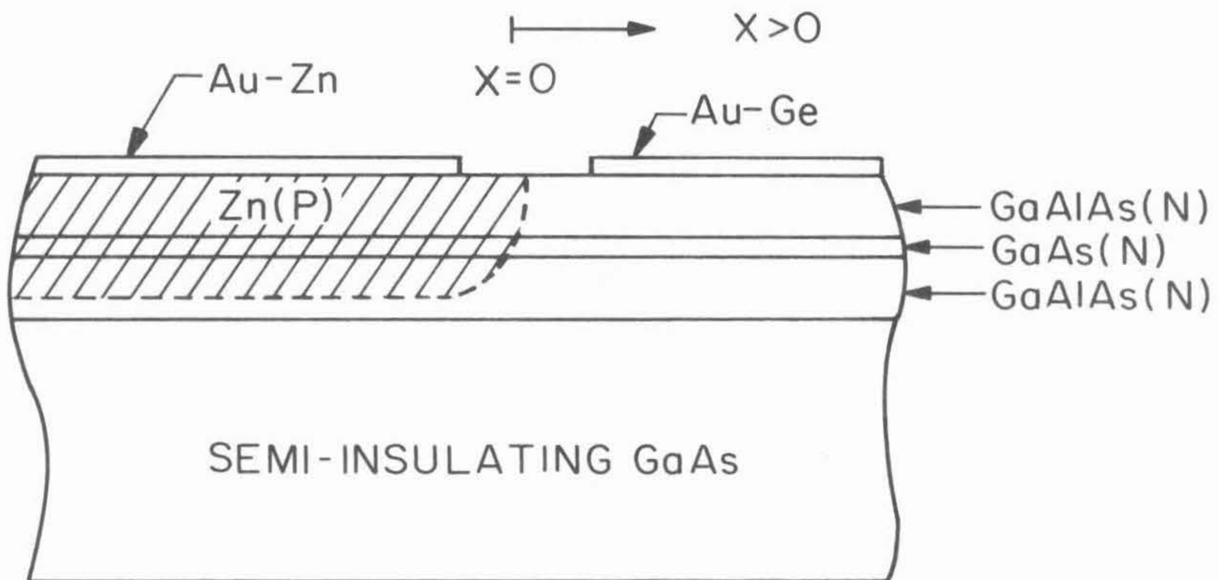

Fig. 4-21 The schematic drawings of the cross sections of (a) a crowding effect laser, and (b) a lateral injection laser.

where β is the propagation constant in the z direction (normal to the plane of the figure), ω is the angular frequency and c is the speed of light in vacuum. The dependence of the field on y (the direction perpendicular to the epilayers) can be treated independently using regular refractive index guiding and will not be considered here. For a guided wave E(x) must be zero as x goes to infinity. We also take E(0) = 0 since there is a large refractive index difference between GaAs and air in the case of crowding effect lasers and a strong absorption in the heavily doped P type GaAs region in the case of lateral injection lasers. The boundary conditions for a guided wave are thus

$$E = 0 \text{ at } x = 0 \text{ and } x \to \infty \tag{4-40}$$

Substituting

$$\xi = 2d\sqrt{iA}\,\frac{\omega}{c}\,e^{-x/2d} \tag{4-41}$$

into eq. (4-39) we can convert eq. (4-39) into a Bessel equation

$$\xi^2 \frac{d^2E}{d\xi^2} + \xi \frac{dE}{d\xi} + \left\{ \xi^2 - 4d^2[\beta^2 - (\varepsilon_r - i\beta) \frac{\omega^2}{c^2}] \right\} E = 0 \tag{4-42}$$

The solution of this equation is

$$E = DJ_\nu(\xi)$$

where D is an arbitrary constant and

$$\nu = 2d[\beta^2 - (\varepsilon_r - iB) \frac{\omega^2}{c^2}]^{1/2} \tag{4-44}$$

The other independent solution $Y_\nu(\xi)$ (Bessel function of the second kind) is not allowed since the solution needs to be bounded at $\xi = 0$ (i.e., $x \to \infty$). The eigenvalues ν are determined by the boundary condition at $x = 0$, i.e.,

$$J_\nu(4\pi \frac{d}{\lambda} \sqrt{iA}\,) = 0 \tag{4-45}$$

Here we have used the relation $\frac{\omega}{c} = \frac{2\pi}{\lambda}$, where λ is the wavelength in free space. Since $J_\nu(\xi)$ is a complex function of x we can write it as

$$J_{\nu_k} = r_k(x)\, e^{i\theta_k(x)} \tag{4-46}$$

where the index k indicates the mode number, $r_k(x)$ is the amplitude and $\theta_k(x)$ is the phase term. The electric field of the kth mode is then

$$D\, r_k(x)\, e^{i\theta_k(x)}\, e^{i(\beta_k z - \omega t)} \tag{4-47}$$

or

$$D\, r_k(x)\, e^{i[\theta_k(x) + \beta_{k,r}z] - i\omega t - \beta_{k,i}z} \tag{4-48}$$

where $\beta_{k,r}$, $\beta_{k,i}$ are the real part and the imaginary part of β_k respectively. The wavefronts of the modes are now described by

$$\beta_{k,r}z + \theta_k(x) = \text{constant} \tag{4-49}$$

Because of $\theta(x)$, the wavefronts of the modes are x dependent and no longer planar and perpendicular to the z direction. The eigenvalues

of β are obtained from eq. (4-44)

$$\beta_k = \left[\frac{\nu_k^2}{4d^2} + (\varepsilon_r - iB)\frac{\omega^2}{C^2}\right]^{1/2} \tag{4-50}$$

Since ε_r is dominant on the right hand side, β_k can be expanded by taking the first two terms of the Taylor series

$$\beta_k = \frac{\omega}{C}\sqrt{\varepsilon_r} + i\left(2\sqrt{\varepsilon_r}\ \frac{\omega}{C}\right)^{-1}\left(\frac{\nu_{k,r}\,\nu_{k,i}}{2d^2} - B\frac{\omega^2}{C^2}\right) \tag{4-51}$$

where $\nu_{k,r}$ and $\nu_{k,i}$ are the real part and the imaginary part of ν_k. Using the relations $\sqrt{\varepsilon} = n$ and $\frac{B\omega}{2nC} = \alpha$, we get

$$\beta_k = \frac{\omega}{C}n + i\left(\frac{\nu_{k,r}\,\nu_{k,i}\,C}{4d^2 n\,\omega} - \alpha\right) \tag{4-52}$$

where n is the refractive index of the medium and α is the loss coefficient in the medium. The imaginary part of β_k is the net gain (or loss) of the kth mode, which is

$$g_k = \beta_{k,i} = \frac{\nu_{k,r}\,\nu_{k,i}\,C}{4d^2 n\,\omega} - \alpha \tag{4-53}$$

The net gain is now separated into two parts. The first term is the gain coefficient and the second term is the loss coefficient. When g_k is positive the mode possesses net gain. When it is negative the mode is lossy.

As shown in eq. (4-46) the profile of the kth mode at a constant phase plane is described by $r_k(x)$. Fig. 4-22 is the numerical plot

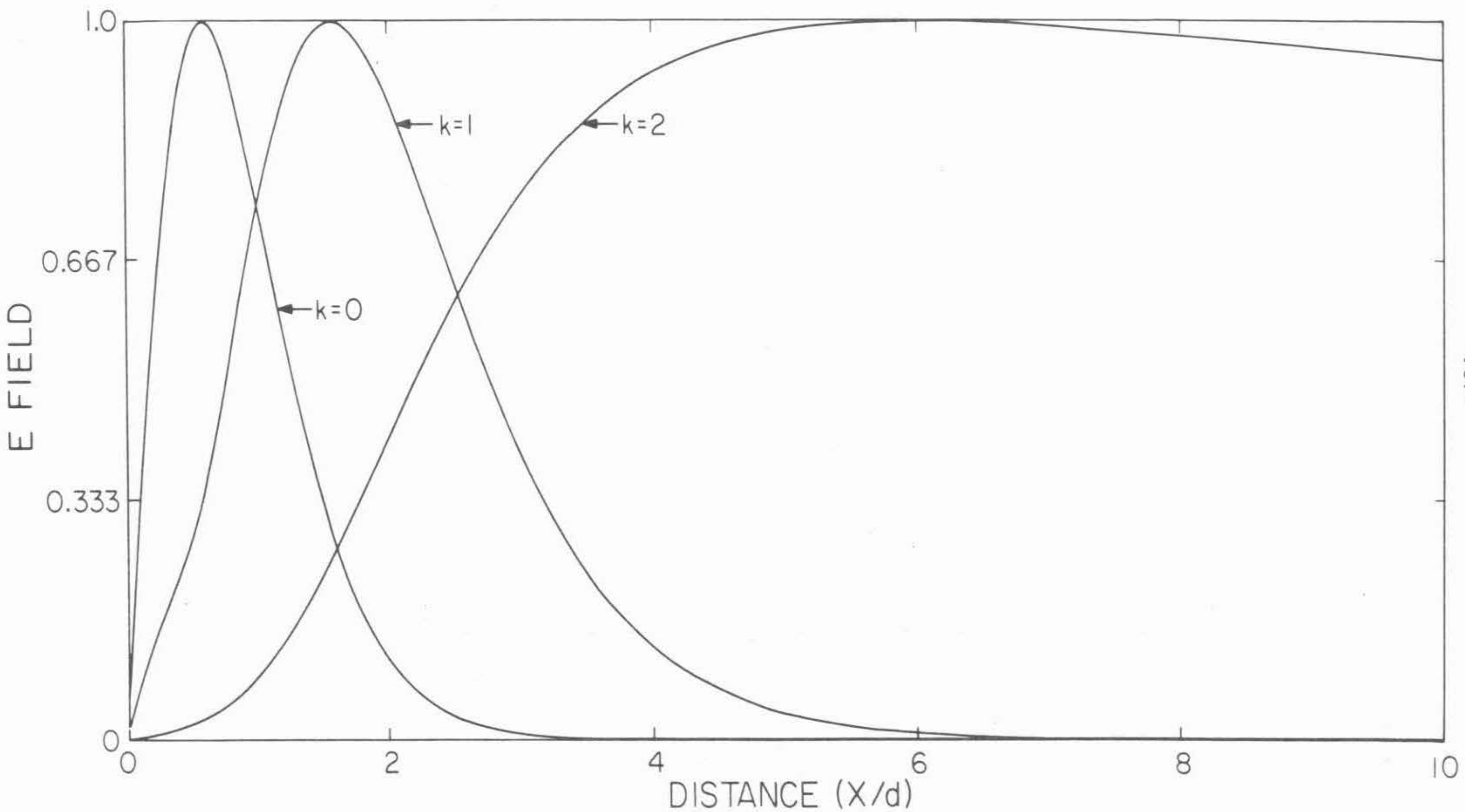

Fig. 4-22 Plots of the three modes calculated for a waveguide with $4\pi\frac{d}{\lambda}\sqrt{iA} = 10+10i$. The amplitudes of all the modes are normalized to 1.

of the modes when $4\pi \frac{d}{\lambda} \sqrt{iA} = 10 + 10i$. The zeros of $J_\nu(10 + 10i)$ were solved numerically and lie at values of 5.71+8.83i, 2.57+7.93i and 0.034+7.17i. There are thus three modes. An interesting feature of the mode profiles is that there are no zero crossings for the higher order modes. This is different from the situation in which the modes are guided by a real refractive index where the reflective boundaries produce standing waves in the waveguide and thus always give rise to zero crossings for the higher order modes. The wavefronts of these modes shown in Fig. 4-22 are determined by eq. (4-49) and are plotted in Fig. 4-23. Here we have taken GaAs as the guiding medium. The wavelength λ is taken to be 0.88 μm and index of refraction 3.6. As shown in the plot, the wavefronts are not perpendicular to the z axis. The normal direction of these wavefronts point toward $x > 0$ (lossy side). Therefore, as the modes are emitted from the laser cavity they propagate toward the $x > 0$ side. This satisfactorily explains why we observe the asymmetric far field distributions with peaks off to one side in our lasers. (see Fig. 4-10 and Fig. 4-17) For the particular case $4\pi \frac{d}{\lambda} \sqrt{iA} = 10+10i$, if we take $d = 6\lambda$ and $A = 2.714 \times 10^{-3}$ the angles between the normals of the wavefronts and the z axis are about 6.5^o. The gain of each mode can be readily calculated from eq. (4-53). If we take the loss constant α in the medium to be 125 cm^{-1}, the mode gains in our example are 50.87 cm^{-1}, -54.026 cm^{-1} and -124.063 cm^{-1} for the 0th, 1st and 2nd order mode respectively. Only the 0th order mode has net gain. The other two modes are lossy. This result is understandable since

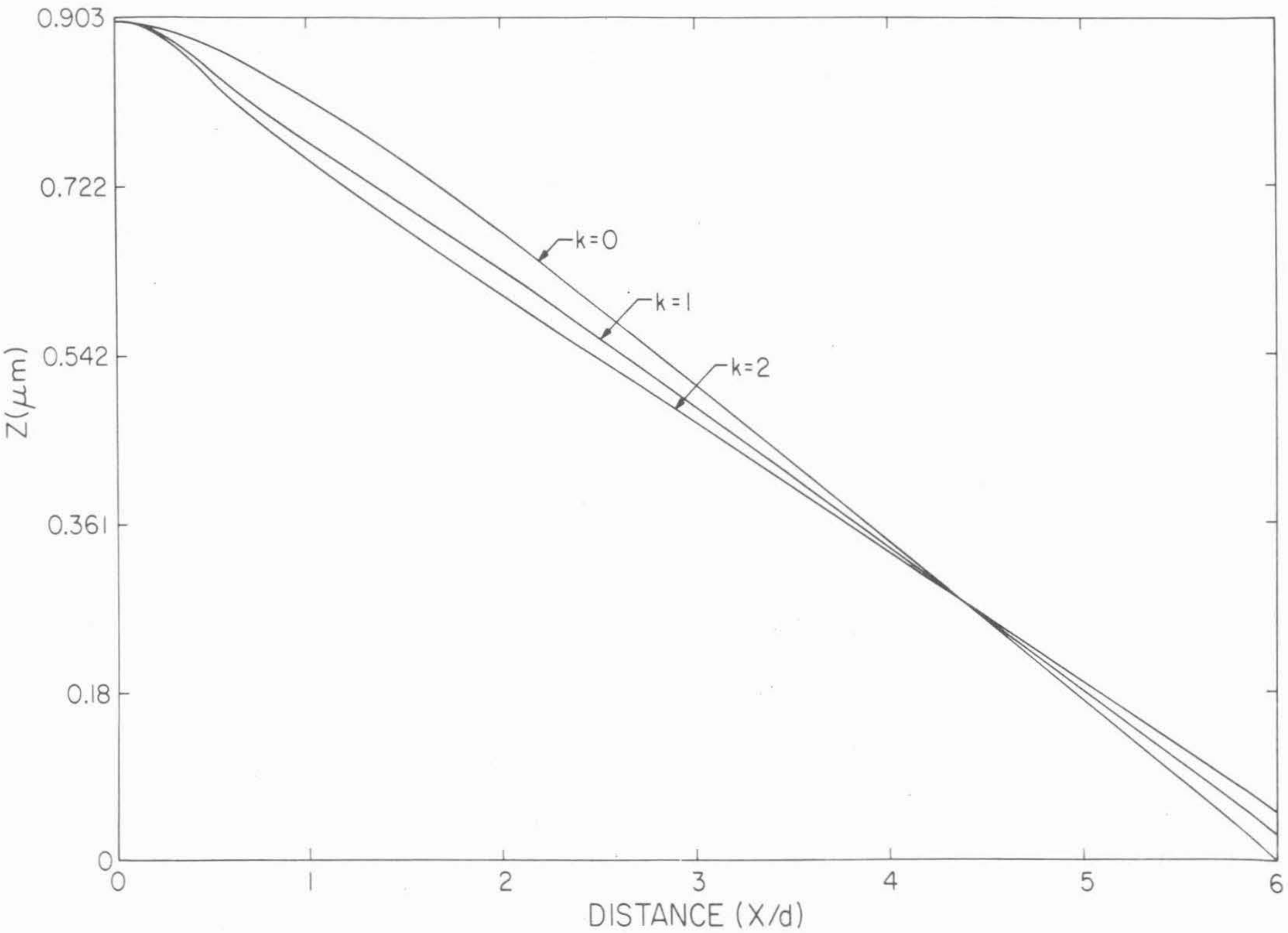

Fig. 4-23 Plots of the wavefronts of the three modes shown in Fig. 4-22.

the 0th order mode concentrates the intensity near $x = 0$ and consequently experiences the highest gain.

IV.5 Monolithic Integration of Injection Lasers with Electronic Devices

As mentioned in the introduction to this chapter the difficulty of integrating injection lasers with electronic devices on a single chip of GaAs is due to the fact that all GaAs lasers reported today have been fabricated on N^+ GaAs substrates. Because of the highly conductive substrates, electrical isolation, which is necessary for integration, is difficult to achieve. The idea of fabricating GaAs lasers on semi-insulating substrates was conceived with the aim of solving this problem. Using the non-conductive substrate we can perform the electrical integration on epilayers without worrying about the current leakage through the substrate and the parasitic interactions between the devices and the substrate. Furthermore, we can take advantage of the already developed GaAs planar technology to perform the integration.

In this section several examples of integration are discussed. The integration of a crowding effect laser and a Gunn oscillator, which we have demonstrated,[13] is discussed in IV.5.1. The possible integration of lasers with metal-semiconductor field-effect transistors (MESFET) is discussed in IV.5.2.

IV.5.1 Integration of a crowding effect laser with a Gunn oscillator on a semi-insulating substrate

GaAs injection lasers are of great interest as transmitters for high bit-rate fiber optical communication systems. One of the most attractive features of GaAs laser is the capability of high speed modulation into the GHz range.[33] A number of modulation schemes have been proposed and investigated. However, all the schemes modulate the lasers with external circuits. Because of high speed operation, special care has to be taken in wiring, connections, packing etc. to eliminate undesired parasitic capacitances and inductances. Monolithic integration, which does not suffer from these problems, is therefore much more attractive. However, monolithic integration was difficult and not seriously attempted till our success with the fabrication of lasers on semi-insulating substrates.

The first realization of this kind of integration was obtained by fabricating a crowding effect laser and a Gunn oscillator on a piece of semi-insulating substrate. The cross section of the structure is schematically shown in Fig. 4-24. The laser and the Gunn device are integrated in series, so that the high frequency oscillating current pulses from the Gunn device pass through the laser and modulate the light output. The advantage of using a Gunn device lies in the fact that it can supply fast current pulses of constant waveforms without any shaping, and it can be easily fabricated.

The structure of the crowding effect laser used for this integrated device is similar to the one described in section IV.2 except that the

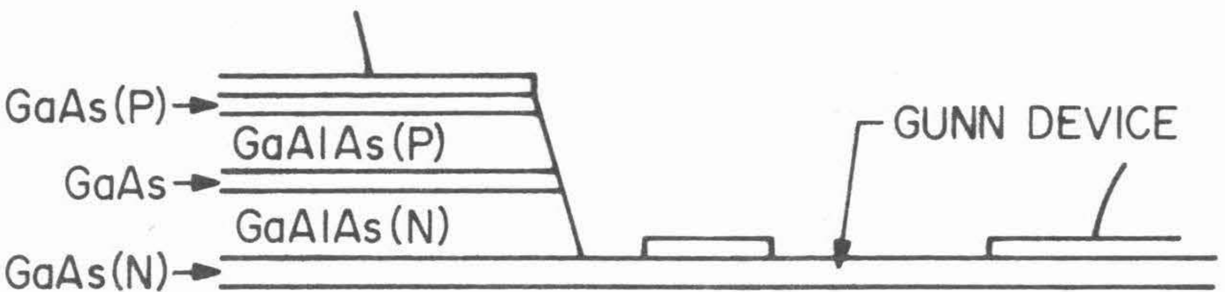

Fig. 4-24 The schematic drawing of the integrated Gunn-Laser device. The electrode on the left side of the Gunn device was not used. The voltage was applied between the electrode to the right and the P type contact on top of the mesa.

N type layers lie below the P type layers. The reason for doing this is that only N type GaAs displays the Gunn effect.[8]

Gunn oscillation was first discovered by Gunn in 1963.[34] He found that when the applied electric field across a short N type sample of GaAs or InP exceeded a critical threshold value of several thousand volts per centimeter, coherent microwave output was generated. The frequency of oscillation was approximately equal to the reciprocal of the carrier transit time across the length of the sample. Later, Kromer pointed out that this oscillation was due to a differential negative resistance in the material.[35] The mechanism responsible for the differential negative resistance is a field-induced transfer of conduction-band electrons from a low-energy, high mobility valley to a higher energy, low-mobility valley. When this negative resistance appears (at certain high fields) current oscillation occurs. Of the semiconductor materials displaying Gunn effect, N type GaAs is the most widely understood and used.

The fabrication procedure of our integrated "laser-Gunn" device is the same as that described in IV.2.2. After the N type contact (Au-Ge) was evaporated,a stripe 140 μm was opened in the metal using photolithographic methods. The N GaAs layer under the window serves as the drift region of the Gunn oscillator. The cross section of the final structure is shown in Fig. 4-24.

If the voltage across the two electrodes of the Gunn device is higher than some critical value,Gunn oscillation occurs. The

oscillating current pulses flow through the PN junction in the mesa region and modulate the light. If the range of the current oscillation is higher than the lasing threshold current, the laser light will be modulated. If the threshold current of the laser lies in the range of the current oscillation the laser will be turned on and off repetitively at the oscillation frequency. The frequency of oscillation depends on the distance between the electrodes of the Gunn device and is higher when the distance is smaller.

The sheet resistance of the N type GaAs layer is an important parameter for this device because it determines the threshold of the Gunn oscillation and the effect of current crowding in the laser. We have chosen a doping concentration $\sim 10^{16}cm^{-3}$ for this layer and a thickness $\sim$ 3μm. For a 300 μm long device the typical threshold current for Gunn oscillation is about 200 mA and the lasing threshold is about 160 mA.

We have operated this integrated Gunn diode-laser as a two terminal device. The voltage was applied across the P type contact on top of the mesa and the cathode of the Gunn device. The laser (which serves as one of the Gunn oscillator's electrodes) and the Gunn device are thus integrated crystallographically since they use the same epitaxial layer for the series connection.

Fig. 4-25 shows a typical oscillogram of the current pulse and the light pulse. Trace 1 is the light pulse and trace 2 is the current pulse. Oscillation can be seen on top of both pulses. In this case even the minima of the current exceed the lasing threshold current ($\sim$170 mA)

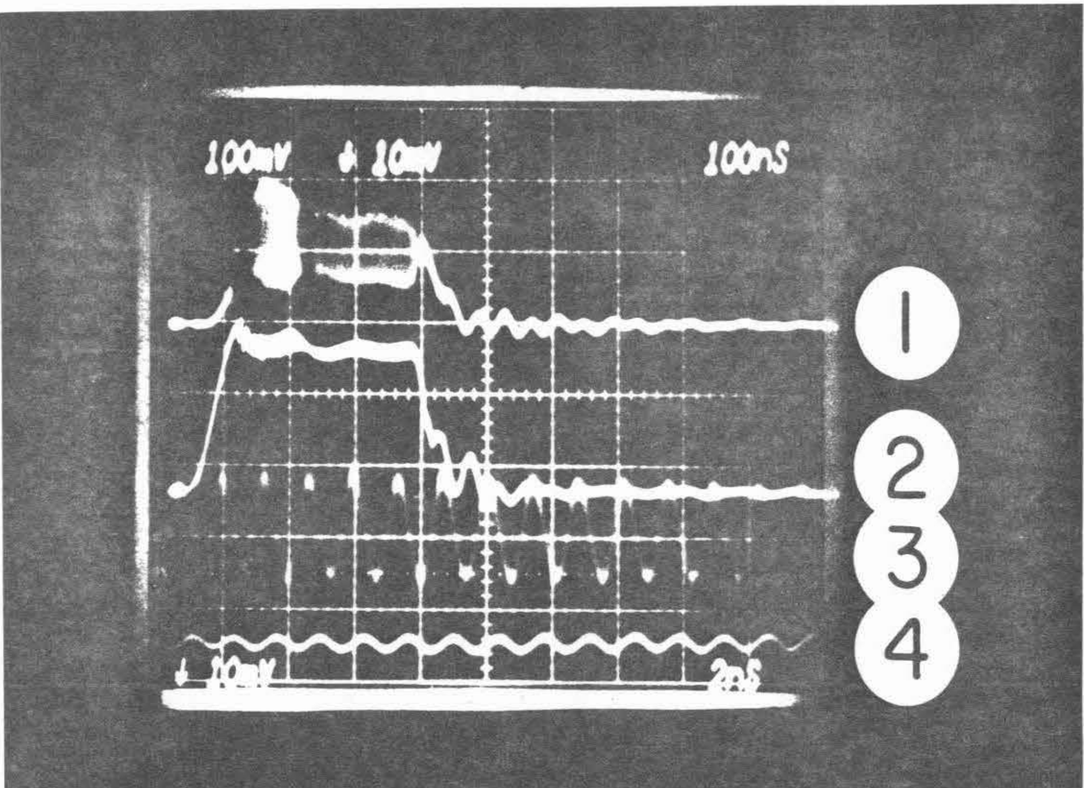

Fig. 4-25 The oscillogram of the current and the light output of an integrated Gunn-Laser device. (1) is the light pulse, and (2) is the current Pulse. The expanded traces of (1) and (2) are shown by (3) and (4) respectively. The time scale is 100 nsec/div for (1) and (2) and 2 nsec/div for (3) and (4).

and the laser is not turned off. Because of the nonlinear light current characteristics of lasers, the modulation depth of the laser output ($\sim$ 70%) is much larger than that of the current ($\sim$ 15%). Traces 3 and 4 are expanded traces of the light and the current, respectively. The frequency of oscillaion is about 0.75 GHz. 1 GHz modulation has been achieved with a smaller separation between the Gunn electrodes.

For three-terminal operation it is possible to add a Schottky gate on the Gunn device and use the gate to trigger the Gunn oscillation. In this way a single short laser pulse can be achieved.

IV.5.2 Integration of injection lasers with MESFET's

In the past few years, the GaAs metal-semiconductor field-effect transistor (FET) has become the most attractive high speed microwave transistor. This is due to its capability of high gain, low noise and high speed performance.[10] GaAs MESFET's are usually fabricated on N type epilayers or ion-implanted layers on semi-insulating substrates.

Integrating a MESFET with a crowding effect laser or a lateral injection laser on a common semi-insulating substrate can be easily conceived.[36] Fig. 4-26 shows two examples of the integration. The upper one in the figure is an integrated device consisting of a lateral injection laser and a MESFET, and the lower one shows the integration of a crowding effect laser with a MESFET. The fabrication procedure of these devices will consist of epitaxial growth, selective

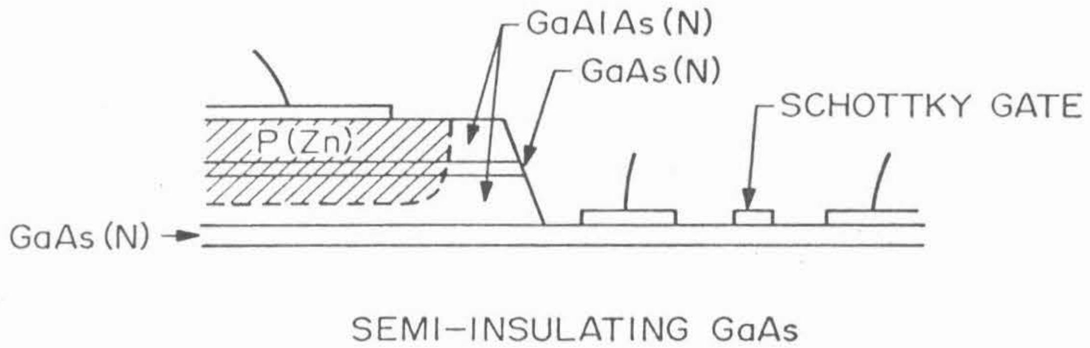

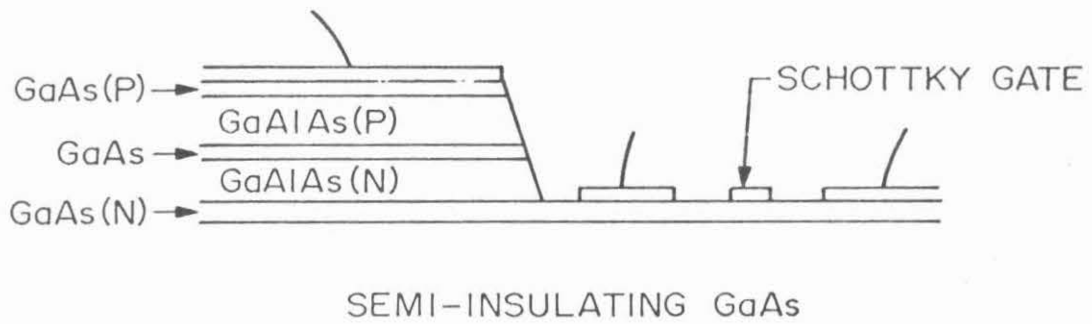

Fig. 4-26 These are two examples of the integration of a GaAs-GaAlAs laser with a Schottky gate FET. The upper one uses a lateral injection laser and the lower one uses a crowding effect laser.

etching, selective diffusion and metallization. The current passing through the FET is modulated by the signals from the Schottky gate and the laser light is, in turn, modulated by the current.

Since the laser and the FET are integrated on a single chip of GaAs crystal, it is possible to operate it at very high speed. Using today's know-how in GaAs microwave devices and the technology which we developed of fabricating GaAs lasers on semi-insulating substrates, considerable integration of high speed electronics and lasers can be expected in the near future.

REFERENCES FOR CHAPTER IV

(1) T. Tsukada, "GaAs-$Ga_{1-x}Al_xAs$ buried-heterostructure injection lasers", J. Appl. Phys. 45, 4899 (1974)

(2) H. Namizaki, "Transverse-junction-stripe lasers with a GaAs p-n homojunction", IEEE J. Quantum Electron. QE-11, 427 (1975)

(3) K. Aiki, M. Nakamura, T. Kuroda, J. Umeda, R. Ito, N. Chinone, and M. Maeda, "Transverse mode stablized $Al_xGa_{1-x}As$ injection lasers with channeled-substrate-planar structure", IEEE J. Quantum Electron. QE-14, 89 (1978)

(4) S. Somekh, E. Garmire, A. Yariv, H. L. Garvin, and R. G. Hunsperger, "Channel optical waveguides and directional couplers in GaAs-imbedded and ridged", Appl. Opt. 13, 327 (1971)

(5) F. L. Leonberger, J. P. Donnelly, and C. O. Bozler, "Low loss GaAs $p^+n^-n^+$ three- dimensional optical waveguides", Appl. Phys. Lett. 28, 616 (1976)

(6) F. L. Leonberger, J. P. Donnelly, and C. O. Bozler, "GaAs $p^+n^-n^+$ directional coupler switch", Appl. Phys. Lett. 29, 652 (1976)

(7) F. K. Reinhart, J. C. Shelton, and R. A. Logan, "Densely packed electrooptic $Al_{1-y}Ga_yAs$-$Al_xGa_{1-x}As$ rib waveguide modulators and switches", Topical Meeting on Integrated and Guided Wave Optics, paper MD2-1, Salt Lake City, Utah (1978)

(8) S. M. Sze, Physics of Semiconductor Devices, John Wiley & Sons Inc., New York (1969)

(9) J. A. Copeland and S. Knight, "Applications utilizing bulk negative resitance", in Semiconductors and Semimetals Vol.7, edited by R. K. Willardson and A. C. Beer, Academic Press (1971)

(10) C. A. Liechti, "Microwave field-effect transistors-1976", IEEE Trans. Microwave Theory Tech. MIT-24, 279 (1976)

(11) C. P. Lee, S. Margalit, and A. Yariv, "Double-heterostructure GaAs-GaAlAs injection lasers on semi-insulating substrates using carrier crowding", Appl. Phys. Lett. 31,281 (1977)

(12) C. P. Lee, S. Margalit, I. Ury, and A. Yariv, "GaAs-GaAlAs injection lasers on semi-insulating substrates using laterally diffused junctions", Appl. Phys. Lett. 32, 410 (1978)

(13) C. P. Lee, S. Margalit, I. Ury, and A. Yariv, "Integration of an injection laser with a Gunn oscillator on a semi-insulating GaAs substrate", Appl. Phys. Lett. 32, 806 (1978)

(14) G. R. Cronin and R. W. Haisty, "The preparation of semi-insulating GaAs by chromium doping", J. Electrochem. Soc. 111, 874 (1964)

(15) R. Zucca, " Electrical compensation in semi-insulating GaAs", J. Appl. Phys. 48, 1987 (1977)

(16) See for example, Pritchard, Electrical Characteristics of Transistors, McGraw Hill (1967)

(17) M. Abramowitz and I. A. Stegun, Handbook of Mathematical Functions, Dover Publications, Inc., New York (1970)

(18) H. Namizaki, H. Kan, M. Ishii, and A. Ito, "Transverse-junction-stripe-geometry double-heterostructure lasers with very low threshold current", J. Appl. Phys. 45, 2785 (1974)

(19) H. Namizaki, H. Kan, M. Ishii, and A. Ito, "Characteristics of the junction-stripe-geometry double heterostructure lasers", Japan J. Appl. Phys. 13, 1618 (1974)

(20) W. Susaki, T. Tonaka, H. Kan, and M. Ishii, "New structures of GaAlAs lateral-injection laser for low-threshold and single mode operation", IEEE J. Quantum Electron. QE-13, 587 (1977)

(21) L. R. Weisberg, "Diffusion in GaAs", Trans. TMS-AIME 230, 291 (1964)

(22) C. P. Lee, S. Margalit, and A. Yariv, "Dependence of Zn diffusion on the Al content in $Ga_{1-x}Al_xAs$", Solid State Electron.(to be published)

(23) B. J. Baliga and S. K. Ghandhi, "Lateral diffusion of Zinc and Tin in GaAs", IEEE Trans. Electron Device. ED-21, 410 (1974)

(24) D. Kendall, in Semiconductors and Semimetals Vol.4, edited by R. K. Willardson and A. C. Beer, Academic Press (1968)

(25) I. L. Chang and G. L. Pearson, "Diffusion mechanism of Zn in GaAs and GaP based on isoconcentration diffusion experiments", J. Appl. Phys. 35, 1960 (1964)

(26) H. Rupprecht and C. Z. Lemay, "Diffusion of Zn into GaAs under the pressure of excess arsenic vapor",J. Appl. Phys. 35,1970 (1964)

(27) R. A. Logan and F. K. Reinhart, "Optical waveguides in GaAs-GaAlAs epitaxial layers", J. Appl. Phys. 44, 4172 (1973)

(28) E. Garmire, D. F. Lovelace, and G. H. B. Thompson, "Diffused two-dimensional optical waveguides in GaAs", Appl. Phys. Lett. 26, 239 (1975)

(29) H. Kogelnik, "On the propagation of Gaussion beam of light through lens like media including those with loss or gain variation" Appl. Optic. 4, 1562 (1965)

(30) D. Marcuse, Light Transmission Optics, Van Nostrand, New York (1972)

(31) D. D. Cook and F. R. Nash, "Gain-induced guiding and astigmatic output beam of GaAs lasers", J. Appl. Phys. 46, 1660 (1975)

(32) C. P. Lee, S. Margalit, and A. Yariv, "Waveguiding in an exponentially decaying gain medium", Optics Comm. 25, 1 (1978)

(33) G. Arnold and P. Russer, "Modulation behavior of semiconductor injection lasers", Appl. Phys. 14, 255 (1977)

(34) J. B. Gunn, "Microwave oscillation of current in III-V semiconductors", Solid State Comm. 1, 88 (1963)

(35) H. Kromer, "Theory of the Gunn effect", Proc. IEEE, 52, 1736 (1964)

(36) C. P. Lee, S. Margalit, and A. Yariv, "GaAs-GaAlAs heterostructure lasers on semi-insulating substrates", IEEE Trans. Electron Device. (to be published)

CHAPTER V

EXPERIMENTAL TECHNIQUES

V.1 Introduction

During the course of studying the various GaAs-GaAlAs laser devices described in the previous chapters, many experimental techniques have been involved. They can be generally divided into three categories: material preparation, device processing, and device characterization and measurements.

All the structures described previously are prepared by a liquid phase epitaxial (LPE) growth system in our laboratory. The grown layers are generally smooth and of good quality. The thicknesses of the layers can be controlled to within a tolerance which is on the order of 0.1 μm. Good devices depend on the ability to grow good quality layers. Thus, material preparation is probably the most important step in the device fabrication. Details of the epitaxial growth are given in the next section.

The device processing includes cleaning, diffusion, photolithography, chemical etching, metallization, packaging, etc. Part of these procedures have been described in the previous chapters. In this chapter we will use the double heterostructure laser as an example of the fabrication procedure.

The characterization of a laser device includes threshold determination, spectrum measurement, and near- and far-field measurements. Since the wavelength of the GaAs laser is around 8500Å, infrared detectors have to be used in these measurements. Details of these

techniques are given in Section V-3.

V.2 GaAs-GaAlAs Liquid Phase Epitaxy

Epitaxy, derived from the Greek word "epi" meaning "on", and the word "taxis" meaning "arrangement", describes a technique of growing a thin crystalline layer on a parent substrate in which the crystallographic orientation of the layer is determined by that of the parent substrate. This technique has been used very widely in the fabrication of various types of semiconductor devices. For GaAs-GaAlAs heterostructure devices the epitaxial growth is especially important, because the multilayer structure cannot be achieved by techniques such as diffusion or ion implantation.

During the last ten years or so three kinds of epitaxial growth techniques for the GaAs-GaAlAs system have been developed. They are (1) vapor phase epitaxy (VPE) in which the material for growth is in the form of chemical compounds in the vapor phase, and in which GaAs or GaAlAs is deposited on the substrate by chemical reaction; (2) liquid phase epitaxy (LPE) in which the epitaxial layer is precipitated on the substrate from a saturated liquid solution; (3) molecular beam epitaxy (MBE) in which the constituents of the growth in the form of an atomic beam impinge upon the surface of the substrate in an ultrahigh vacuum system. Among these three techniques liquid phase epitaxy is by far the most popular and most reliable method for preparing high quality epilayers for optoelectronic devices. All the devices described in the previous chapters were fabricated in our laboratory using this technique.

In order to control the material composition of the epitaxial layers grown from the liquid phase, the composition-temperature relations for the Al-Ga-As system must be known. A number of studies reporting phase diagrams for GaAs-GaAlAs are available[1-3]. The resulting phase diagrams that describe the liquid and solid compositions that are in equilibrium at a given temperature are used to establish the necessary compositions of the liquid to be used for the growth of a given $Ga_{1-x}Al_xAs$ layer.

V.2.1 Growth system

The liquid phase epitaxial growth system used by the author is shown in Fig. 5-1. This is a so-called horizontal sliding boat system which was first developed by Panish et al.[4] In this system all the epitaxial layers can be grown during a single growth cycle without any intervening handling steps. The system consists of three major parts: a furnace, a quartz tube, and a graphite boat.

A photograph of the boat is shown in Fig. 5-2. It consists of three pieces of graphite. The upper piece has a number of wells which contain the growth solutions. Under this piece is a long slider on which the substrates are seated. The horizontal sliding bar rests on a bottom slab of graphite. The top surface of the sliding bar forms the floor for the solution wells. A small quartz tube is used to hold this boat in position relative to the furnace. This holding tube is sealed at the end which is in the furnace, and a thermocouple is inserted into the tube from the other end. The temperature of the boat is monitored

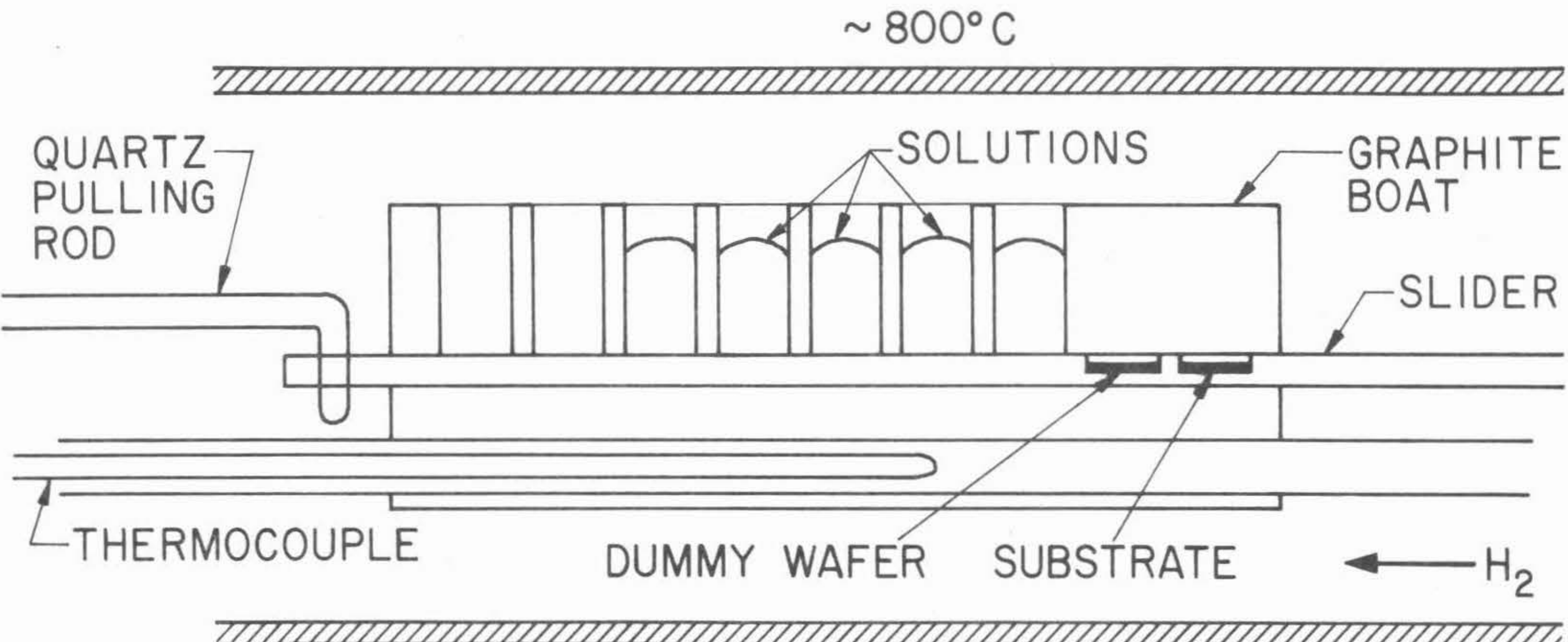

Fig. 5-1 The liquid phase epitaxial growth system used in this work

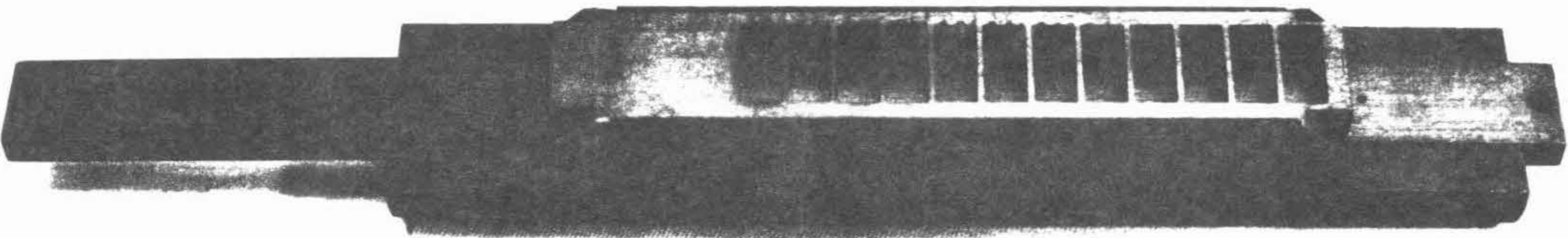

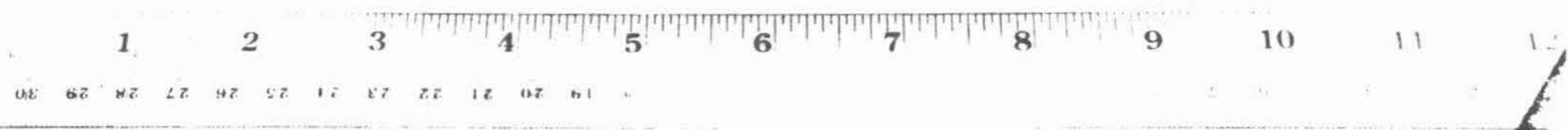

Fig. 5-2 The graphite boat used in this work

by this thermocouple during the entire growth cycle. The slider, which holds the growth substrates, can be moved relative to the solutions by a quartz rod so that the substrate can be translated from one well position to another under the various solutions. As illustrated in Fig. 5-1, the boat is placed into a quartz tube in a windowless resistance furnace. In order to assure a uniform growth on the substrate, the temperature profile along the furnace is kept very uniform. In a 25-inch long range near the center of the furnace, where the boat is located, the temperature variation is less than 0.5°C.

Elimination of oxygen in the growth system is one of the key factors in achieving good quality crystals. The GaAs substrates and the solutions, especially those which contain Al, can be easily oxidized at high temperatures. The oxidation prevents wetting between the substrate and the Ga solution, and results in irregular growth. In our system the whole quartz processing tube is airtight and kept in high purity hydrogen atmosphere with a constant flow of palladium-diffused hydrogen. The oxygen content in the system is monitored by an oxygen monitor. In normal conditions, the oxygen content in our system is less than 0.1 ppm.

V.2.2 Growth procedure

GaAs-GaAlAs LPE growth is usually carried out using Ga as a solvent. Other materials such as GaAs, Al, and dopants are added to the Ga to form the required liquid solution. If this solution is supersaturated with arsenic at an appropriate temperature ($\sim$ 800°C) and is brought in contact with a GaAs substrate, a solid epitaxial layer will be precipitated on the surface of the substrate. The supersaturation is

usually achieved by cooling the solution, and the growth rate of the epilayer depends on the rate of cooling.

The entire growth cycle consists of several steps. The first step is to bake the solvent-Ga. In the case of a four-layer double heterostructure as an example, we put Ga in the first four wells of the boat with each well containing four grams of Ga, and then insert the boat inside the quartz tube and heat it in the furnace at 800°C for about three or four hours. This baking step is very important for the growth, especially for GaAlAs because it cleans the Ga and drives out the residual oxygen which is dissolved in the Ga. After baking, the boat is taken out of the quartz tube and other materials are added to the Ga solvents. For a double heterostructure, the first layer is N GaAlAs, so GaAs, Al and Sn are put in the first well. The second layer is the GaAs active layer which is usually not intentionally doped, so only GaAs is added to saturate the Ga melt. The third layer, P GaAlAs, is similar to the first layer except for being P type, so instead of Sn we add Ge as the dopant. The last layer is P^+ GaAs, so we add GaAs and Ge in the fourth well.

Sn and Ge are the dopants we usually use for N type and P type layers, respectively. The aluminum concentration in the liquid is determined on the basis of the desired concentrations in the solid using the solidus and liquidus phase data.[3,5] GaAs is used to saturate the solutions at the growth temperature. At the same time we put these materials in the Ga melts, two pieces of GaAs substrate are placed on the graphite slider. The reason for using two substrates will be explained below. In most instances the substrates are (100) N type GaAs doped in

the range $n = 10^{18}$ to $10^{19} cm^{-3}$ with silicon or tellurium. They are cleaned and etched with $H_2SO_4:H_2O_2:H_2O$ (4:1:1) to remove possible surface damage. The size of each substrate is 7.5 mm x 14.5 mm.

After the boat is loaded and inserted back into the quartz tube, the whole system is flushed with hydrogen for about two or three hours before it is heated up. Heating the system from room temperature to the growth temperature, ∿800°C, takes about 40 minutes. After it reaches this temperature we usually leave it there for three or four hours so that complete thermal equilibrium can be reached inside the solutions. We then set up a cooling rate to lower the temperature of the furnace, and use the quartz pulling rod to bring the GaAs substrates into contact with the different solutions successively from the first solution to the last. As the temperature drops, the saturated material in the solutions precipitates on the substrates to form the epitaxial layers. The cooling rate determines the growth rate and is usually set at 0.1°/min to 1°/min. For embedded epitaxy, since the growth rate is higher than that of the usual growth, a much lower cooling rate was used.

The two GaAs substrates which are put on the slider are used in the growth for different purposes. The first one, which is closer to the solutions in the starting position, is called the "dummy" wafer (see Fig. 5-1). The second one is the "actual" wafer, on which we need to grow the layers. The dummy wafer is introduced under each solution before the second wafer. Therefore, it brings the solutions into equilibrium with respect to arsenic concentration before the growth takes place on the actual substrate. This technique was first used by Dawson,[6] and is

called "near equilibrium" growth. With this technique the layer thickness and the growth rate can be easily controlled because the growth starts on the "actual" wafer from an almost equilibrium solution. At temperatures near 800°C the GaAs epilayer grows with a rate of about 1 μm for every one degree of cooling. The $Ga_{1-x}Al_xAs$ layer grows at a slower rate, and the higher the Al content the slower it grows. When $x = 0.4$ the growth rate is about 0.5 μm/°C. The thickness of each layer is thus controlled by the temperature drop during the growth. Figure 5-3 shows a typical growth cycle of a GaAs-GaAlAs double heterostructure and the corresponding layer thicknesses. A photograph of a typical wafer after a four-layer growth is shown in Fig. 5-4. Except for a few small spots and for the areas near the edges, the surface of the growth is usually smooth and mirror-like.

V.3 Laser Diode Fabrication

In this section we use the case of a regular double heterostructure laser as an example to describe the fabrication procedures of a laser diode. The compositions, dimensions and sequence of the layers are the same as those shown in Fig. 1-3. After the layers are grown, the sample is taken out of the growth system and then cleaned with hot methanol and hydrochloric acid to remove the residual Ga drops which remain on the surface of the wafer. The sample is then rinsed in distilled water and blown dry with high purity nitrogen. Following that, it is placed into a vacuum chamber and P type contact metal is evaporated on the surface of the top epilayer. The metal used for P type contact is usually either a Cr-Au or a Au-Zn alloy. Cr-Au requires two steps of evaporation: a thin

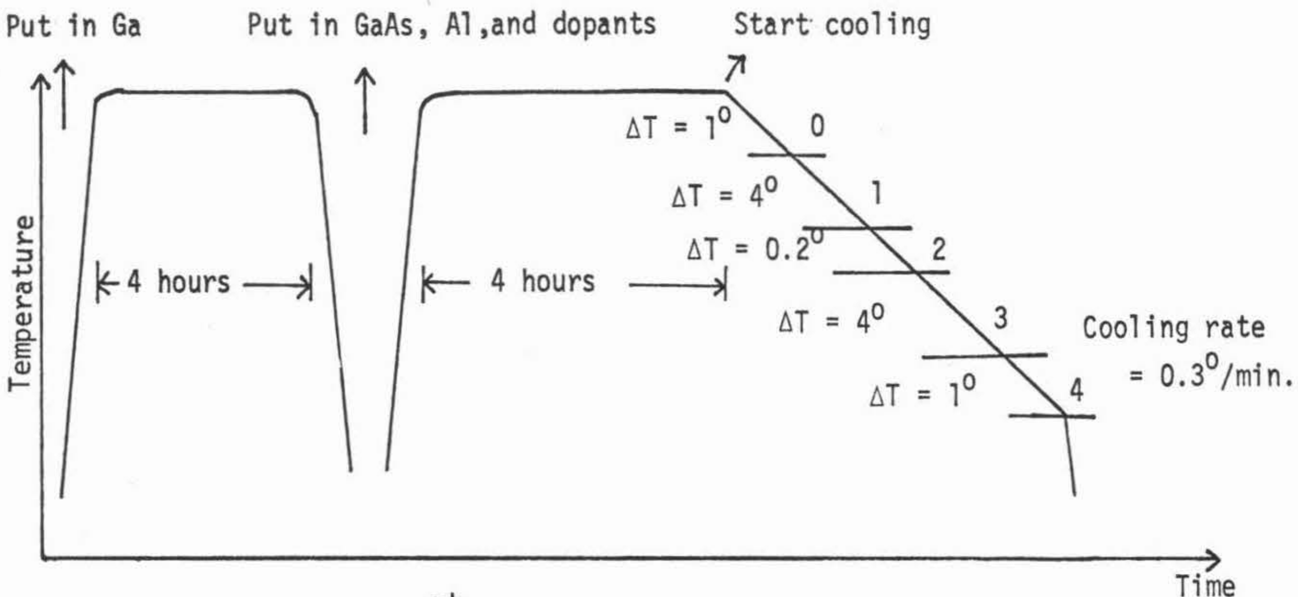

0: Dummy piece under the 1st solution

1: Actual piece under the 1st solution, dummy piece under the 2nd solution
growth of N $Ga_{0.6}Al_{0.4}As$ layer (2μm)

2: Actual piece under the 2nd solution, dummy piece under the 1rd solution
growth of GaAs active layer (0.2μm)

3: Actual piece under the 3rd solution, dummy piece under the 4th solution
growth of P $Ga_{0.6}Al_{0.4}As$ layer (2μm)

4: Actual piece under the 4th solution
growth of P^+ GaAs layer (1μm)

Fig. 5-3 A typical growth cycle of a four-layer double heterostructure laser

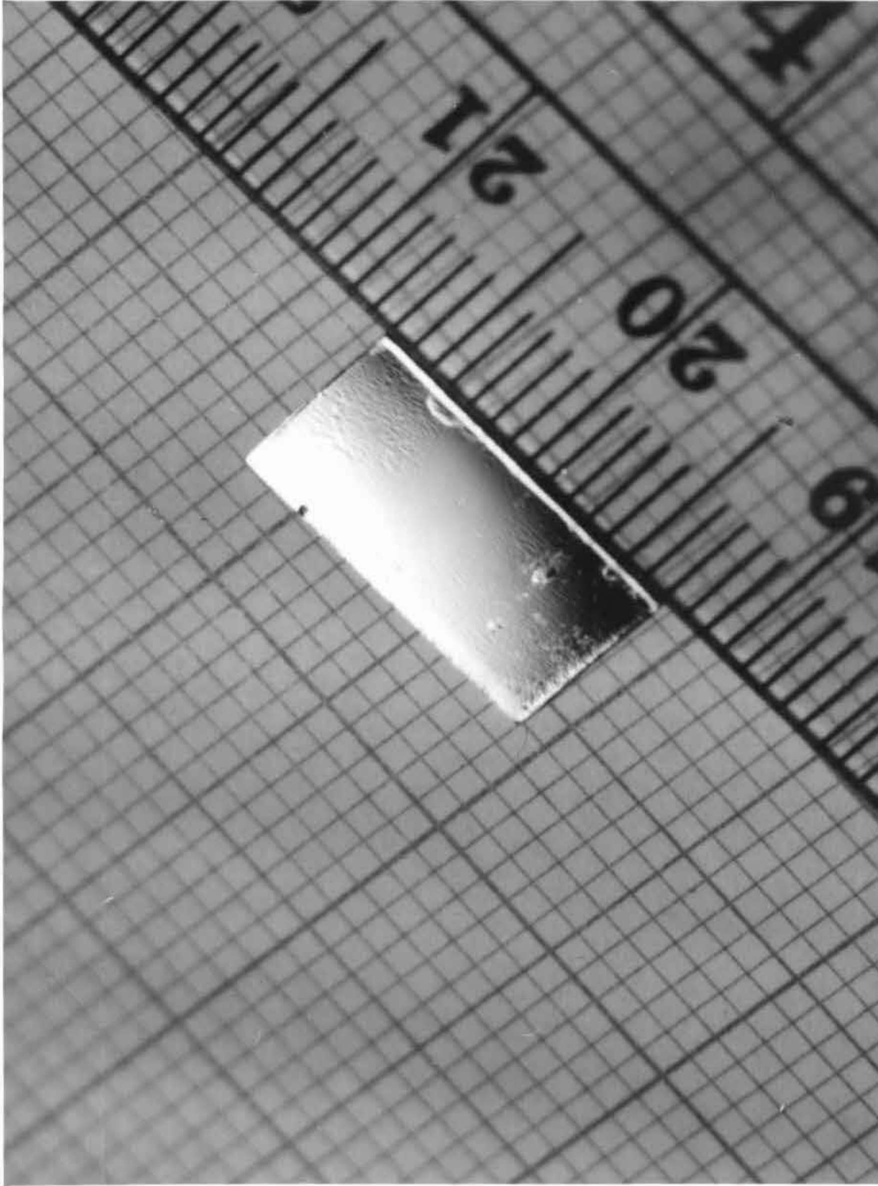

Fig. 5-4 A typical top view of a wafer after a four-layer epitaxial growth. The dimension of the wafer is 7 X 14 mm^2.

layer of Cr (∿ 500Å) is evaporated first, and then a thick Au layer (∿ 3000Å) is evaporated. During evaporation, the wafer is heated at ∿500°C (for Cr) and then ∿200°C (for Au) for better adhesion and better ohmic contact. Au-Zn alloy, containing 95% Au and 5% Zn, is evaporated on the wafer in a single step. The sample is subsequently heated in H_2 atmosphere at 500°C for 5 minutes. After the P type contact is prepared, the n side (substrate) of the wafer is lapped until the total wafer thickness is about 100 μm. The lapped surface is cleaned briefly in H_2SO_4:H_2O_2:H_2O (4:1:1) and rinsed with water, and then the N type metal contact is applied on it. We have used electrodeless plating of Au-Sn and evaporation of Au-Ge to deposit this contact layer. When the former is used, the P side of the wafer is masked with a plating resist and then the wafer is immersed for about 30 seconds in an electrodeless plating solution which deposits gold and a small amount of tin on the lapped surface. The plating-resist mask is then removed and the wafer is placed on a hot stage with a hydrogen atmosphere, heated to 450°C, and cooled rapidly. When Au-Ge alloy (86% Au and 14% Ge) is used, the sample is placed in a vacuum system and the metal layer is evaporated on the lapped surface. Following that, the contact is thermally alloyed at 430°C for one minute. Alloying the metal contact with the semiconductor is an important step in making good ohmic contact. Recently we found that alloying of Au-Ge on N type GaAs can also be achieved using a Q-switched ruby laser.(7) The short laser pulse (15 nsec) raises the temperature of the contact instantaneously above the eutectic point and makes it alloy. The resulting contact has more uniform surface quality and lower contact resistance ($\sim 7 \times 10^{-5} \Omega\text{-cm}^2$) compared with that of conventional thermal

alloying techniques.

After the contacts are applied, the sample is cleaved into bars in the [110] direction. The bars are 300-500 μm wide with the smooth cleaved edges comprising the partially reflecting mirrors for the laser cavities. The bars are cut into slices ∿100 μm wide with a microsaw. Each slice is thus an individual laser. The lasers are then mounted on copper heat sinks for subsequent testing.

V.4 Optical Measurements

V.4.1 Threshold current, differential quantum efficiency and spectrum

After a laser is fabricated, several optical measurements are performed. The first one is the determination of the threshold current and the differential quantum efficiency. Threshold current is usually found by plotting the curve of light intensity versus driving current, as those shown in Figs. 2-11, 4-8, and 4-19. The current at the point where the curve has a dramatic change in slope, viz., when the light output starts to go up rapidly with current, is the threshold current. The light intensity was measured with a S1 photomultiplier.

The differential quantum efficiency of a laser is defined by[8]

$$\eta_d = \frac{d(P_o/h\nu)}{d\left(\frac{I - I_{th}}{q}\right)} \qquad (5\text{-}1)$$

where P_o is the power output at current I, $h\nu$ is the photon energy, q is the electronic charge, and I_{th} is the threshold current. The power output was measured with a calibrated silicon photodetector, and η_d, as defined

in eq. (5-1) was taken as the slope of the light-current curve.

The spectra of our lasers were measured with a Czerny-Turner scanning spectrometer (SPEX #1600). The laser light was focused onto the input slit of the spectrometer and the signals from the output slit were picked up by a water-cooled GaAs photomultiplier. The grating in the spectrometer was slowly rotated by a driving motor and the signals from the photomultiplier were integrated by a boxcar integrator, and then recorded on a strip chart recorder.

V.4.2 Near field measurements

The laser light mode profile in the direction perpendicular to the cavity is usually obtained by measuring the light distribution at one of the cavity mirrors. This mirror illumination is called the near field pattern of the laser. The experimental setup used by us to perform this measurement is shown in Fig. 5-5. The near-field pattern at a cleaved end of a laser was imaged by means of a microscope objective onto a 20 μm wide slit placed in front of a S1 photomultiplier located 0.35 meters from the imaging objective. The microscope objective used in the setup had a magnification factor of 43:1, a focal length of 4 mm, and a numerical aperture (N.A.) of 0.85. The resolution, as determined by Rayleigh criterion,[9] was

$$S = \frac{1.22\lambda}{2\ NA} = \frac{1.22 \times 0.85}{2 \times 0.85}$$

$$= 0.65\ \mu m \tag{5-2}$$

where we have taken the wavelength λ to be 0.85 μm.

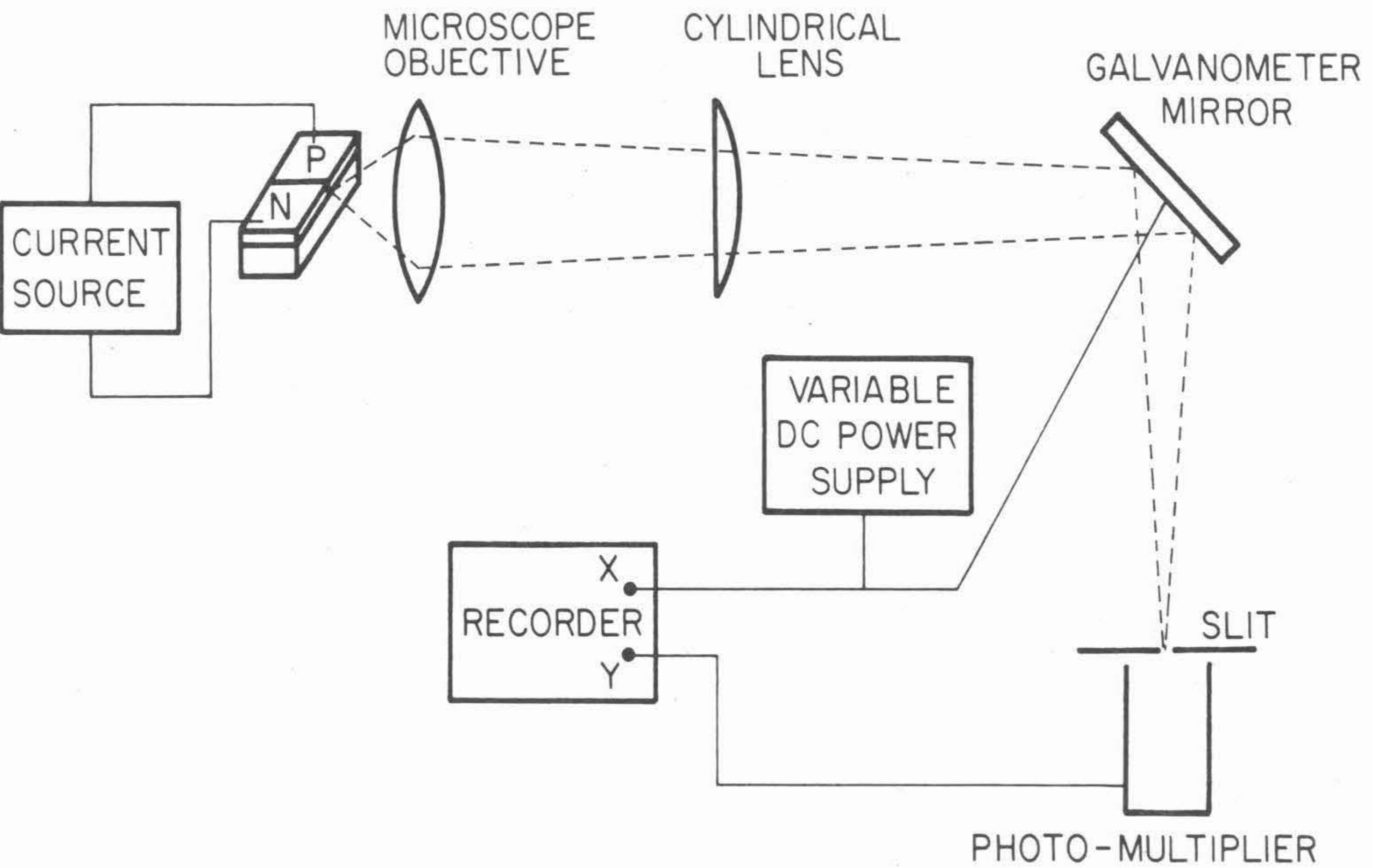

Fig. 5-5 Set-up for measuring lasers' near field patterns.

The magnification of the whole system, as the ratio of the image distance and the focal length of the objective, was 87.5. Since the diameter of the Rayleigh disk imaged onto the slit was about 57 μm ($\simeq$ 87.5 x 0.65 μm) the system resolution was determined by eq. (5-2) as opposed to the width of the slit which was 20 μm.

The mode profiles were obtained by scanning, via a galvanometer mirror, the imaged patterns over the slit of the photomultiplier. The galvanometer mirror was driven by a variable D.C. power supply which was manually controlled. The output of the photomultiplier went to a boxcar integrator and the integrated signal was recorded on an X-Y recorder whose X base was driven by the same D.C. voltage which drove the galvanometer mirror.

V.4.3 Far field measurements

The far field radiation pattern of a laser is the spatial distribution of the laser light at a distance much greater than the dimension of the light source, i.e., the near field. From the far field pattern one can tell how the light propagates after it is emitted from the laser cavity. For example, Fig. 4-17, the far field of a lateral injection laser, tells us that the laser light propagates to one side instead of being emitted perpendicular to the front mirror. Also, owing to the finite dimension of the near field, the far field tells us how the light is diffracted and the divergence of the beam.

Far fields are usually given as functions of the angle between the observation direction and the normal of the front mirror. The experimental setup used to perform the far field measurements is shown in Fig. 5-6. The laser was put at the center of a rotating table where

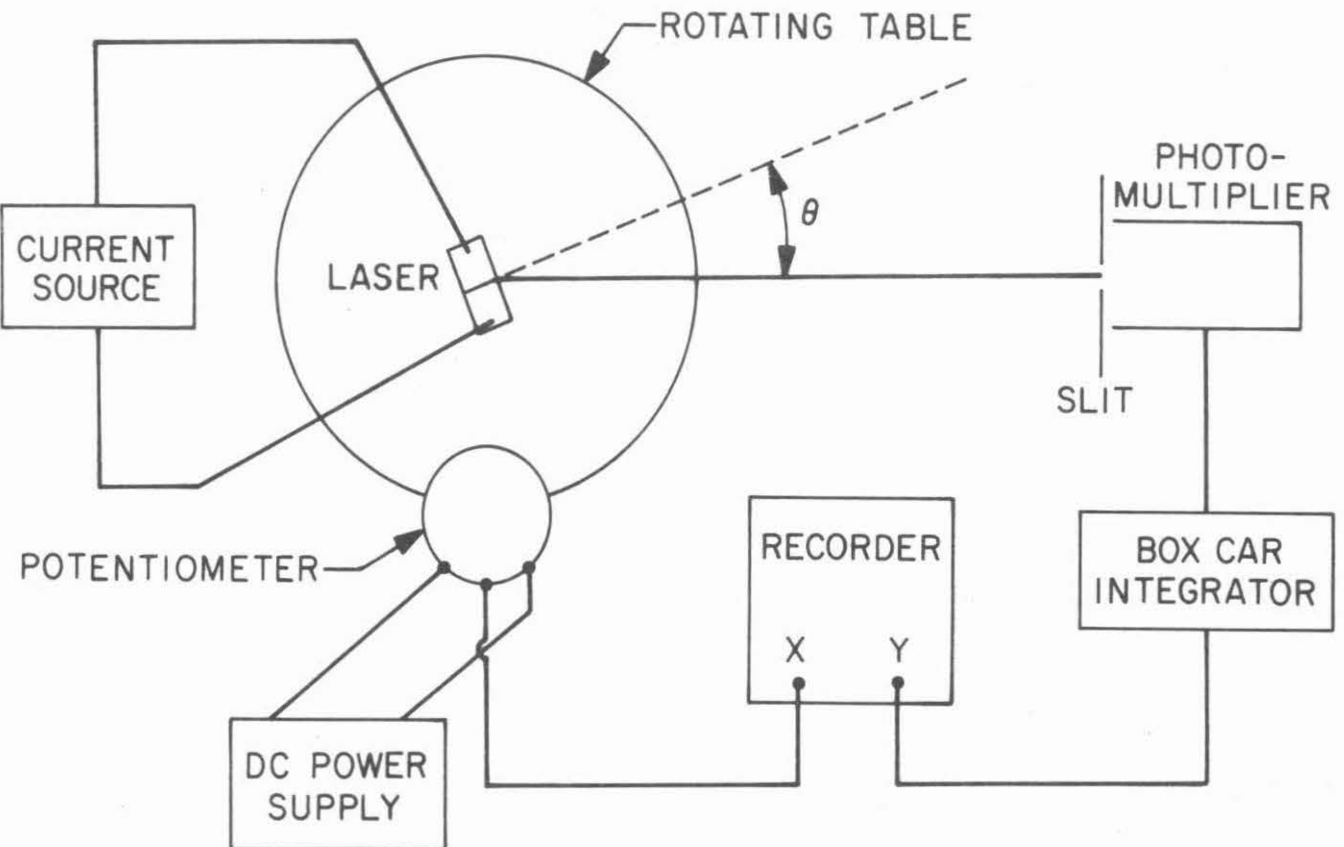

Fig. 5-6 Set-up for measuring lasers' far field patterns

angles could be accurately measured. The photomultiplier was placed behind a slit 8 cm away from the diode. A D.C. power supply and a potentiometer, which was attached to the table, were used to convert the angle of rotation into voltage which served as the X drive of an X-Y recorder. The output of the photomultiplier was integrated by a boxcar integrator and then coupled to the Y drive of the recorder. The measured angular distribution of light had a resolution determined by the angle spanned by the slit opening with respect to the light source. The slit width used in our measurements was 1 mm, which corresponds to a resolution of 0.7°.

REFERENCES FOR CHAPTER V

1. M. B. Panish and S. Sumski, "Ga-Al-As phase, thermodynamic and optical properties", J. Phys. Chem. Solids 30, 129 (1969)
2. M. Ilegems and G. L. Pearson, "Derivation of the Ga-Al-As ternary phase diagram with applications to liquid phase epitaxy", in 1968 Proc. Symp. Gallium Arsenide, London (1969)
3. M. B. Panish and M. Ilegems, "Phase equilibria in ternary III-V systems", in Progress in Solid State Chemistry, 7, (Pergamon Press, 1972)
4. M. B. Panish, S. Sumski, and I. Hayashi, "Preparation of multilayer LPE heterostructures with crystalline solid solutions of $Al_xGa_{1-x}As$ heterostructure lasers," Met. Trans. 2, 795 (1971)
5. K. Gamo, T. Inada, I. Samid, C. P. Lee, and J. W. Mayer, "Analysis of $Ga_{1-x}Al_xAs$-GaAs heteroepitaxial layers by proton backscattering", in Ion Beam Surface Layer Analysis 1 (Plenum Press, New York, 1976)
6. L. R. Dawson, "Near-equilibrium LPE growth of GaAs-$Ga_{1-x}Al_xAs$ double heterostructures", J. Cryst. Growth 27, 86 (1974)
7. D. Fekete, C. P. Lee, S. Margalit, D. M. Pepper, and A. Yariv, "Q-switched ruby laser alloying of ohmic contacts in GaAs epilayers", to be published
8. A. Yariv, Introduction to Optical Electronics (Holt, Reinhart and Winston, Inc., New York, 1971)
9. F. A. Jenkins and H. E. White, Fundamentals of Optics, 3rd Ed. (McGraw-Hill, New York, 1957)